Handbook of Clay Science
Edited by F. Bergaya, B.K.G. Theng and G. Lagaly
Developments in Clay Science, Vol. 1

Chapter 2

STRUCTURES AND MINERALOGY OF CLAY MINERALS

M.F. BRIGATTI[a], E. GALAN[b] AND B.K.G. THENG[c]

[a]*Dipartimento di Scienze della Terra, Università di Modena, I-41100 Modena, Italy*
[b]*Departamento de Cristalografía, Mineralogía y Química Agrícola, Facultad de Química, Universidad de Sevilla, ES-41071 Sevilla, Spain*
[c]*Landcare Research, Palmerston North, New Zealand*

2.1. GENERAL STRUCTURAL INFORMATION

Phyllosilicates considered in this section ideally contain a continuous tetrahedral sheet. Each tetrahedron consists of a cation, T, coordinated to four oxygen atoms, and linked to adjacent tetrahedra by sharing three corners (the basal oxygen atoms, O_b) to form an infinite two-dimensional 'hexagonal' mesh pattern along the *a*, *b* crystallographic directions (Fig. 2.1). In the octahedral sheet, connections between each octahedron, M, to neighbouring octahedra are made by sharing edges. The edge-shared octahedra form sheets of hexagonal or pseudo-hexagonal symmetry (Fig. 2.2). Common tetrahedral cations are Si^{4+}, Al^{3+}, and Fe^{3+}. Octahedral cations are usually Al^{3+}, Fe^{3+}, Mg^{2+}, and Fe^{2+}, but other cations, such as Li^{+}, Mn^{2+}, Co^{2+}, Ni^{2+}, Cu^{2+}, Zn^{2+}, V^{3+}, Cr^{3+}, and Ti^{4+} were identified. Octahedra show two different topologies related to (OH) position, i.e., the *cis*- and the *trans*-orientation (Fig. 2.2).

The free corners (the tetrahedral apical oxygen atoms, O_a) of all tetrahedra point to the same side of the sheet and connect the tetrahedral and octahedral sheets to form a common plane with octahedral anionic position O_{oct} (O_{oct} = OH, F, Cl, O) (Fig. 2.3). O_{oct} anions lie near to the centre of each tetrahedral 6-fold ring, but are not shared with tetrahedra. The 1:1 layer structure consists of the repetition of one tetrahedral and one octahedral sheet, while in the 2:1 layer structure one octahedral sheet is sandwiched between two tetrahedral sheets (Fig. 2.3).

In the 1:1 layer structure, the unit cell includes six octahedral sites (i.e., four *cis*- and two *trans*-oriented octahedral) and four tetrahedral sites. Six octahedral sites and eight tetrahedral sites characterize the 2:1 layer unit cell. Structures with all the six octahedral sites occupied are known as trioctahedral (Fig. 2.4a). If only four of the six octahedra are occupied, the structure is referred to as dioctahedral (Fig. 2.4b). The structural formula is often reported on the basis of the half unit-cell content, i.e., it is based on three octahedral sites.

DOI: 10.1016/S1572-4352(05)01002-0

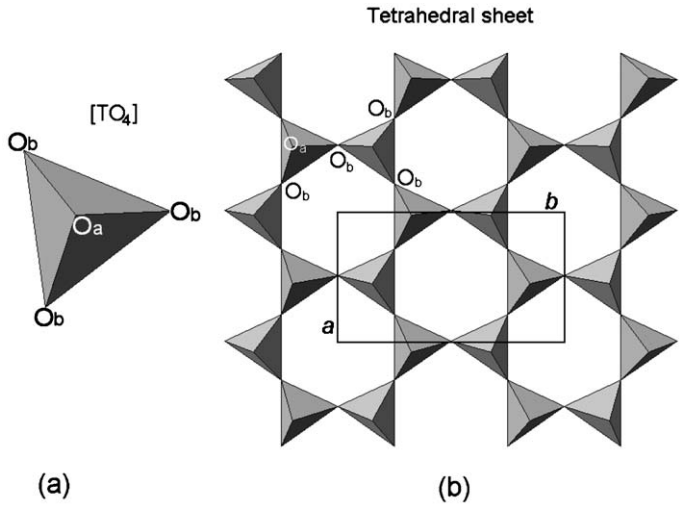

Fig. 2.1. (a) Tetrahedron $[TO_4]$; (b) tetrahedral sheet. O_a and O_b refer to apical and basal oxygen atoms, respectively. *a* and *b* refer to unit-cell parameters.

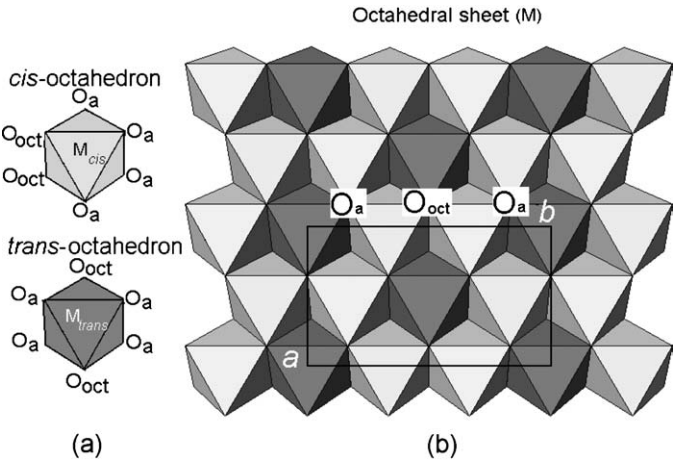

Fig. 2.2. (a) O_{oct} (OH, F, Cl) orientation in *cis*-octahedron and *trans*-octahedron; (b) location of *cis*- and *trans*-sites in the octahedral sheet. O_a and O_b refer to apical and basal oxygen atoms, respectively. *a* and *b* refer to unit cell parameters.

In the 1:1 or TM phyllosilicates (e.g., dioctahedral kaolinite and trioctahedral serpentine) each layer is about 0.7 nm thick (Fig. 2.5a). One surface of the layer consists entirely of oxygen atoms (O_b) belonging to the tetrahedral sheet, while the other surface is composed of O_{oct} (mostly OH groups) from the octahedral sheet (Fig. 2.3). In the 2:1 or TMT layer the tetrahedral sheets are inverted and two-thirds of the octahedral

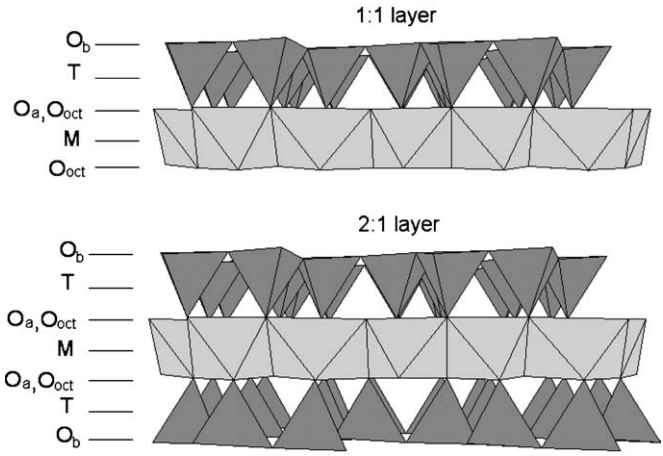

Fig. 2.3. Models of a 1:1 and 2:1 layer structure. O_a, O_b, and O_{oct} refer to tetrahedral basal, tetrahedral apical, and octahedral anionic position, respectively. M and T indicate the octahedral and tetrahedral cation, respectively.

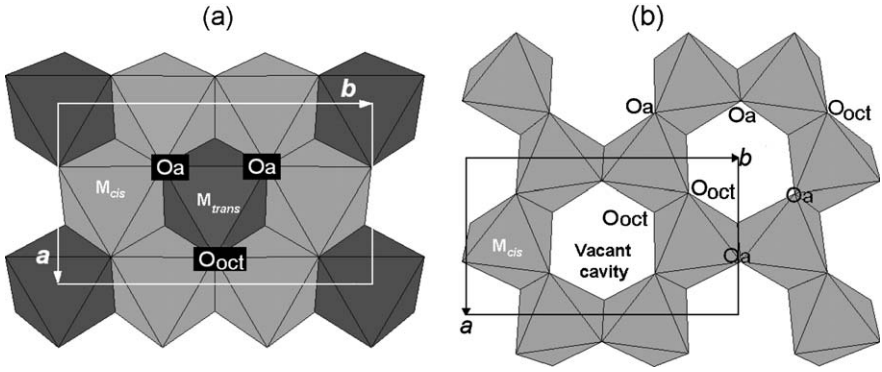

Fig. 2.4. (a) trioctahedral sheet; (b) dioctahedral sheet. O_a represents the apical oxygen atoms shared with tetrahedra, and O_{oct} is the anionic site shared between adjacent octahedra. *a* and *b* are unit-cell parameters.

hydroxyl groups are replaced by tetrahedral apical oxygen atoms (Fig. 2.3). Both surfaces of such a layer consist of tetrahedral basal oxygen atoms O_b. The periodicity along the *c*-axis varies from 0.91–0.95 nm in talc and pyrophyllite (Fig. 2.5b) to 1.40–1.45 nm in chlorite (Fig. 2.5e). The higher values for chlorite are due to interlayer occupancy. In talc, the interlayer space is empty, whereas in mica and illite (Fig. 2.5c) it is occupied by anhydrous alkaline and alkaline-earth cations (layer periodicity $\approx$1.0 nm). The interlayer space of smectite and vermiculite (Fig. 2.5d) contains alkaline or alkaline-earth cations together with water molecules (layer periodicity is about

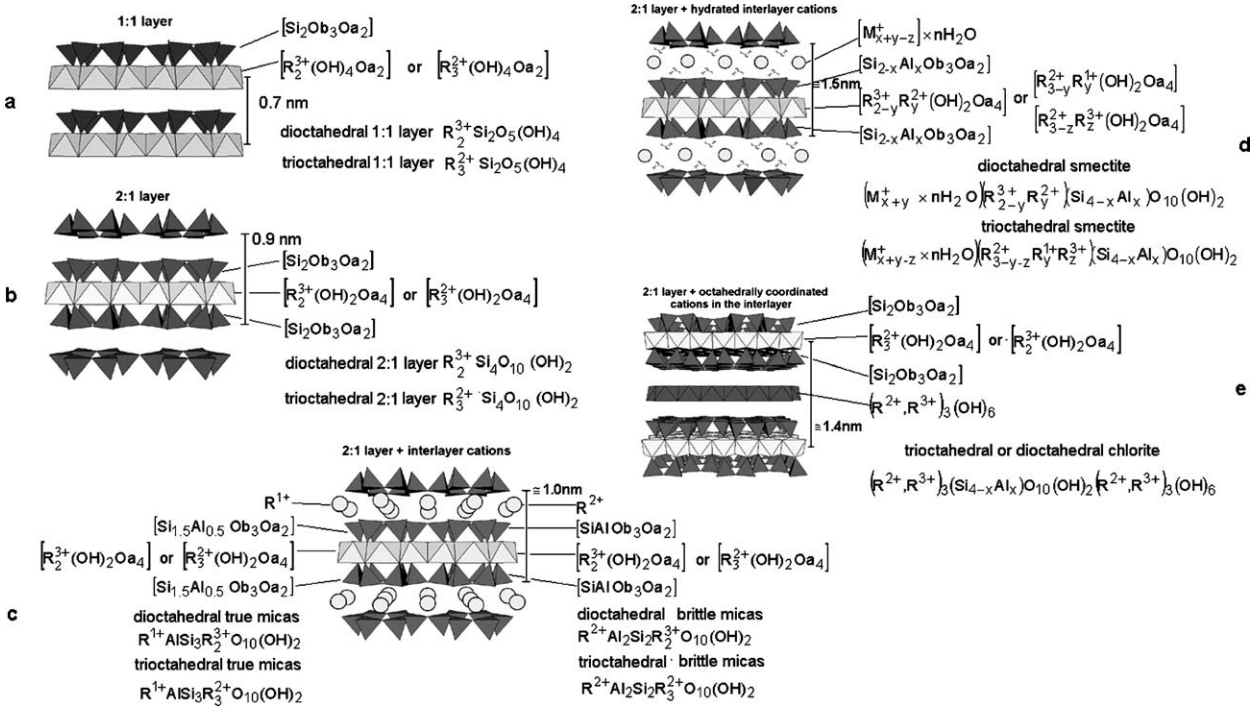

Fig. 2.5. Different layer structures: (a) 1:1 layer (i.e., kaolinite- and serpentine-like layer); (b) 2:1 layer (i.e., pyrophillite- and talc-like layer); (c) 2:1 layer with anhydrous interlayer cations (i.e., the mica-like layer); (d) 2:1 layer with hydrated interlayer cations (i.e., smectite- and vermiculite-like layer); (e) 2:1 layer with octahedrally coordinated interlayer cations (i.e., chlorite-like layer).

1.2 nm when the interlayer position is occupied by cations with low-field strength and water molecules, about 1.5 nm when the interlayer is occupied by high-field strength cations and water molecules, and more than 1.5 nm when water molecules are exchanged by different polar molecules). On the contrary, in chlorite (Fig. 2.5e) the interlayer is occupied by a continuous octahedral sheet, thus showing a $TMTM_{int}$ sequence (where M_{int} is the octahedral interlayer sheet).

The lateral dimension of the tetrahedral sheet is usually greater than that of the octahedral sheet. The lateral misfit between the two sheets requires an adjustment in one or both sheets, causing the layer structure to deviate from ideal hexagonal symmetry. Layer distortion, following from the matching of tetrahedral and octahedral lateral dimensions, usually follows three different mechanisms: (i) the rotation of adjacent tetrahedral as evaluated by the angle α (i.e., the deviation from 120° of each angle in the ring (Fig. 2.6a); (ii) the increase in thickness of the tetrahedral sheet, thereby reducing the basal area of each tetrahedron as evaluated by the angle τ (i.e., the deviation from 109°28′ of O_a–T–O_b triads, Fig. 2.6b); and (iii) the tilting of the tetrahedral basal oxygen plane as evaluated by the Δz parameter (Fig. 2.6c). More

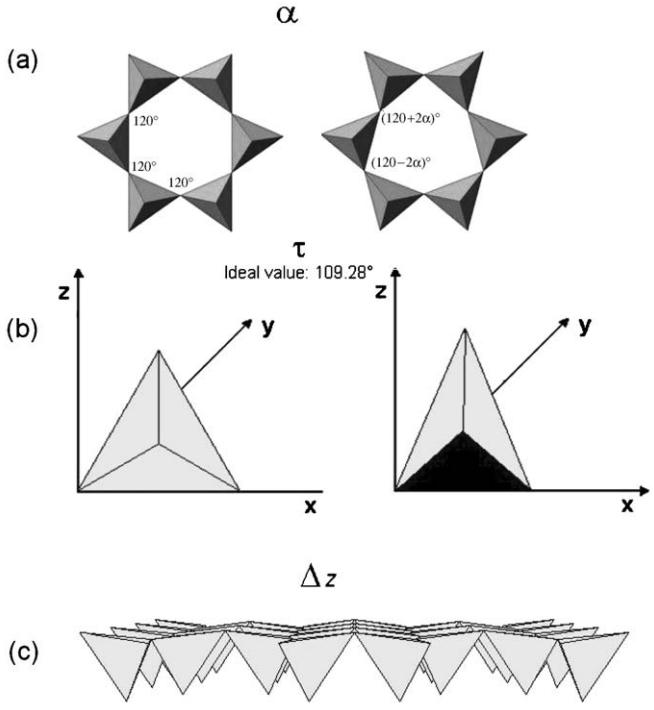

Fig. 2.6. Individual tetrahedra and tetrahedral sheet adjustments in order to accommodate the tetrahedral sheet to the octahedral sheet. (a) tetrahedral ring rotation, α parameter; (b) tetrahedral flattening, τ parameter; (c) tetrahedral tilting, Δz parameter.

details are provided by Brindley and Brown (1980), Bailey (1988a), de la Calle and Suquet (1988), Evans and Guggenheim (1988), Giese (1988), Güven (1988), Wicks and O'Hanley (1988), Moore and Reynolds (1989), Brigatti and Guggenheim (2002).

2.2. LAYER CHARGE (*X*)

When the tetrahedral and octahedral sheets are joined in a layer, the resulting structure can be either electrically neutral or negatively charged. Electrical neutrality exists if (i) the octahedral sheet contains trivalent cations (R^{3+}) in two octahedral sites (usually Al^{3+} and Fe^{3+}), with a vacancy ($\square$) in the third octahedron [$R_2^{3+}(OH)_6$]; (ii) divalent cations (R^{2+}, usually Fe^{2+}, Mg^{2+}, Mn^{2+}) occupy all the octahedral sites [$R_3^{2+}(OH)_6$]; and (iii) the tetrahedral sheet contains Si^{4+} in all tetrahedra. A negative layer charge arises from (i) substitution of Al^{3+} for Si^{4+} in tetrahedral sites; (ii) substitution of Al^{3+} or Mg^{2+} for lower charge cations in octahedral sites, and (iii) the presence of vacancies. This charge variability is recognized as one of the most important features of 2:1 phyllosilicates and micas, because it induces occupancy of the interlayer space by exchangeable cations. In 2:1 phyllosilicates the (negative) layer charge ranges from 0.2 in montmorillonite and hectorite to 2.0 in brittle micas, calculated on the basis of their structural formulae (i.e., half unit-cell content). In 1:1 phyllosilicates the layer charge is usually close to zero.

2.3. POLYTYPISM

A compound is polytypic if it occurs in several different structural modifications for which layers of identical structure and composition are stacked in different ways. In a polytypic series the two-dimensional translations within the layers are (essentially) preserved. The periodicity normal to the layers varies between polytypes according to the number of layers involved in the stacking sequence. Thus, small deviations from stoichiometry (up to 0.20 atoms per formula unit) within a same polytypic series are admissible in the case of phyllosilicates. The theoretical principles of polytypism have been reviewed by Baronnet (1978), Bailey (1988a), Takeda and Ross (1995), Ďurovič (1997, 1999), and Nespolo et al. (1997) and will not be further discussed. Polytypism will only be mentioned when we describe relevant features of clay mineral structures.

2.4. MIXED-LAYER STRUCTURES

Mixed-layer phyllosilicates or interstratified phyllosilicates can be built up by two or more different components. Structures with more than two components are less common, possibly because it is difficult to recognize all the different layers. Interstratified clay minerals can have (i) ordered or regular mixed-layer structures if different layers

alternate along the c^* direction in a periodic pattern (e.g., the stacking of generic type A and type B layers can be … ABABAB … or … AABAABAA … or … AAA-ABAAAABAAAAB … etc.) and (ii) disordered or irregular mixed-layer structures, if the stacking along the c^* direction of type A and B layers is random (e.g., … AB-BABAA … or … AAABABBAAAAABABA …). Fig. 2.7 shows an example of interstratification between 2:1 anhydrous layers with periodicity of about 1 nm and 2:1 hydrated layers with periodicity of about 1.4 nm. Regular sequences are identified by special names. For example, the name 'rectorite' is attributed to a regular interstratification of dioctahedral mica and dioctahedral smectite; 'tosudite' is a regular interstratification of dioctahedral chlorite and dioctahedral smectite; 'corrensite' represents a regular interstratification of trioctahedral vermiculite with trioctahedral chlorite; 'aliettite' is a regular interstratification of talc and trioctahedral smectite (saponite or vermiculite) (Bailey, 1982). The criterion adopted by the AIPEA Nomenclature Committee to attribute special names to regular 1:1 interstratification is that the sequence gives rational reflections. A test of rationality for the diffraction pattern is provided by calculating the coefficient of variability (CV) applied to at least ten $00l$ reflections

$$CV = 100\left[\sum_{i=1}^{n}\frac{\left(X_i - \bar{X}\right)^2}{(n-1)}\right]^{1/2}\frac{1}{\bar{X}}$$

where $X_i = l \times d_{(001)}$ and $\bar{X} = \sum_{i=1}^{n} X_i/n)$ <0.75 (Bailey, 1982)

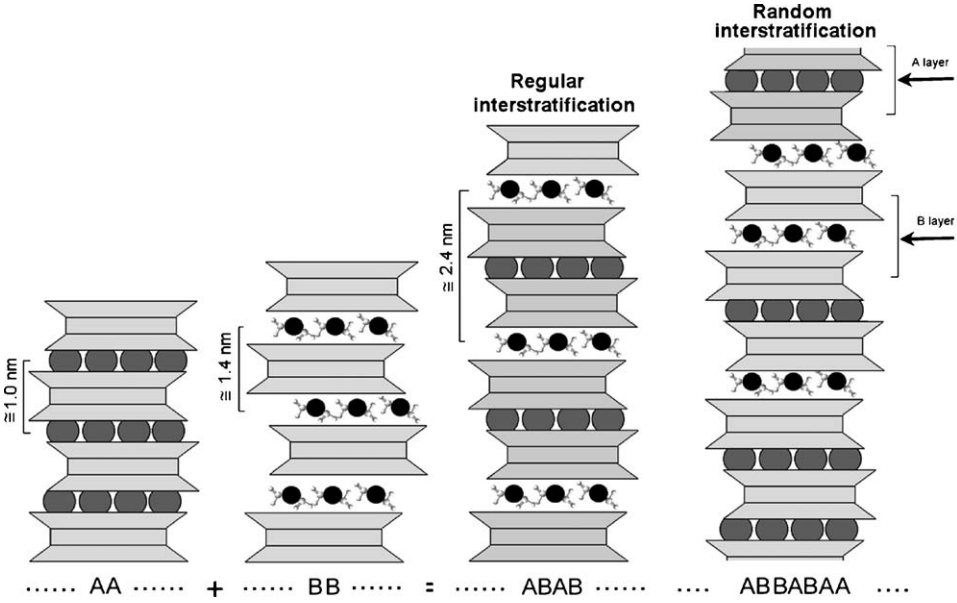

Fig. 2.7. Regularly and randomly interstratified phyllosilicates. A and B are layers with different periodicity along the c direction.

If a two-component type having different $d(001)$ periodicity is randomly interstratified, the mineral is identified by using the name of the components such as illite–smectite, illite–chlorite, illite–vermiculite, and kaolinite–smectite. In randomly stacked mixed layer structures, layer sequence can be 'completely different'. Examples are the irregular stacking of (i) illite (1 nm) and smectite (1.4 nm), (ii) integral multiples of serpentine (0.7 nm) and chlorite (1.4 nm), or (iii) layers with similar basal spacing but with different local structure such as the random stacking of *trans*-vacant and *cis*-vacant illite layers (Drits, 1997). A 'completely different' $d_{(001)}$ distance is measured by X-ray diffraction (XRD). The basal reflections $d(00l)$ form a succession that does not correspond to a series of rational and integral values of l indices. This deviation from the Bragg rule arises from the random variation of the basal periodicity along $\boldsymbol{c}^*$ and can be a good criterion to identify the presence of irregular interstratified structures (Drits and Tchoubar, 1990). When the interstratified material is made up from sequences of different layers with the same thickness, or a thickness that is an integer multiple of the other (e.g., chlorite–serpentine), the XRD pattern looks like that of a regular phase.

Recognition of the interstratified character of a sequence requires a precise analysis of the position intensity and of the profile width of basal reflections, in conjunction with high-resolution transmission electron microscopy (HRTEM) (Moore and Reynolds, 1989; Banfield and Bailey, 1996). Finally, the analysis of XRD patterns can provide useful guidance even in the case of equal layer distance of the component. For example, the sequence of *cis*- and *trans*-vacant sites in adjacent illite layers, produces displacements along the a direction, yielding $d(110)$ reflections that violate the individual layer symmetry.

Useful references to the application of statistical methods to the interpretation and prediction of interstratified mineral structures have been provided by Nadeau et al. (1984, 1985), Reynolds (1988), Drits and Tchoubar (1990), Baronnet (1992), Veblen (1992), and Drits (1997).

2.5. THE 1:1 LAYER

2.5.1. Dioctahedral 1:1 Minerals: The Kaolin Group

The clay minerals in the kaolin group consist of dioctahedral 1:1 layer structures with a general composition of $Al_2Si_2O_5(OH)_4$. Kaolinite, dickite, and nacrite are polytypes. The kaolinite stacking sequence consists of identical layers with an interlayer shift of $2a/3$. Dickite and nacrite have a two-layer stacking sequence where the vacant site of the octahedral sheet alternates between two distinct sites (Brindley and Brown, 1980). Halloysite is a hydrated polymorph of kaolinite with curved layers and a basal spacing of 1 nm that decreases to about 0.7 nm on dehydration. The composition of the kaolin group minerals is characterized by a predominance of Al^{3+} in octahedral sites, although some isomorphous substitution of Mg^{2+}, Fe^{3+}, Ti^{4+}, and V^{3+} for Al^{3+} can occur.

A. Kaolinite

Pauling (1930) was the first to outline the crystal structure of kaolinite using models based on idealized polyhedra. Gruner (1932b) reported the first structural interpretation of the kaolinite powder XRD pattern. He indicated that the mineral belonged to the monoclinic *Cc* symmetry with $d(001) = 1.43$ nm, corresponding to a two-layer structure. This was subsequently confirmed by Hendricks (1938b). Brindley and Robinson (1945, 1946) found that many reflections in the powder pattern could not be indexed correctly on the basis of a monoclinic structure, and suggested a lowering of layer symmetry to the triclinic *C*1. This symmetry is consistent with a 1:1 layer structure built up by stacking of identical layers with a translation of $-a/3$. Kaolinite, dickite, and nacrite consist of sequences with different position of octahedral vacancies in adjacent layers. Bailey (1963) has demonstrated that both kaolinite and dickite have a 1*M* stacking sequence of layers. Octahedral site vacancies alternate in dickite, whereas in kaolinite the location of the vacancy is the same in adjacent layers. Three polytypes, all based on a 1*M* structure, are found for 1:1 dioctahedral phyllosilicates. The 1*M* structure presents three possible locations for the vacant octahedral site, commonly referred as A, B, or C site vacancy (Adams, 1983; Thompson and Withers, 1987; Bish and Von Dreele, 1989; Bukin et al., 1989; Smrčok et al., 1990; Bish, 1993). The structure is chiral if the vacant site is B or C, and achiral if the vacant site is A. All naturally occurring kaolinites are chiral (Fig. 2.8).

Hobbs et al. (1997) have modelled the kaolinite structure by an all-atom ab initio energy minimization method. Their results confirm the space group *C*1, and predict significantly different Si–O bond lengths for the basal and apical tetrahedral oxygen atoms. A low-temperature neutron powder diffraction study by Bish (1993) indicates that low temperatures influence the interlayer separation but has little effect on tetrahedral and octahedral parameters. The structure refinement, derived by Neder et al. (1999) from single-crystal synchrotron data, confirms the *C*1 symmetry and provides

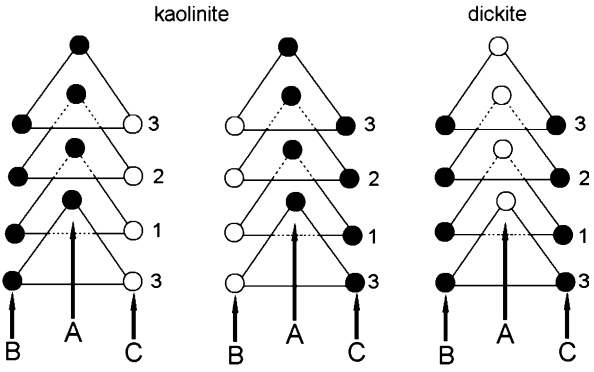

Fig. 2.8. Projection on the (001) plane of the octahedral sites in kaolinite and dickite showing the possible placement of the vacant octahedral site (open circles). Closed circles represent Al^{3+} octahedra. Modified after Bailey (1963).

the following unit-cell parameters: $a = 0.5154(9)$ nm, $b = 0.8942(4)$ nm, $c = 0.7401(10)$ nm, $\alpha = 91.69(9)^\circ$, $\beta = 104.61(5)^\circ$, and $\gamma = 89.82(4)^\circ$. Except for the slight difference in β-angle, these values are very similar to those obtained by Bish and Von Dreele (1989), using X-ray and neutron powder diffraction, i.e., $a = 0.5156(1)$ nm, $b = 0.89446(2)$ nm, $c = 0.740485(2)$ nm, $\alpha = 91.697(2)^\circ$, $\beta = 104.862(2)^\circ$, and $\gamma = 89.823(2)^\circ$. The refinement indicates that tetrahedra are significantly distorted with the Si–O_a bond shorter by 0.0013 nm than the average Si–O bond distances. On the other hand, the octahedral Al–O_a bonds are significantly longer than the Al–O_{oct} (i.e., Al–OH) bonds.

The interlayer OH vectors associated with H-bonding are nearly normal to (001), forming three interlayer hydrogen bonds as shown in Fig. 2.9. Previous studies generally agreed on the position of the Si, Al, and O atoms. However, some uncertainties remain as to the position of the OH groups. The kaolinite layer is essentially neutral and any two contiguous layers are linked through –Al–O–H···O–Si– hydrogen bonding. The primitive unit cell contains four crystallographically distinct O–H groups. Three of them (labelled OH_2, OH_3, OH_4) are located at the inner surface and one (labelled OH_1) is inside the layer as shown in Fig. 2.9a. These hydroxyl groups form strong hydrogen bonds if they are oriented nearly perpendicular to the layer but are not involved in H-bonding if they are parallel to the layer (Fig. 2.9). The extensive research into OH group orientation has been reviewed by Giese (1988). The crystal structure refinement of a deuterated kaolinite (Akiba et al., 1997) confirms that the three inner OD vectors point toward the tetrahedral sheet, and form H-bonding with basal oxygen atoms of the adjacent kaolinite layer. One of these three, however, differs from the other two in bond angle, thus, suggesting a different orientation of the bond. Benco et al. (2001a–c) have explained interlayer

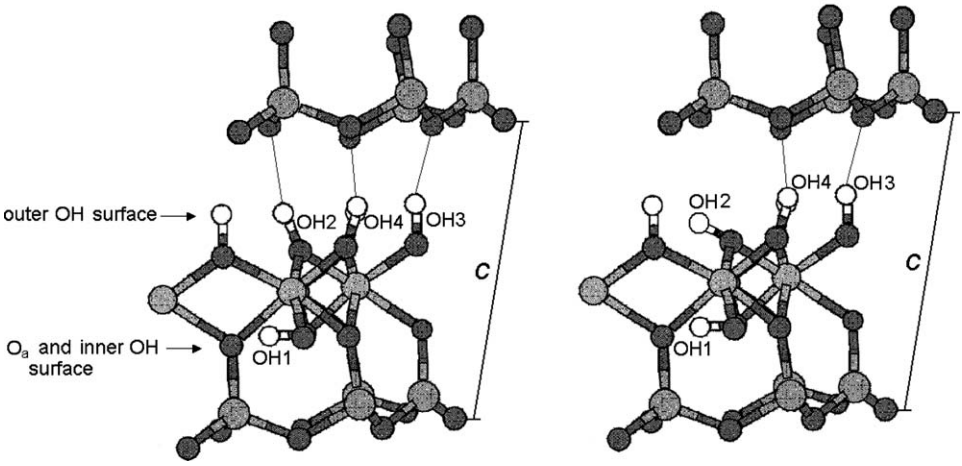

Fig. 2.9. Different OH orientations on the octahedral surface of kaolinite. Modified after (Benco et al., 2001a).

H-bonding in kaolinite by ab initio molecular dynamic simulations of a hypothetical isolated layer. They identify four distinct OH groups, two of which (OH_3 and OH_4) form weak H bonds with O–H···O distances between 0.18 and 0.26 nm, while the other two (OH_1 and OH_2) do not participate in H bonding (Fig. 2.9b).

The poor structural order commonly observed in kaolin minerals may be explained in terms of a series of stacking faults or defects in the *ab* plane and along the *c*-axis. This feature accounts for the well-known tendency of kaolin minerals to form a wide variety of ordered and disordered polytypes as well as twins (Dornberger-Schiff and Ďurovič, 1975; Plançon et al., 1989; Zvyagin and Drits, 1996). The diffraction patterns of ordered kaolinite are significantly different from those of disordered kaolinite. Ordered kaolinite shows sharp and narrow peaks, while its disordered counterpart gives less well-defined, broad, and asymmetrical peaks. The *hkl* reflections with $k = 3n$ (where n is an integer) are generally less affected than those with $k \neq 3n$ (Brindley and Robinson, 1946; Murray, 1954). In extreme cases, peaks lose their identity and merge to form a two-dimensional modulated band of diffracted intensity.

Structural order/disorder in kaolinite can be assessed by different tests. The most widely used (Fig. 2.10) are those based on changes in two groups of XRD

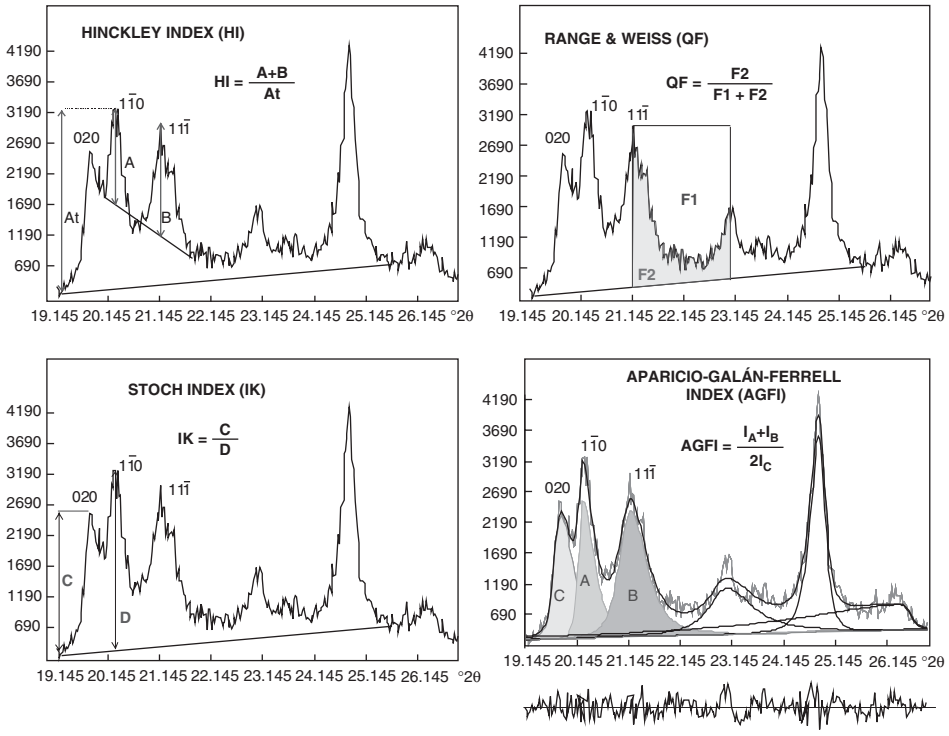

Fig. 2.10. XRD-based methods for assessing the degree of structural order in kaolinite. The 2θ values refer to CuKα radiation.

reflections: (i) the 02*l* and 11*l* sequences (20–23° 2θ using Cu Kα) that are sensitive to arbitrary and special interlayer displacements (such as $b/3$) and (ii) the 13*l* and 20*l* sequences (35–40° 2θ using Cu Kα) that are affected by arbitrary displacements (Cases et al., 1982). Some of these tests are (i) the Hinckley index (HI) (Hinckley, 1963) and Range–Weiss index (QF) (Range and Weiss, 1969); (ii) the Stoch index (IK) (Stoch, 1974), measured in the same zone as the previous two indices but is less sensitive to the presence of quartz; and (iii) the Liétard index (R2) (Liétard, 1977) that is sensitive to the presence of arbitrary defects only (Cases et al., 1982). Aparicio and Galán (1999) have investigated the influence of mineral and amorphous phases, associated with kaolin and kaolinitic rock, on kaolinite order–disorder measurements by XRD. Both the Hinckley and Range–Weiss indices appear to be influenced by quartz, feldspar, iron gels, illite, smectite, and halloysite. On the other hand, the Stoch index can be used in the presence of quartz, feldspar, iron, and silica gels, while the Liétard index is not affected by phases other than halloysite. As a result, Aparicio et al. (1999) have proposed the Aparicio–Galán–Ferrell index. Derived from the intensity of reflections in the 02*l* and 11*l* sequence, and obtained by pattern fitting, this index is less influenced by peak overlap (Aparicio et al., 2001).

On the other hand, Plançon and Zacharie (1990) have proposed 'an expert system' that runs on a compatible PC and describes the structural defects of kaolinite based on direct measurements of the diffraction pattern. The results of this system are acceptably consistent with the theoretical and experimental diffractograms for kaolinite. The expert system describes kaolinite defects and provides a global abundance of translation defects, but cannot distinguish between the t_0 translation (roughly $t_1 - b/3$) and the t_2 translation (roughly $t_1 + b/3$). It gives the number of different phases in the sample (1 or 2 phases). For bi-phase samples, it establishes the percentage of low-defect or well-crystallized phases (%wp). In the case of single-phase samples, it fixes the amount of the *C* layers (W_C), the variation of interlayer translations about the mean values (δ), the proportion of translation defects (p), and the mean number of layers (M).

Aparicio and Galán (1999) have suggested that the expert system of Plançon and Zacharie (1990) is the best method for determining the degree of order–disorder in kaolinite, although it is highly affected by the presence of other phases, particularly when more than 25% of well-crystallized kaolinite is present. However, the system can be used with single-phase kaolinite (disordered kaolinite), which is not affected by the presence of phases other than halloysite, thus seemingly increasing the amount of translation defects. In any case, the expert system should not be used with kaolinite of medium order–disorder because the well-ordered phase is present in a low amount (<10%).

B. Dickite

Gruner (1932a) was the first to propose a structural refinement for dickite (general formula $Al_2Si_2O_5(OH)_4$). Subsequent refinements were proposed by Hendricks (1938b), Newnham and Brindley (1956), and Newnham (1960). On the basis of these

refinements, the crystal structure of dickite belongs to the monoclinic space group *Cc* with the vacant cavity alternating in adjacent layers between B and C sites (Fig. 2.8). Symmetry requirements (site A of Fig. 2.8) are met by placing the vacant cavity at the *trans*-site (Bailey, 1963). The cell parameters are as follows: $a = 0.5138(1)$ nm, $b = 0.8918(2)$ nm, $c = 1.4389(2)$ nm, $\beta = 96.74(2)^\circ$ (Joswig and Drits, 1986). As with kaolinite, the vector orientation of inner and outer OH groups, and the strength of interlayer H-bonding, have attracted much attention (Giese and Datta, 1973; Adams and Hewat, 1981; Rozhdestvenskaya et al., 1982; Sen Gupta et al., 1984; Joswig and Drits, 1986; Giese, 1988; Bukin et al., 1989; Johnston et al., 1990).

Using polarized single-crystal Fourier-transform infrared microscopy, Johnston et al. (1990) have deduced that the angle between the inner OH_1 vector and the *b*-axis is 47°, while the inner-surface OH-group vectors are oriented at different angles with respect to the *b*-axis ($OH_3 = 22^\circ$; OH_2 and $OH_4 = 45^\circ$). Benco et al. (2001a–c) have assessed the orientation of OH vectors using ab initio molecular dynamics and total energy calculations. They suggest that the inner hydroxyl and one inner-surface hydroxyl are horizontally oriented, while the other two hydroxyls are involved in interlayer bonding. Bish and Johnston (1993) have provided a low-temperature structural refinement for dickite. The structure is the same as that deduced previously from room temperature measurments, except for the orientation of OH vectors. In particular, the inner hydroxyl group is almost parallel to (001), inclined by 1.3° towards the tetrahedral sheet. The internuclear O–H_3···O distance increases as well as the Al–OH_1–Al. The two-dimensional crystal structure refinement at 535 °C suggests that the OH groups on the surface are completely removed.

C. Nacrite

The first crystal structure refinement of nacrite was reported by Hendricks (1939) who suggested the space group *Cc*. The structure is made up by stacking six layers, closely approaching rhombohedral symmetry with a pseudo-space group *R*3*c*. Blount et al. (1969) have confirmed that the ideal structure of nacrite is based on a 6*R* stacking sequence of kaolinite layers (TM layers), in which each successive layer is shifted relative to the layer below by –1/3 of the 0.89 nm lateral repeat direction. This direction is referred to as *x* in nacrite, contrary to the usual convention for layer silicates, because of the positioning of the (010) symmetry planes normal to the 0.51 nm repeat direction. Alternate layers are also rotated by 180°. The pattern of vacant octahedral sites reduces the symmetry to *Cc* and permits description of the structure as a two-layer form with an inclined *z*-axis. Adjacent tetrahedra are twisted by 7.3° in opposite directions so that the basal oxygen atoms are nearer to both the Al^{3+} cations in the same layer and the surface hydroxyls of the layer below. Interlocking corrugations in the oxygen and hydroxyl surfaces of adjacent layers run alternately parallel to the [110] and $[1\bar{1}0]$ axes in the adjacent layers. The upper and lower O–Al–O groups in each Al octahedron are rotated by 5.4° and 7.0° in opposite directions resulting in the shortening of shared edges. Nacrite has a greater interlayer separation and smaller lateral dimensions than dickite and kaolinite, and the

observed β-angle deviates by 11–12° from the ideal value. These features, and the overall lower stability, of nacrite are ascribed to the less-favourable positioning of the basal O_b atoms relative to the directed interlayer H-bonds. The nacrite crystal structure, refined by Zvyagin et al. (1972, 1979) using high-voltage electron diffraction (ED), is very similar to that proposed by Blount et al. (1969). However, the tetrahedral rotation angle in the structure of Zvyagin et al. (1972, 1979) is smaller. Zheng and Bailey (1994) have confirmed the crystal structure reported by Blount et al. (1969), giving the following unit-cell parameters: $a = 0.8906(2)$ nm, $b = 0.5146(1)$ nm, $c = 1.5664(3)$ nm, and $\beta = 113.58(3)°$. The location of hydrogen atoms is deduced from different electron density maps. The inner OH_1 vector points exactly towards the vacant octahedron and is depressed by −18.6° away from the level of the octahedral cations. All three surface OH groups have OH vectors at 50–66° to (001), although OH_2 may not participate in interlayer hydrogen bonding. All three interlayer OH–OH contacts (between 0.294 and 0312 nm) are bent at angles between 132 and 141°.

Ben Haj Amara et al. (1997, 1998) have described the structure of hydrated and dehydrated nacrite. The hydrated form is characterized by a basal distance of 0.842 nm, containing one water molecule per $Si_2Al_2O_5(OH)_4$ in the interlayer space. The interlayer water molecule is placed above the vacant octahedral site of the layer and is embedded in the ditrigonal cavity of the tetrahedral sheet of the upper layer.

D. Halloysite

Halloysite may be regarded as a hydrated kaolinite phase. Hofmann et al. (1934) showed by XRD that water was present in the interlayer space, giving a general formula of $Si_2Al_2O_5(OH)_4 \times 2H_2O$. As hydrated halloysite has a layer periodicity (basal spacing) close to 1 nm (10 Å) (Brindley and Robinson, 1948), it is often denoted as 'halloysite-(10 Å)'. The interlayer water in halloysite can be easily removed. The resultant dehydrated form with a basal spacing close to 0.72 nm (7.2 Å) is referred to as 'halloysite-(7 Å)' although the name 'metahallysite' is sometimes used. The particles of halloysite can adopt different morphologies, such as spheres, tubes, plates, and laths (e.g., Churchman and Theng, 1984). More often than not, the long tubular forms are relatively well crystallized. In most cases the direction of particle orientation coincides with the *b*-axis (Zvyagin et al., 1966).

The interlayer water in halloysite can be irreversibly removed by heating (Zvyagin et al., 1966). Costanzo and Giese (1985) have suggested a continuous sequence of hydration states, ranging from fully hydrated through partially hydrated to dehydrated halloysite. Costanzo et al. (1984) have identified two types of interlayer H_2O: (i) 'hole' H_2O located in the ditrigonal cavities of the tetrahedral sheet and (ii) 'associated' H_2O forming a discontinuous layer of mobile molecules. The 0.84 and 0.86 nm hydrates have only 'hole' H_2O, whereas the 1 nm hydrates and natural halloysite contain both 'hole' and 'associated' H_2O. Hole water is H-bonded to the basal oxygen atoms of the tetrahedral sheet. Associated water forms intermolecular

H-bonds approximately equal in strength to that in liquid water, and is less strongly bonded to the clay surface than hole water.

The dehydration of halloysite has been discussed by Bhattacherjee (1973) and Mizuki et al. (1985) who indicated dehydration at 70–100 °C and collapse of the structure at approximately 400 °C. Okada and Ossaka (1983) suggested that the halloysite layer periodicity changed coherently from 1 to 0.7 nm and that dehydration progressed perpendicular to the layers of each particle.

Kohyama et al. (1978) have determined the unit-cell parameters for 1 nm- and 0.7 nm-halloysites, both of which have a two-layer structure in the space group Cc with unit-cell parameters $a = 0.514(4)$ nm, $b = 0.890(4)$ nm, $c = 2.07(1)$ nm, $\beta = 99.7^\circ$ and $a = 0.514(4)$ nm, $b = 0.890(4)$ nm, $c = 1.49(1)$ nm, $\beta = 101.9^\circ$. Bayliss (1989) has refined the halloysite unit-cell parameters in the hexagonal system.

E. Hisingerite

Hisingerite, first described in 1810, has been variously regarded as a non-crystalline silicate, a ferric allophane, a ferric halloysite, and a poorly crystallized nontronite. On the basis of TEM data, Frost et al. (1997) and Eggleton and Tilley (1998) have interpreted hisingerite to be the iron analogue of spherical halloysite.

2.5.2. Trioctahedral 1:1 Minerals: The Serpentine Group

The trioctahedral 1:1 layer silicates have been investigated by many authors (e.g., Wicks and O'Hanley, 1988) using well-crystallized phases similar to those found in the clay fraction of soils and sediments.

Lizardite, antigorite, and chrysotile are Mg-rich 1:1 trioctahedral layer minerals with an ideal composition of $Mg_3Si_2O_5(OH)_4$. Although chemically simple, they are structurally complex. Lizardite has an ideal layer topology, whereas antigorite is modulated and chrysotile is bent (Wicks and Whittaker, 1975; Wicks and O'Hanley, 1988; Veblen and Wylie, 1993).

These structural differences are recognized by the AIPEA Nomenclature Committee (Martin et al., 1991). Like lizardite, the trioctahedral 1:1 minerals berthierine, amesite, cronstedtite, nepouite, kellyite, fraipontite, and brindleyite have been classified as serpentine minerals with a planar structure. Other minerals, traditionally referred to as serpentine, show a modulated layer structure. They are subdivided into minerals with tetrahedral sheet strips such as antigorite and bementite, or with tetrahedral sheet islands such as greenalite, caryopilite, pyrosmalite, manganpyrosmalite, ferropyrosmalite, friedelite, mcgillite, schallerite, and nelenite.

Suitable crystals of Mg-rich serpentine minerals for high-quality three-dimensional structural studies were not available until 1980. Since then, however, Mellini and co-workers (Mellini, 1982; Mellini and Zanazzi, 1989; Mellini and Viti, 1994) have performed a structural study on two polytypes of lizardite: $1T$ and $2H_1$ in the space group $P31m$, whereas $2H_1$ polytype structure belongs to the space group $P6_3cm$ (Mellini and Zanazzi, 1987). Brigatti et al. (1997) examined the $2H_2$ form of

lizardite in the space group $C2/c$. The effect of pressure on the structure of $1T$ lizardite has been determined by Mellini and Zanazzi (1989). Guggenheim and Zhan (1998) reported a high-temperature study on both $1T$ and $2H_1$ lizardite crystals. The overall structure of lizardite consists of two submodules: the 1:1 layer itself and the empty space where two adjacent 1:1 layers meet through interfacing hexagonally close-packed oxygen atoms. The internal dimension of 1:1 layer shows only minor changes after chemical substitutions, increasing pressure or temperature. On the contrary, the interlayer thickness varies significantly with composition (Chernoski, 1975) or when the pressure increases (Mellini and Zanazzi, 1989). As the interlayer thickness decreases, the ditrigonalization of the tetrahedral sheet increases either in a positive or in a negative way. In the $1T$ polytype the ditrigonal ring distortion changes from -1.5° to approximately 0° when the temperature changes from 20 to 480 °C. In the $2H_1$ polytype this structural parameter changes from 1.8° to 1.3° at 300 °C and remains unchanged up to 475 °C. For the $2H_1$ polytype the O–O distance in the interlayer O–H···O bond increases linearly from 0.308 to 0.315 nm as the temperature increases from 20 to 475 °C. On the contrary, for the $1T$ polytype this distance remains nearly constant up to 360 °C. Above this temperature the O–O distance increases slightly. Thus, the $2H_1$ polytype appears to have weaker hydrogen bonding than the $1T$ polytype (Guggenheim and Zhan, 1998).

Antigorite is characterized by a large superstructure along the [100] direction. On the basis of X-ray and optical diffraction, Zussman (1954) has suggested that the superstructure is a result of a repeating wave structure. The structure has been subsequently studied by Kunze (1956, 1958, 1959), who identified the super-cell unit as '*A*' and the sub-cell unit as '*a*'. Aruja (1945) derived a value of about 0.455 nm for the *A* parameter. Uehara and Shirozu (1985) defined the superstructure in terms of the number (M) of sub-cells ($a = 0.544$ nm) along the x-axis, with $M = A/a$. They also suggested that samples of antigorite might be classified into three structural types. In the first type $M = n$ (where n is an integer); in the second type $M = (2n+1)/2$; and in the third type M is different from $n/2$. The first type contains an odd number of tetrahedra (n) and an even number of octahedra ($n-1$) in the superstructure period A (space group Pm). The structure of the second type derives from that of the first type but is different from the structure proposed by Kunze (1959), where M is an even number in the space group $P2/m$. The model based on $M = (2n+1)/2$ is obtained by shifting Kunze's model at each wave limit along the y direction by $b/2$ (resulting in lattice C-centered). The model contains an even number of tetrahedra (m) and an odd number of octahedra ($m-1$). The third structure, with M different from $n/2$, is a mixture of the two structures described above in coherent domains. This structure is commonly found in poorly crystallized disordered materials (Uehara, 1987).

Difficulties in studying single crystals of chrysotile can be related to fibre intergrowth, polygonalization of the layer, polytype intergrowth, and crystal bending.

Amesite with an ideal composition of $(Mg_2Al)(SiAl)O_5(OH)_4$ can have an ordered or disordered cation distribution in the 1:1 layer. Thus, differences in both polytypic arrangements and ordering patterns inside the same polytype can occur. Four

regular polytypes ($2H_1$, $2H_2$, $6R_1$, and $6R_2$) as well as random stacking polytypes have been determined (Steinfink and Brunton, 1956; Hall and Bailey, 1976; Anderson and Bailey, 1981; Wiewióra et al., 1991; Zheng and Bailey, 1997). Since cations of different size and charge occur both in tetrahedral and octahedral sites, there is a very strong tendency for ordering. All amesites are therefore presumed to be ordered. As a result, the hexagonal or rhombohedral symmetry of the ideal polytypes is reduced to triclinic symmetry with complete cation disorder, and the β unit-cell angle deviates slightly from 90° ($90.2 \leqslant \beta \leqslant 90.3°$).

Carlosturanite, an octahedrally modulated structure (Compagnoni et al., 1985), has the general formula of $M_{21}[T_{12}O_{28}(OH)_4](OH)_{30} \times H_2O$ where M is predominantly Mg^{2+} with small amounts of Fe^{3+}, Mn^{3+}, Ti^{4+}, Cr^{3+}, and T is Si^{4+}, Al^{3+}. The unit-cell parameters are $a = 1.670$ nm, $b = 0.941$ nm, $c = 0.7291$ nm, $\beta = 101.1°$, and the space group is *Cm*. The model structure consists of a continuous planar octahedral sheet and a discontinuous 'tetrahedral sheet'. The latter is modified to strips, six tetrahedra in width, running parallel to the *b*-axis.

Greenalite is a 1:1 structure having the tetrahedral sheet completely occupied by Si^{4+}, and the octahedral sheet mostly occupied by Fe^{2+}, with a significant substitution of Mg^{2+} for Fe^{3+} (Floran and Papike, 1975). The greenalite structure has been investigated by Guggenheim et al. (1982) using ED, HRTEM, and optical imaging techniques. They have suggested that the tetrahedral sheet is made up of 'islands' of six-member tetrahedral rings, with four and three-members ring at the island borders. More detailed information on greenalite can be found in the review by Guggenheim and Eggleton (1998).

2.6. THE 2:1 LAYER

The layer of 2:1 phyllosilicates consists of an octahedral sheet sandwiched between two opposing tetrahedral sheets. In pyrophyllite (dioctahedral) and talc (trioctahedral), the layer is electrically neutral. In the other 2:1 phyllosilicates (e.g., smectite, vermiculite, mica, chlorite), the layer is usually negatively charged. The magnitude of the layer charge (X) measures the deviation of charge from neutrality. For true micas X is close to -1, while for brittle micas it is approximately equal to -2; in both cases the space between two adjacent layers is occupied by anhydrous cations. Illite is a micaceous clay mineral that occurs widely in soils and sediments. A fractional value for layer charge and the presence of hydrated cations in the interlayer space characterize the most common 2:1 clay minerals, such as smectites and vermiculites. In smectites, the negative charge per half-unit-cell ranges from 0.2 to 0.6, while in vermiculites this value is between 0.6 and 0.9. In chlorite, the negative layer charge is neutralized by the presence of a positively charged octahedral sheet in the interlayer space. Most chlorites are trioctahedral; dioctahedral chlorites, and intermediate forms with alternating dioctahedral and trioctahedral sheets, are rare. As in 1:1 phyllosilicates, the 2:1 layer structure can be non-planar. For example,

minnesotaite (traditionally considered as a variety of talc) has a modulated structure with tetrahedral strips. Other 2:1 layer silicates, such as sepiolite, palygorskite, and loughlinite also show a modulated structure but the strips are made up of octahedral sheets (Martin et al., 1991).

2.6.1. Pyrophyllite, Talc, and Related Minerals

The ideal layer structure of pyrophyllite (dioctahedral) and talc (trioctahedral) is electrically neutral, and hence no charge-balancing cation is present in the interlayer space. Contiguous layers are held together by van der Waals interactions. This affects both the mechanical properties of the minerals and the quality of crystals for structural investigation.

Pyrophyllite with an ideal structural formula of $Al_2Si_4O_{10}(OH)_2$, is not known to vary greatly in composition. Only limited substitution of Al^{3+} for Si^{4+} and minor amounts of Fe^{2+}, Fe^{3+}, Mg^{2+}, and Ti^{4+} have so far been found. Although structural investigations of this mineral are complicated by its small size and irregular layer stacking, polytypism in pyrophyllite has been identified by several authors (Zvyagin et al., 1968; Shitov and Zvyagin, 1972; Evans and Guggenheim, 1988). There are two dominant polytypes, a two-layer monoclinic ($2M$), and a one-layer triclinic ($1Tc$). Investigations into the pyrophyllite structure date back to Gruner (1934), Hendricks (1938a). Rayner and Brown (1966) have proposed the space group $C2/c$ and Cc with $a = 0.517$ nm, $b = 0.892$ nm, $c = 1.866$ nm, $\beta = 99.8^\circ$ as unit-cell parameters. Brindley and Wardle (1970) determined the XRD powder patterns of pyrophyllite samples from different localities, and showed the existence of both one-layer triclinic and two-layer monoclinic forms. Some samples were mixtures of the two forms, while others were so disordered, either naturally or by mesh grinding, that differentiation was not possible. The powder pattern of the best-crystallized sample gave the following parameters: $a = 0.5173$ nm, $b = 0.8960$ nm, $c = 0.9360$ nm, $\alpha = 91.2^\circ$, $\beta = 100.4^\circ$, $\gamma = 90^\circ$ for the triclinic form; and $a = 0.5172$ nm, $b = 0.8958$ nm, $c = 1.867$ nm, $\beta = 100.0^\circ$ for the monoclinic form. The corresponding anhydrous phases gave the following parameters: $a = 0.5140$ nm, $b = 0.9116$ nm, $c = 0.9504$ nm, $\alpha = 91.2^\circ$, $\beta = 100.2^\circ$, $\gamma = 90^\circ$ for the triclinic form, and $a = 0.5173$ nm, $b = 0.9114$ nm, $c = 1.899$ nm, $\beta = 100.0^\circ$ for the monoclinic form. The expansion of the b parameter was attributed to a relaxation of the twisted Si–O network. After dehydroxylation, the Al^{3+} ion coordination appeared to change only slightly, possibly causing the structures to be constrained in the ***a*** direction (Wardle and Brindley, 1972).

The first three-dimensional crystal structure refinement of pyrophyllite (polytype $1Tc$, space group symmetry $C\bar{1}$) has been carried out by Lee and Guggenheim (1981). The mean tetrahedral cation-oxygen bond length (0.1618 nm) is consistent with the lack of significant Al^{3+} for Si^{4+} substitutions. Similarly, the octahedral cation-oxygen distance (0.1912 nm) indicates a nearly complete Al occupancy. The OH vector points away from the (001) plane and forms an angle of about 26° (Giese, 1973). This

value is much higher than that commonly found for muscovite containing K^+ in the interlayer space. This feature is explained in terms of the sole contribution of Al^{3+} cations to the attainment of a theoretical equilibrium position. Molecular dynamic modelling by Teppen et al. (1997) gives results that are in good agreement with experimentally derived values, although the OH vector is predicted to be less inclined than what is observed. Since van der Waals interactions are primarily involved in keeping adjacent 2:1 layers together, interlayer cohesion is weak.

Isomorphous substitution in pyrophyllite has been suggested by Kodama (1959). A pale blue sample containing V^{3+} (44–190 ppm), Cr^{3+} (30–80 ppm), Sn^{4+} (20–50 ppm), Ni^{2+}, Co^{2+}, Pb^{2+}, and Ga^{3+} shows the following unit-cell parameters: $a = 0.517$ nm, $b = 0.895$ nm, $c = 1.864$ nm, $\beta = 99.8°$.

Substitution in the octahedral sheet of pyrophyllite has also been indicated by theoretical ab initio calculations. Mg^{2+} for Al^{3+} substitutions tend to be distributed in the octahedral sheet, whereas Fe^{3+} for Al^{3+} substitutions tends to be clustered (Sainz-Diaz et al., 2002).

Even if pyrophyllite is characterized by the near absence of layer charge, the mineral can react with heavy metals in solution. For instance, Scheidegger et al. (1997) found that pyrophyllite can adsorb Ni^{2+} from aqueous solution using X-ray absorption fine structure (XAFS). Their data suggest the formation of multinuclear Ni^{2+} complexes after a reaction time of few minutes. The size of these complexes increases with time. Ni–Ni bond distances (0.299–0.303 nm) are similar to those in mixed Ni–Al hydroxides, but distinctively shorter than in $Ni(OH)_2$.

The thermal transformation of pyrophyllite, analysed by different techniques (^{27}Al and ^{29}Si MAS-NMR, thermal analysis DTA-TG, dilatometry, and XRD), suggests that dehydroxylation occurs above 800 °C. The ^{27}Al NMR obtained on the mineral after heating at 800 °C suggests the occurrence of Al in a distorted five-fold coordination. At 1000 °C, the tetrahedral sheet breaks down and a partial segregation of amorphous SiO_2 occurs. This process is consistent with the rearrangement of aluminium ions, favouring the formation of small disordered nuclei of mullite and cristobalite. The formation of $[AlO_5]$ polyhedra during pyrophyllite dehydroxylation has also been detected by Klevtsov et al. (1987).

Recently, the structure of brinrobertsite, an ordered, mixed-layered, dioctahedral pyrophyllite–smectite, has been modelled from TEM data. TEM images show sequences of dominant 2.4 nm periodicity, produced by 2:1 layers with alternate pyrophyllite-like (low-charge) and smectite-like (high-charge) interlayers.

The chemical composition of talc-like minerals does not usually differ significantly from that of the end-member ($Mg_3Si_4O_{10}(OH)_2$), even if limited substitution of Al^{3+} or Fe^{3+} for Mg^{2+} occurs. Charge balance is usually achieved by tetrahedral $^{[IV]}Al^{3+}$ for $^{[IV]}Si^{4+}$ substitutions and/or by insertion of vacancies in octahedral position. Talc-like minerals are kerolite (hydrated variety), minnesotaite (Fe-rich variety), and willemseite (Ni-rich variety). Different polytypic sequences have been derived by Weiss and Ďurovič (1984) who found ten non-equivalent polytypes but only seven of these may actually be distinguished by XRD.

2.6.2. True and Brittle Micas

Brigatti and Guggenheim (2002) have discussed the structural and chemical features of more than 200 mica crystals. Most of these are true micas, belonging to the $1M$, $2M_1$, $3T$, $2M_2$, and $2O$ polytypes. The dominant polytype in trioctahedral true micas is $1M$, whereas in dioctahedral micas, the most common stacking sequence is $2M_1$. The structure refinements of brittle micas confirm that the $1M$ polytype is generally trioctahedral whereas the $2M_1$ polytype is dioctahedral. The $2O$ structure has been found for the trioctahedral brittle mica anandite (Giuseppetti and Tadini, 1972; Filut et al., 1985) and recently for a phlogopite from the Kola Peninsula (Ferraris et al., 2000).

In some naturally occurring true micas, Si^{4+} nearly fills all of the tetrahedral sites (e.g., polylithionite, tainiolite, norrishite, and celadonite), whereas in the most common mica species (muscovite and phlogopite) Al^{3+} substitutes for Si^{4+} in a ratio close to 1:3. In some true micas and brittle micas, the Al^{3+} for Si^{4+} substitution corresponds to a ratio of Al:Si = 1:1 (e.g., ephesite, preiswerkite, siderophyllite, margarite, and kinoshitalite) whereas the trioctahedral brittle mica, clintonite, has an unusually high Al^{3+} content with a ratio of Al:Si = 3:1 (Bailey, 1984a–c). Evidence of Fe^{3+} tetrahedral substitution was reported on the basis of optical observations (Farmer and Boettcher, 1981; Neal and Taylor, 1989), spectroscopisc studies (Dyar, 1990; Rancourt et al., 1992; Cruciani et al., 1995), and crystal-structure refinements (Guggenheim and Kato, 1984; Joswig et al., 1986; Cruciani and Zanazzi, 1994; Medici, 1996; Brigatti et al., 1996a; Brigatti et al., 1999). In tetra-ferriphlogopite, tetra-ferri-annite, and anandite Fe^{3+} is the only Si^{4+}-substituting cation, with a Fe:Si ratio of about 1:3 (Giuseppetti and Tadini, 1972; Semenova et al., 1977; Hazen et al., 1981; Filut et al., 1985; Brigatti et al., 1996a, b; Mellini et al., 1996; Brigatti et al., 1999). Two mica end-members contain boron (boromuscovite) (Liang et al., 1995) and berillium (bityite) (Lin and Guggenheim, 1983), and some synthetic micas contain Ge in the tetrahedral sheet (Toraya et al., 1978a, b; Toraya and Marumo, 1981). Most mica structures show a disordered distribution of tetrahedral cations, with the exception of some brittle mica species, such as margarite (Guggenheim and Bailey, 1975, 1978; Kassner et al., 1993), anandite (Giuseppetti and Tadini, 1972; Filut et al., 1985), bityite (Lin and Guggenheim, 1983), and a few true micas, e.g., polylithionite-3T (Brown, 1978) and muscovite-3T (Güven and Burnham, 1967).

As already mentioned, the dimensions of an ideal octahedral sheet in the (001) plane are commonly less than those of an ideal and unconstrained tetrahedral sheet. In order to obtain congruence, the difference in size between the octahedral and tetrahedral sheets is adjusted by mechanisms involving both sheets (Mathieson and Walker, 1954; Newnham and Brindley, 1956; Zvyagin, 1957; Bradley, 1959; Radoslovich, 1961; Radoslovich and Norrish, 1962; Brown and Bailey, 1963; Donnay et al., 1964; Lee and Guggenheim, 1981; Bailey, 1984b).

Three translationally independent octahedral cation sites characterize the 2:1 layer. One site, called M(1), is *trans*-coordinated by OH (or F and/or Cl, but rarely by S).

Both the remaining two sites are *cis*-coordinated and are referred to as M(2) if a relevant symmetry plane exists in the layer. Otherwise, the two *cis*-sites are labelled M(2) and M(3), respectively. In dioctahedral micas, M(1) is usually vacant, whereas in trioctahedral micas all three octahedral sites are occupied. The cation distribution in octahedral sites may be summarized as (i) all octahedra are occupied by the same kind of 'crystallographic entity', i.e., the same kind of ion or a statistical average of different kinds of ions, including voids (homo-octahedral micas; Ďurovič (1981, 1994)); (ii) two octahedra are occupied by the same kind of 'crystallographic entity' and the third by a different entity in an ordered way (meso-octahedral micas); or (iii) each of the three sites is occupied by a different 'crystallographic entity' in an ordered way (hetero-octahedral micas). Several phlogopite and tetra-ferriphlogopite crystals (space group $C2/m$) show the same kind of cations (or a disordered cation distribution) in M(1) and M(2) octahedra. Some Li-rich micas (space group $C2$) have different cation ordering in M(1), M(2), and M(3) sites, e.g., zinnwaldite-1M (Guggenheim and Bailey, 1977), lepidolite-1M (Backhaus, 1983), zinnwaldite-2$M1$ (Rieder et al., 1998), ferroan polylithionite-1M, and lithian siderophyllite-1M (Brigatti et al., 2000).

A. Illite

A recent review on illite has been provided by Brigatti and Guggenheim (2002). Illite is a dioctahedral 2:1 phyllosilicate of common occurrence in soils and sedimentary rocks. The term 'illite' is used for 2:1 minerals with a non-expandable layer and a wide variety of chemical compositions. For this reason, Rieder et al. (1998) have suggested that 'illite' be used as a series name. The composition of illite differs from that of dioctahedral mica muscovite, $[^{[XII]}K^{[VI]}Al_2^{[IV]}(Si_3Al)O_{10}(OH)_2]$ in having heterovalent substitutions of the type $^{[IV]}Si^{4+}_{-1}{}^{[VI]}Al_{3+}{}^{[IV]}Al^{3+}_{-1}{}^{[VI]}(Fe_{2+}, Mg_{2+})$ and $^{[IV]}Si^{4+}_{-1}{}^{[VI]}Al_{3+}{}^{[XII]}(\square, H_2O)^{[XII]}K_{-1}$, homovalent substitution of the type $^{[VI]}Fe_{3+}{}^{[IV]}Al^{3+}_{-1}$, and a layer charge between -0.6 and -0.9 (Bailey, 1986).

Different chemical compositions have been found for samples from diverse genetic environments, such as hydrothermally alterated igneous rocks (Środoń et al., 1992), shales, and mudstones (Lindgreen et al., 1991). Zöller and Brockamp (1997) have also reported different chemical compositions for co-existing $1M$ and $2M_1$ illites.

A high-quality three-dimensional structure refinement for illite is still missing, even if some models show a good fit with (thermal gravimetric analysis) TGA and XRD data. Drits et al. (1984, 1993) have suggested a statistical distribution of cations over all three octahedral sites. Bailey (1984a) and Drits et al. (1984) have established a relationship between the intralayer shift (i.e. the displacement along parameter a between two adjacent 2:1 layers) and octahedral site size (Bailey, 1984a). This intralayer shift is larger than the theoretical value ($1/3$ a) for *trans*-vacant illite and smaller for *cis*-vacant illite, allowing the *trans*- or *cis*-vacant structure to be identified by XRD.

A great deal of research has been carried out on the variation of the (001) XRD reflection in different illitic materials. The half-height-width value of this reflection,

known as the 'Kübler index', is measured using the $<2\,\mu m$ fraction of air-dried illite and Cu Kα radiation (Kübler, 1964, 1967; Kübler and Goy-Eggenberger, 2001). The 'Kübler index', expressed as small changes in the Bragg angle ($\Delta 2\theta$), has been used to identify the diagenesis-archizone and archizone-epizone metamorphic boundaries (Antonelli et al., 2003). Standardization of sample preparation and instrumental-measuring conditions have been discussed. Besides being influenced by experimental conditions and sample preparation, the Kübler index is affected by (i) the mean size of domains that scatter X-rays coherently; (ii) lattice strain; and (iii) the amount of swelling part in the interstratified component. Nevertheless, this index can serve as a useful indicator of diagenesis and low-temperature metamorphism in different geotectonic environments (Guggenheim et al., 2002 and references therein). Other indices using illite features to indicate the grade of diagenesis and incipient metamorphism of clastic rocks are the 'Weaver index' (Weaver, 1960), the 'Weber index' (Weber, 1972), the 'Flehmig index' (Flehmig, 1973), and the 'Watanabe index' (Watanabe, 1988).

Zöller and Brockamp (1997) have observed that $1M$- and $2M_1$-illite polytypes are distinct in composition, and hence should be considered as different mineral phases. Peacor et al. (2002) have reported that dioctahedral clay minerals, including illite-montmorillonite and illite, proceed from a partially disordered $1M_d$ stacking to a $2M_1$ type during normal prograde diagenetic and low-grade metamorphic sequence, and that $1M$ does not normally occur as an intermediate polytype.

Extended X-ray absorption fine structure spectroscopy (EXAFS) studies have suggested that the Fe^{2+} cations in the octahedral sheet of Fe-rich illites preferentially occupy the *cis*-sites, giving rise to domains of different size (Drits et al., 1997a, b). Sainz-Diaz et al. (2002) have confirmed the clustering of Fe^{2+} atoms in the octahedral sheet by theoretical calculations. Furthermore, illites with *cis*-vacant (cv) 2:1 layers have higher dehydroxylation temperatures than those with *trans*-vacant (tv) 2:1 layers (Drits et al., 1996).

The phase changes that take place when Fe-rich illites are heated have been discussed by Murad and Wagner (1996). Fe^{2+} is completely oxidized at 250 °C, and the layer gradually dehydroxylates between about 350 and 900 °C. At 900 °C the illite structure breaks down, and hematite clusters appear.

The stability of illite in natural environments is the subject of much controversy. Evidence for the metastability of 'illite' with respect to ideal muscovite plus pyrophyllite has been discussed by Rosenberg (2002).

2.6.3. *Smectites*

Smectites are 2:1 phyllosilicates with a total (negative) layer charge between 0.2 and 0.6 per half unit cell. Except for the layer charge and hydration of the interlayer cations, their structure is similar to that of other 2:1 phyllosilicates already described. The octahedral sheet may either be dominantly occupied by trivalent cations (dioctahedral smectites) or divalent cations (trioctahedral smectites). The general formula for

dioctahedral smectites is $(M^{+}_{x+y} \times nH_2O)(R^{3+}_{2-y}R^{2+}_{y})(Si^{4+}_{4-x}Al^{3+}_{x})O_{10}(OH)_2$and that for trioctahedral species (e.g., saponite) is $(M^{+}_{x} \times nH_2O)(R^{2+}_{3-y}R^{3+}_{y})(Si_{4-x-y}Al_{x+y})O_{10}(OH)_2$ where x and y indicate the layer charge resulting from substitutions in tetrahedral and octahedral sites, respectively; R^{2+} and R^{3+} refer to a generic divalent and trivalent octahedral cation, respectively; M^{+} refers to a generic monovalent interlayer cation (equivalent numbers of cations of different valency may be indicated by $M^{n+}_{x+y/n}$).

A wide range of cations can occupy tetrahedral, octahedral, and interlayer positions. Commonly Si^{4+}, Al^{3+}, and Fe^{3+} are found in tetrahedral sites. Substitution of R^{3+} for Si^{4+} in tetrahedral sites creates an excess of negative charge on the three basal oxygens and the apical oxygen. This affects the total charge of the 2:1 layer as well as the local negative charge at the layer surface. Al^{3+}, Fe^{3+}, Fe^{2+}, Mg^{2+}, Ni^{2+}, Zn^{2+}, and Li^{+} generally occupy octahedral sites. In dioctahedral smectites, substitution of divalent cations for trivalent cations creates an excess of negative layer charge, whereas substitution of trivalent for divalent cations in trioctahedral smectites generates an excess of positive charge. These events have implications for many physical properties of smectites such as swelling and rheological behaviour.

Most of the technological uses of smectite are related to reactions that take place in the interlayer space. Na^{+}, K^{+}, Ca^{2+}, and Mg^{2+}, which balance the negative 2:1 layer charge, are commonly hydrated and exchangeable. Smectites contain water in several forms. The water held in pores may be removed by drying under ambient conditions. Water may also be associated with layer surfaces and in interlayer spaces (Güven, 1992). Usually, three modes of hydration (recognized as pH-dependent) are distinguished: (i) interlayer hydration (of internal surfaces) of primary clay mineral particles; (ii) continuous hydration relating to an unlimited adsorption of water on internal and external surfaces; and (iii) capillary condensation of free water in micropores. The main elements of interlayer hydration are (i) hydration of interlayer cations, (ii) interaction of clay surfaces with water molecules and interlayer cations, and (iii) water activity in the clay–water system.

A voluminous literature exists on the hydration of interlayer cations (Hendricks et al., 1940; Mooney et al., 1952; Norrish, 1954; van Olphen, 1965, 1969; Suquet et al., 1975, 1977; MacEwan and Wilson, 1980; Suquet and Pezerat, 1987). The interlayer hydration complexes of smectites, arising from intercalation of a discrete number of water layers, can be distinguished by X-ray or neutron diffraction. This number ranges from zero to three, corresponding to the formation of zero-, one-, two- or three-layer hydrates. The main factors affecting the interlayer hydration of smectites are: (i) hydration energy of the interlayer cation; (ii) polarization of water molecules by interlayer cations; (iii) variation of electrostatic surface potentials because of differences in layer charge location; (iv) activity of water; (v) size and morphology of smectite particles. Two types of hydration complexes can form in the interlayer space: 'inner-sphere' and 'outer sphere' complexes. In the former case the cation is directly bound to the clay surface on one side and to a number of water molecules on the other side, whereas in outer sphere hydration complexes, the interlayer cation is completely surrounded by water molecules and interacts with the clay mineral

surface through its water ligands. The interactions between clay minerals and water molecules are further described in Chapter 3, while the reviews by McEwan and Wilson (1980), Sposito and Prost (1982), Parker (1986), Newman (1987), McBride (1989), Güven (1992) and Brown et al. (1995) should be consulted for more details.

Swelling of smectites occurs in a stepwise fashion, through the sequential formation of integer-layer hydrates (Norrish, 1954), and hence may be viewed as a series of phase transitions between such hydrates (Laird, 1994). At total water contents intermediate between phases, a two-phase coexistence is observed in the form of interstratified or mixed layer hydrates (Cases et al., 1997). Many theoretical approaches, such as Monte Carlo simulation, have been applied to investigating the interlayer cation-water interaction. In Na^+-exchanged smectites each Na^+ ion is surrounded by five water molecules, while its position depends on the layer charge location. In montmorillonite, Na^+ is located above the hexagonal cavity just over the octahedron where Mg^{2+} substitutes for Al^{3+}, whereas in beidellite, Na^+ is located near the Al^{3+}-substituted tetrahedron (Chatterjee et al., 1999). Water shows a strong preference to forming an intermolecular hydrogen-bonded network, while the hydrogen bonds to the aluminosilicate surface are weak and short-lived (Boek and Sprik, 2003).

The location of isomorphous substitution in the layer (i.e., whether the layer charge derives from substitution in the tetrahedral or octahedral sheet) is an important factor affecting smectite hydration. In electrically neutral layers the basal oxygen atoms act as a weak Lewis base (electron donor), forming weak hydrogen bonds with water molecules. When isomorphous substitution occurs, the basal oxygen atoms have an excess of negative charge, and their electron-donating capacity increases. Sposito (1984) has shown that H-bonding between water molecules and basal oxygens is stronger for tetrahedral than for octahedral sheet substitution. The surface charge density (δ) of a smectite with layer charge x_j (in electrons) can be computed by the equation: $\sigma = x_j/a \times b$ where a and b denote the unit-cell parameters.

Another type of surface having variable charge develops along the edges of clay mineral particles where Si–O–Si and Al–O–Al bonds are 'broken' and may convert into Si–OH and Al–OH groups (Güven, 1992). The surface potential ($\psi 0$) at these edges is related to the pH of the ambient solution, and the proton concentration at the point of zero charge (PZC) of the edge surface.

The propensity of smectites for sorbing cationic species from solution is given as the cation exchange capacity (CEC) (see Chapter 12.9). CEC values are expressed in centimole of positive charge per kilogram of dry clay mineral (cmol(+)/kg) which is numerically equal to the traditional unit of milliequivalents per 100 g clay (meq/100 g). The exchange between cations balancing the negative layer charge and cations in solution shows the following general features: (i) it is reversible; (ii) it is diffusion-controlled (the rate-limiting step being the diffusion of one charge-balancing ion against another); (iii) it is stoichiometric; and (iv) in most cases there is selectivity of one cation over another (Gast, 1977).

Polymeric hydr(oxides) of aluminium, iron, chromium, zinc, and titanium can intercalate into smectites by cation exchange. After heating, these 'pillared clays' show a

large surface area and porosity, high acidity, and catalytic properties (see Chapters 7.5 and 10.2). Likewise, cationic organic molecules (e.g., aliphatic and aromatic amines, pyridines, methylene blue) may replace the inorganic exchangeable cations in the interlayer space, while non-ionic polar organic molecules may replace adsorbed water on external surfaces and in the interlayer space. As a result, the surface of smectite particles becomes hydrophobic, losing its tendency to bind water (see Chapter 7.3).

Species of smectites may be differentiated according to the following criteria: (i) dioctahedral or trioctahedral nature of the octahedral sheet; (ii) predominant octahedral cation; and (iii) density and location of the layer charge.

The most important end-members of dioctahedral smectites have the following general compositions:

Montmorillonite	$(M_y^+ \times nH_2O)(Al_{2-y}^3 Mg_y^{2+})Si_4^{4+}O_{10}(OH)_2$
Beidellite	$(M_x^+ \times nH_2O)Al_2^{3+}(Si_{4-x}^{4+}Al_x^{3+})O_{10}(OH)_2$
Nontronite	$(M_x^+ \times nH_2O)Fe_2^{3+}(Si_{4-x}^{4+}Al_x^{3+})O_{10}(OH)_2$
Volkonskoite	$(M_x^+ \times nH_2O)Cr_2^{3+}(Si_{4-x}^{4+}Al_x^{3+})O_{10}(OH)_2$

The most important species of trioctahedral smectites are:

Hectorite	$(M_y^+ \times nH_2O)(Mg_{3-y}^2 Li_y^+)Si_4^{4+}O_{10}(OH)_2$
Saponite	$(M_x^+ \times nH_2O)Mg_3^{2+}(Si_{4-x}^{4+}Al_x^{3+})O_{10}(OH)_2$
Sauconite	$(M_x^+ \times nH_2O)Zn_3^{2+}(Si_{4-x}^{4+}Al_x^{3+})O_{10}(OH)_2$

Intermediate compositions can occur as swinefordite, a dioctahedral-trioctahedral lithium-rich species (Tien et al., 1975). Moreover, significant differences in chemical composition with respect to end-members occur for both dioctahedral and trioctahedral smectites.

2.6.4. Vermiculite

Vermiculite is generally trioctahedral. As in smectite the 2:1 layers are separated by hydrated cations occupying the interlayer space. However, the (negative) layer charge of vermiculite (>0.6 per formula unit), arising mostly from substitution of Al^{3+} for Si^{4+} in tetrahedral sites, is larger than that of smectite. Furthermore, vermiculite particles ('crystals') are often large enough for detailed structural studies to be performed. Stacking disorder produces 'streaking' in the diffraction pattern parallel to $\boldsymbol{c}^*$ for $0kl$ reflections where $k \neq 3n$. This feature, involving semi-random layer displacement of $\pm b/3$, is always found in Mg^{2+}-vermiculite (Shirozu and Bailey, 1966; Slade et al., 1985). For the 2-layer hydrates of Na^+- and Ca^{2+}-vermiculites that develop at a relative humidity (P/P_0) >0.5, sharp diffraction patterns can be obtained, indicative of a high degree of stacking order. In this instance, the ditrigonal cavities of adjacent silicate layers face each other across the interlayer (Slade et al., 1987; de la Calle and Suquet, 1988). This arrangement

(of adjacent silicate layers) contrasts with that found in natural semi- ordered Mg^{2+}-vermiculite (Mathieson and Walker, 1954; Shirozu and Bailey, 1966; Alcover and Gatineau, 1980), where tetrahedral bases of a given silicate layer can lie opposite ditrigonal cavities of an adjacent silicate layer. This leads to a structure in which the interlayer Mg^{2+} ions are positioned between the bases of aluminium tetrahedra. In the two-layer hydrates of Na^{+}- and Ca^{2+}-vermiculites, Na^{+} and Ca^{2+} cations have a high probability of occurring between the bases of silicon tetrahedra, but Ca^{2+} ions also occur between ditrigonal cavities (Slade et al., 1985). The nature of the interlayer cation and the relative position of adjacent silicate layers influence the organization of the interlayer water molecules. In general, these molecules show an ordered arrangement, although they are somewhat mobile. The oldest structural study on vermiculite was carried out by Gruner (1934). The results of many investigations that followed have been reviewed (e.g., de la Calle and Suquet, 1988). Here, we focus on more recent contributions that are of general interest.

The structure of vermiculite from Santa Olalla, Spain, intercalated with different organic cations, such as tetramethylammonium (TMA^{+}), monomethylammonium (MMA^{+}), dimethylammonium (DMA^{+}) and tetramethylphosphonium (TMP^{+}), has been investigated by Vahedi-Faridi and Guggenheim (1997, 1999a, b). In MMA^{+}-exchanged vermiculite, the interlayer MMA^{+} ion occupies two distinct sites (i) where the N–C axis is perpendicular to the basal oxygen plane, and the N atom being offset from the centre of the interlayer by 0.104 nm and (ii) where the N atom is at the centre of the interlayer between adjacent 2:1 layers, and the N–C axis presumably lying parallel to the basal oxygen plane. Similarly, the C–N–C plane of the DMA^{+} ion in DMA^{+}-vermiculite shows two different orientations with respect to the (001) plane. TMA^{+}-vermiculite shows a near-perfect three-dimensional stacking order with the TMA^{+} ion offset from the centre plane between two silicate layers (Vahedi-Faridi and Guggenheim, 1997).

Earlier, Slade et al. (1987) investigated the structure of a vermiculite-anilinium interlayer complex. Intercalation increases the stacking order of adjacent silicate layers, giving rise to sharp single-crystal reflections in the XRD pattern. Apparently, the packing of the intercalated organic cations produces a superstructure and bonding from layer to layer, promoting ordered layer stacking. The principal axes of the anilinium ions, i.e., N–C(1)–C(4), are nearly perpendicular to the silicate layers, while the planes of the aromatic rings are about $\pm 30^{\circ}$ to the a-axis of the unit cell.

2.6.5. Chlorite

The structure of chlorite is made up of a regularly stacked, negatively charged 2:1 layers and a single, positively charged interlayer octahedral sheet that are linked to each other by H bonds. The simplest structural unit of chlorite, therefore, consists of the repetition of a 2:1 layer along $\boldsymbol{c}^{*}$ and an octahedral interlayer sheet with a periodicity along c of about 1.4 nm.

Chlorites are usually trioctahedral with Mg^{2+}, Al^{3+}, and Fe^{2+}, Fe^{3+} in octahedral sites. More rarely octahedra are occupied by Cr^{3+}, Mn^{3+}, Ni^{2+}, V^{3+}, Cu^{2+}, Zn^{2+}, and Li^{+}. Tetrahedral cations are Si^{4+} and Al^{3+} (0.4–1.8 atoms per four tetrahedral positions). Si^{4+} can occasionally be substituted by Fe^{3+}, Zn^{2+}, Be^{2+}, or B^{3+}.

Bailey (1980) has divided chlorites in four sub-groups: (i) trioctahedral chlorites, the most common, where both the interlayer and the 2:1 octahedral sheets are trioctahedral; (ii) dioctahedral chlorites, where both the interlayer and the 2:1 octahedral sheets are dioctahedral (e.g., donbassite); (iii) di-trioctahedral chlorites, where the 2:1 octahedral sheet is dioctahedral and the interlayer sheet is trioctahedral (e.g., cookeite and sudoite); and (iv) tri-dioctahedral chlorites, where the interlayer sheet is dioctahedral and the 2:1 octahedral sheet is trioctahedral (the only mineral with a similar arrangement is franklinfurnaceite, which also contains Ca^{2+} ions, and should be considered as intermediate in structure between chlorites and brittle micas).

Bayliss (1975) introduced a nomenclature for trioctahedral chlorites based on five end-members:

Clinochlore	$(Mg_5^{2+}Al^{3+})\ (Si_3^{4+}\ Al^{3+})\ O_{10}(OH)_8$
Chamosite	$(Fe_5^{2+}Al^{3+})\ (Si_3^{4+}\ Al^{3+})\ O_{10}(OH)_8$
Pennantite	$(Mn_5^{2+}Al^{3+})\ (Si_3^{4+}\ Al^{3+})\ O_{10}(OH)_8$
Nimite	$(Ni_5^{2+}Al^{3+})\ (Si_3^{4+}\ Al^{3+})\ O_{10}(OH)_8$
Baileychlore	$(Zn_5^{2+}Al^{3+})\ (Si_3^{4+}\ Al^{3+})\ O_{10}(OH)_8$

Intermediate compositions and the presence of other cations are identified by adding a prefix or suffix to the end-member name. For example, the name 'kämmererite' in the old nomenclature for a magnesian chlorite with chromium substitution, should now be changed to 'chromian clinochlore'.

Wiewióra and Weiss (1990) have proposed a different chemical classification based on the values of the following variables: (i) R^{3+}, representing the sum of higher charge cations such as Al^{3+}, Fe^{3+}, and Cr^{3+}; (ii) R^{2+}, representing the content of divalent cations, such as Mg^{2+}, Fe^{2+} Mn^{2+}, and Ni^{2+}; (iii) $\square$, representing octahedral vacancies; and (iv) $Si_{(4-x)}$, where x represents the number of trivalent cations substituting for Si. The structural chemical formula of chlorites may thus be given as $(R_u^{2+}R_y^{3+}W_z)\ (Si_{4-x}^{4+}Al_x^{3+})\ O_{10}(OH)_8$ where $u+y+z=6$ and $z=(y-x)/2$. However, this classification has so far not been accepted by the IMA Commission.

The ideal composition of the 2:1 chlorite layer is $(R^{2+},\ R^{3+})_3(Si_{4-x}Al_x)O_{10}(OH)_2$, and that of the interlayer octahedral sheet is$(R^{2+}, R^{3+})_3(OH)_6$. The positive charge of the interlayer octahedral sheet commonly balances the negative charge of the 2:1 layer arising from substitution of Al^{3+} for Si^{4+}. Sometimes, the octahedral sheet in the 2:1 layer contributes to balancing the tetrahedral charge. The charge of the octahedral sheet in the 2:1 layer is positive if the overall tetrahedral charge is <-1, and usually negative when the tetrahedral charge is >-1. Thus, the stable chlorite

configuration is characterized by a total charge of −1 for the 2:1 layer and a total charge of +1 for the interlayer sheet.

The main chemical substitutions in chlorite have been summarized by Bailey (1988b) as

$^{[VI]}Fe^{2+}\ ^{[VI]}Mg^{2+}_{-1}$

$^{[IV]}Si^{4+}_{-1}\ ^{[VI]}R^{2+}_{-1}\ ^{[IV]}Al^{3+}\ ^{[VI]}Al^{3+}$ (Al–Tschermak)

$^{[IV]}Si^{4+}_{-1}\ ^{[VI]}R^{2+}_{-1}\ ^{[IV]}Al^{3+}\ ^{[VI]}Cr^{3+}$ and $^{[IV]}Si^{4+}_{-2}\ ^{[VI]}R^{2+}_{-1}\ ^{[IV]}Al^{3+}_{2}\ ^{[VI]}Ti^{4+}$

$^{[VI]}(Mg^{2+}, Fe^{2+})_{-3}\ ^{[VI]}Al^{3+}_{2}\ ^{[VI]}\square$

$^{[IV]}Si^{4+}\ ^{[VI]}Mg^{2+}\ ^{[IV]}Al^{3+}_{-1}\ ^{[VI]}Al^{3+}_{-1}$ (common in clinochlore)

$^{[VI]}Fe^{2+}_{-1}\ (OH)^{-1}_{-1}\ ^{[VI]}Fe^{3+}O_2$ and $^{[IV]}Si^{4+}\ ^{[VI]}Fe^{2+}\ ^{[IV]}Al^{3+}_{-1}\ ^{[VI]}Al^{3+}_{-1}$ (common in chamosite)

Brown and Bailey (1963) have studied possible polytypism in a 1.4 nm sequence. In the 2:1 layer, each superior tetrahedral sheet is displaced by $a/3$ with respect to the inferior, due to the presence of the octahedral sheet. This displacement can be either positive or negative. The interlayer octahedral sheet can be oriented in two different ways with respect to the 2:1 layer, referred to as type I and type II. In type I, the octahedra in both the interlayer and the 2:1 layer are oriented in the same way as shown in Fig. 2.11. On the other hand, type II is characterized by an opposite orientation of octahedra in the interlayer and 2:1 layer (Fig. 2.12).

The interlayer sheet, in either type I or type II orientation, needs to match the 2:1 layer to form H-bonds between basal oxygen atoms and OH groups of the octahedral interlayer. This requirement is satisfied by six different geometrical arrangements that can be divided into two sets (A and B), composed of three equivalent positions. In set A, one of the three interlayer cations, if projected on the basal plane, overlaps with the H placed at the centre of the hexagonal ring in the matching tetrahedral sheet of the 2:1 layer. In set B, the interlayer sheet is displaced by $a/3$ and thus, the projection of the octahedral cation on the basal plane matches the H

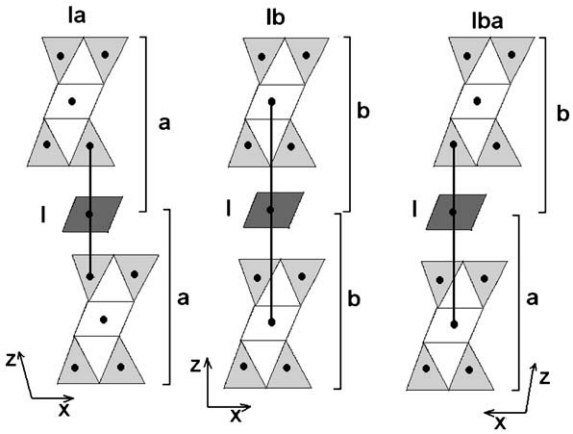

Fig. 2.11. Relationships between the 2:1 layer and the octahedral sheet in I chlorite polytype.

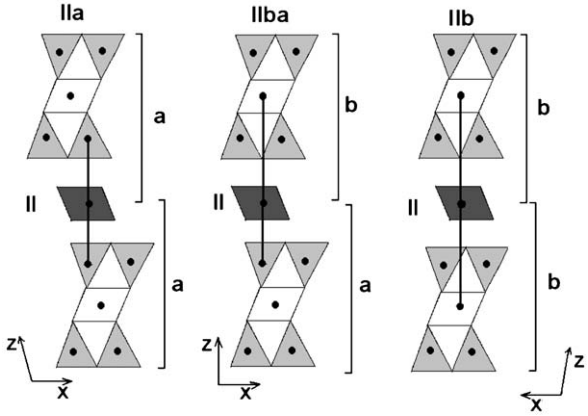

Fig. 2.12. Relationships between the 2:1 layer and octahedral sheet in II chlorite polytype.

position in the adjacent 2:1 layer on the tetrahedral sheet below (Figs. 2.11 and 2.12). These arrangements are referred to as Ia, Ib, IIa, and IIb. Moreover, the overlapping of another 2:1 layer creates six other different orientations. Combination with the four previously derived gives rise to 24 polytypes although only 12 of which are effectively different (Brown and Bailey, 1963). Different notations for chlorite polytypes have been introduced by Bailey (1988a), Zvyagin (1963), and Zvyagin and Mishchenko (1965). The polytypic notation for sequences at 2.8 nm has been proposed by Lister and Bailey (1967) and Drits and Karavan (1969).

Chlorites from clay environments usually present random or semi-random sequences. Random stacking can be identified from the analysis of reflections with $k = 3n$, which are well defined. Broad and very weak reflections, however, characterize spots with $k \neq 3n$.

Single-crystal studies on chlorites have recently been performed (Nelson and Guggenheim, 1993; Smyth et al., 1997; Welch and Marshall, 2001; Kleppe et al., 2003) both at room temperature and at high temperature and pressure. The greatest number of structural refinements pertains to clinochlore.

2.7. ILLITE–SMECTITE AND OTHER INTERSTRATIFICATIONS BETWEEN DIOCTAHEDRAL NON-EXPANDABLE AND EXPANDABLE 2:1 LAYERS

Interstratifications between non-expandable layers of illite and expandable layers of smectite have attracted the attention of many researchers because of their properties (Środoń, 1989), petrogenetic significance (Velde and Köster, 1992), and application in the oil industry (Drits et al., 1997b). In addition to time, temperature, pressure, and K^+ content, Al^{3+} for Si^{4+} substitution and interlayer dehydration are

the main crystal chemical parameters controlling the smectite-to-illite transformation (Środoń and Eberl, 1984; Lindgreen et al., 1991; Huang, 1992; Drits, 1997). The dynamics of this process have been investigated using a wide range of approaches, notably HRTEM and modelling (Bethke and Altaner, 1986).

In the model, developed by Altaner and Ylagan (1997) the crystal structure of illite-smectite (I–S) is interpreted in terms of a non-polar and a polar 2:1 layer. In the non-polar model, individual 2:1 layers are chemically homogeneous, whereas 2:1 layers in the polar model can have a smectite charge on one side and an illite charge on the other. Assuming a polar 2:1 layer model for I–S, the reaction mechanisms required for smectite illitization are (i) solid-state transformation (SST); (ii) dissolution and crystallization (DC); and (iii) Ostwald ripening (OR). SST features the replacement of smectite interlayers by illite interlayers, leading to gradual changes in interlayer ordering, polytype, chemical and isotopic composition, crystal size and shape. Several SST models are possible depending on the nature of the reaction site (framework cations, polyhedra, or interlayers). In contrast, DC models allow for abrupt changes in the structure, composition, and texture of I–S as illitization proceeds. Several DC models are possible depending on the nature of the rate-controlling step, i.e., diffusional transport or surface reactions during crystal growth. The OR model represents the coarsening of a single mineral where the smallest crystals dissolve and nucleate onto existing larger crystals, allowing for evolution in the overgrowth but not in the template crystal. An SST mechanism, involving either reacting polyhedra or reacting interlayers, seems to provide the best model of illitization in rock-dominated systems such as bentonite, while a DC mechanism seems best in describing illitization in fluid-dominated systems such as sandstone and hydrothermal environments. Both DC and SST mechanisms can occur in shale. Differences in reaction mechanism may be related to permeability. The OR model poorly describes illitization because of the progressive mineralogical and chemical changes involved.

In rectorite, there is regular interstratification of one layer of illite and one layer of smectite (… ISIS …), while regular interstratification of one smectite and three illite layers (… IIISIIIS …) gives rise to tarasovite.

Other interstratified minerals composed of non-expandable and expandable 2:1 layers are leucophyllite–smectite (Sokolova, 1982), glauconite–nontronite (Odom, 1984) and celadonite–nontronite (Lipkina et al., 1987).

2.8. ALLOPHANE AND IMOGOLITE

Allophane and imogolite are clay-size hydrous alumino-silicates of short-range order. Although, these minerals have been found in soils of different origins and environments, they are especially abundant in soils derived from volcanic ash and weathered pumice. Not all allophanes, however, are associated with soil environments. A prime example is the type that occurs as a deposit on a stream bed near Silica Springs, New Zealand. The literature also mentions ‘proto-imogolite’, which is a

synthetic alumino-silicate sol formed from the interaction of hydroxyaluminium species and orthosilicic acid in dilute aqueous solutions of pH < 5 (Farmer et al., 1979). The natural analogue of proto-imogolite that occurs in soil is sometimes referred to as 'allophane-like constituents' (Wada, 1995). For more details about the nature, occurrence, and properties of allophane and imogolite, the reader is referred to the reviews by Fieldes and Claridge (1975), Wada (1989), Parfitt (1990), and Harsh (2000).

Since allophane gives broad, diffuse peaks in its XRD pattern (Fig. 2.13), this mineral has often been described as amorphous. HRTEM, however, has consistently shown (Henmi and Wada, 1976; Wada and Wada, 1977; Hall et al., 1985) that the unit particles of allophane consist of nanometre-size hollow spherules, forming micro-aggregates (clusters) of varied size and shape (Fig. 2.14). On this basis, the term

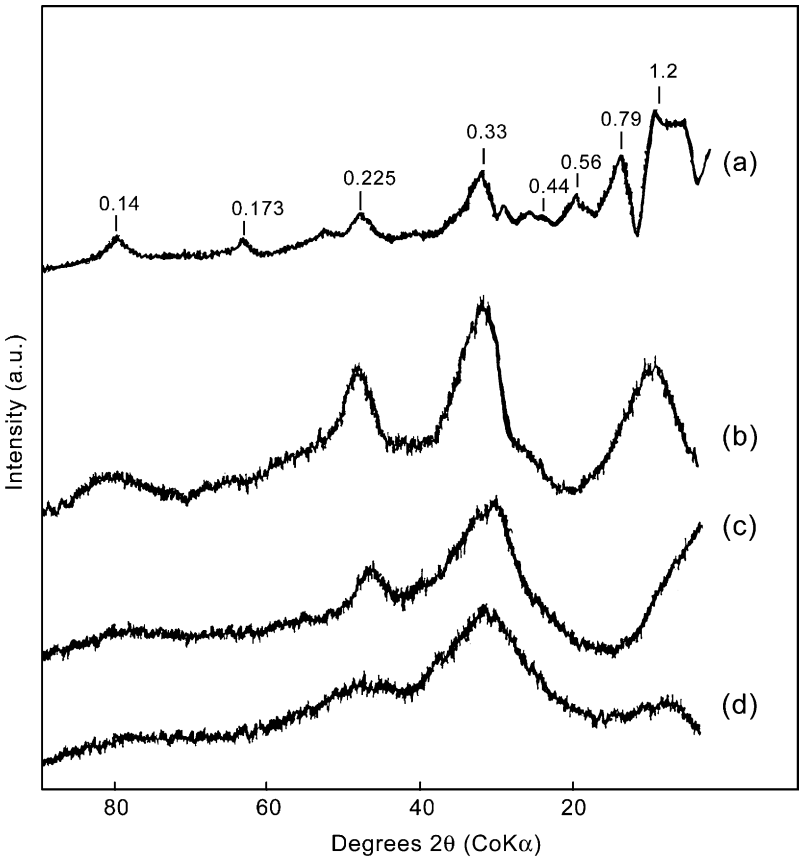

Fig. 2.13. XRD patterns of imogolite and some allophanes: (a) imogolite from soil; (b) imogolite-like allophane (Al/Si = 2.3) from soil; (c) halloysite-like allophane (Al/Si = 1.1) from soil; (d) Silica Springs allophane (Al/Si = 1.7). Adapted from Brown et al. (1978); Childs et al. (1990); Parfitt (1990).

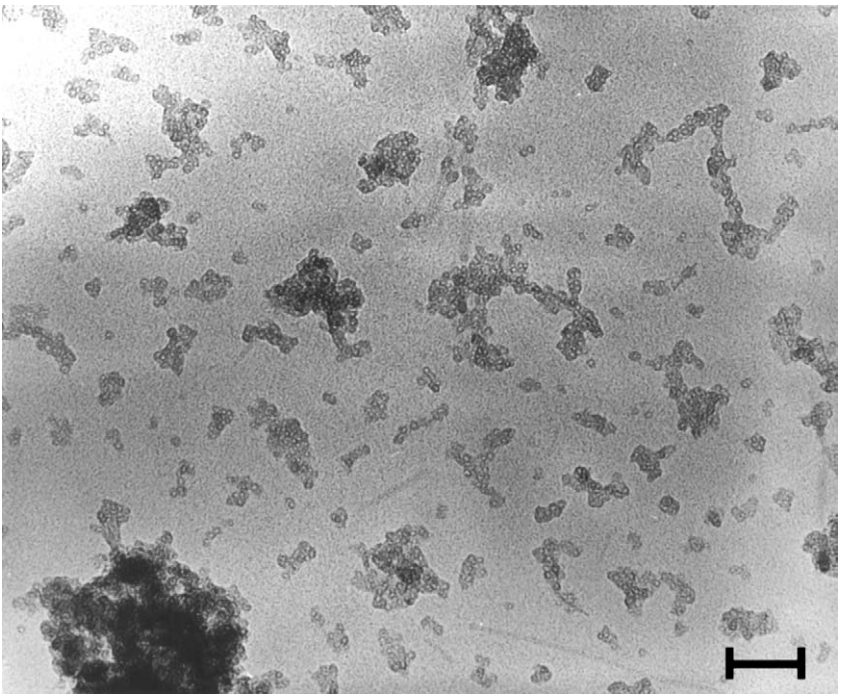

Fig. 2.14. High-resolution transmission electron micrograph of allophane separated from the Kitakami pumice (200 000 × magnification; bar = 50 nm). Courtesy: S.-I. Wada, Kyushu University, Japan.

'short-range order' seems more appropriate than, and preferable to, 'amorphous'. Thus, allophane may be defined as '…a group of clay-size minerals with short-range order which contain silica, alumina, and water in chemical combination' (Parfitt, 1990).

When examined by HRTEM (Fig. 2.15), imogolite appears as slender, hollow tubules forming 10–30 nm thick bundles of several micrometres in length (Henmi and Wada, 1976; Wada, 1989). Further, the XRD pattern of imogolite shows a series of bands (Fig. 2.13) that can be assigned to (*hk*) indices. Similarly, the ring reflections in its ED pattern may be indexed as (*kl*) (Wada, 1995). In having long-range order in one dimension (with a repeat distance of 0.84 nm along the tubule axis), imogolite has been described as para-crystalline. However, there is as yet no generally acceptable terminology to denote the crystalline state of allophane, imogolite, and related minerals. Besides 'short-range order' and 'para-crystalline', the terms 'poorly crystalline', 'non-crystalline', 'sub-crystalline', and 'disordered' have been used in the literature (Brown et al., 1978; Wada, 1995).

Fig. 2.16 shows a cross section of an individual tubule of imogolite as deduced by Cradwick et al. (1972) from chemical, infrared spectroscopic, XRD, and ED analyses.

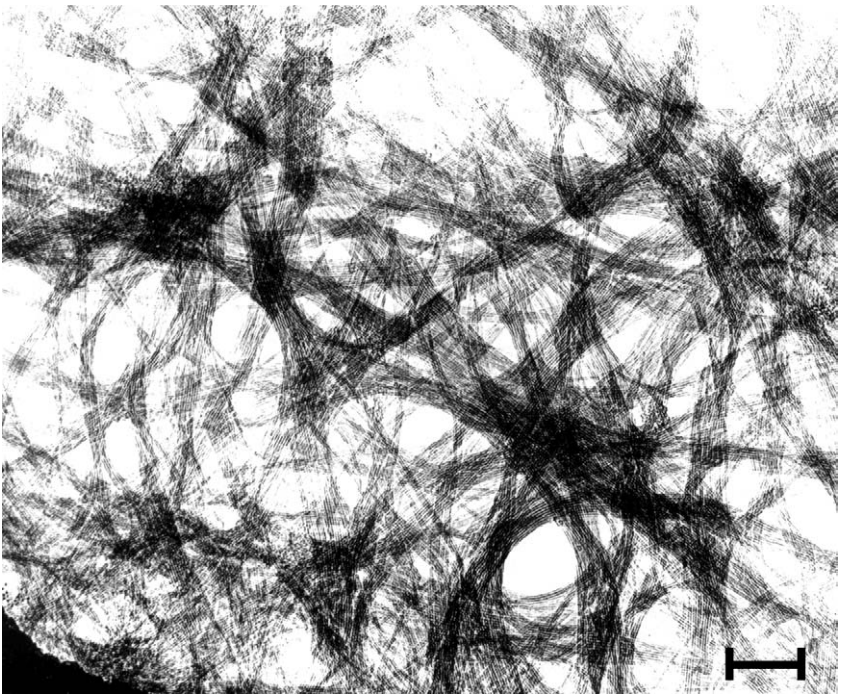

Fig. 2.15. High-resolution transmission electron micrograph of imogolite separated from a gel film of the Kitakami pumice bed (200 000 × magnification; bar = 50 nm). Courtesy: N. Yoshinaga, Ehime University, Japan.

Here, each hollow tubule is depicted as having an outer diameter of 2.14 nm, inner diameter of 0.64 nm, and ten unit cells. The atom positions of two unit cells are shown in detail in Brown et al. (1978). The ideal unit formula of imogolite may thus be written as $SiO_2 \cdot Al_2O_3 \cdot 2H_2O$. The commonly used notation for imogolite, however, is $(OH)_3Al_2O_3SiOH$ giving the sequence of ions from the periphery to the centre of the tubule, and indicating that the orthosilicate group shares three oxygens with aluminium. Fig. 2.16 also gives the structure of gibbsite, drawn to the same scale, to illustrate the similarity between imogolite and gibbsite in terms of atomic arrangement and unit-cell dimensions.

Unlike imogolite, allophane has a variable composition. Although, the Al/Si ratio of some specimens may be as high as four, the vast majority of allophanes have Al/Si ratios between 1 and 2 (Wada, 1989; Parfitt, 1990). Irrespective of chemical composition and origin, however, the unit particle of allophane is a hollow spherule with an outer diameter of 3.5–5.5 nm, and a wall thickness of 0.7–1.0 nm (Fig. 2.17). Because of its similarity in composition to that of imogolite, the Al-rich end-member of allophane (Al/Si$\sim$2) has been referred to as either 'proto-imogilite allophane' (Farmer et al., 1979) or 'imogolite-like allophane' (Parfitt and Wilson, 1985). IR

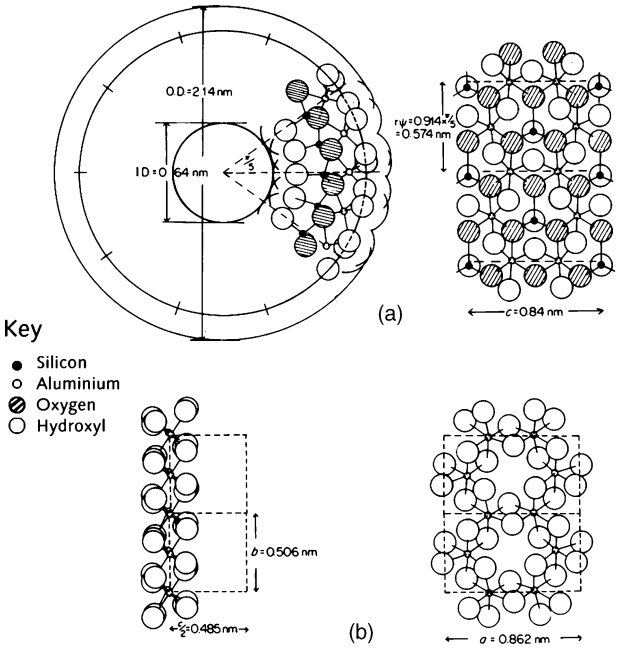

Fig. 2.16. Diagram comparing the structure and unit cell dimensions of imogolite with those of gibbsite. (a) the structure of imogolite viewed down the tubule axis showing the atomic arrangement for two of the 10 unit cells (left); the same projected on a cylinder surface through the centres of the outer hydroxyl groups (right); (b) the structure of a gibbsite sheet showing linked alumina octahedra (left), and projected on the *ab* plane (right). Note that the repeat distance along the tubule axis of imogolite ($c = 0.84$ nm) is close to the *a* dimension of gibbsite ($= 0.862$ nm); OD = outer diameter; ID = inner diameter. From Brown et al. (1978).

(Fig. 2.18) and NMR spectroscopic measurements (Table 2.1) further indicate that this type of allophane is composed of fragments having the imogolite structure over a short range (Parfitt and Henmi, 1980).

By analogy with imogolite (Fig. 2.16), the spherule wall of imogolite-like allophane is apparently composed of an outer gibbsitic sheet to which (O_3SiOH) groups are attached on the inside. Unlike the situation in imogolite, however, the layer structure contains vacancies, particularly in the octahedral sheet. Clusters of such 'defects' give rise to discontinuities or perforations of ~0.3 nm in diameter along the spherule wall, allowing small extraneous molecules, notably water, to enter in the spherule void space (Fig. 2.17). Depending on the ambient solution pH, the (OH)Al(OH_2) groups, exposed at wall perforations, can either acquire or lose protons. Besides being at the source of the pH-dependent charge characteristics, these groups control the reactivity of allophane toward extraneous ionic species, such as phosphate, humic acid, and amino acids. The anion adsorption data further indicate that the wall of individual

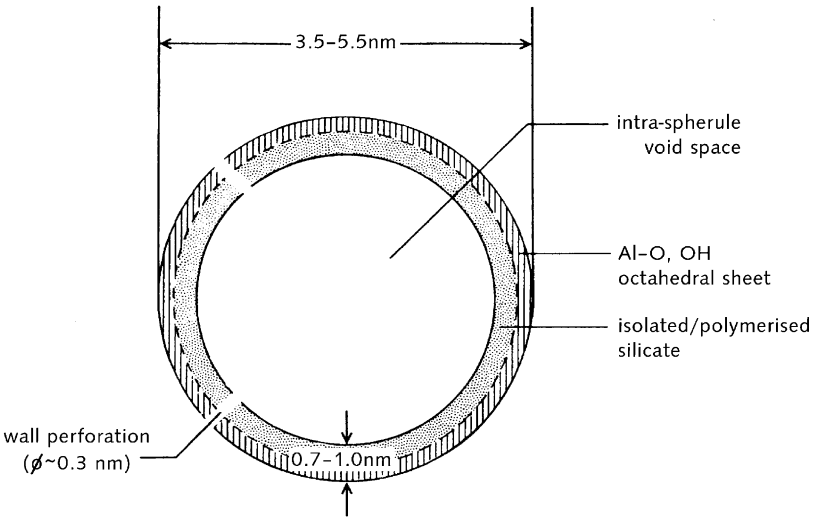

Fig. 2.17. Diagram of a soil allophane unit particle or hollow spherule showing the probable structure of the spherule wall, the intra-spherule void space, and wall perforations. Modified from Wada and Wada (1977).

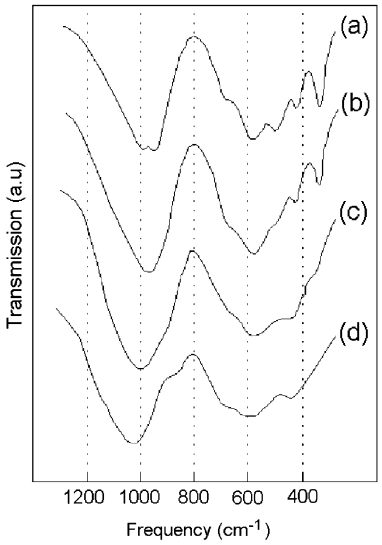

Fig. 2.18. Infrared spectra of imogolite and some allophanes: (a) imogolite from soil; (b) imogolite-like allophane (Al/Si = 2) from soil; (c) halloysite-like allophane (Al/Si = 1.1) from soil; (d) Silica Springs allophane (Al/Si = 1.5). Adapted from Parfitt (1990).

allophane spherules may contain as many as eight perforations (Theng et al., 1982; Hashizume and Theng, 1999; Yuan et al., 2000; Hashizume et al., 2002).

The Si-rich end-member of allophane with an Al/Si ratio of ~1 has been referred to as either 'defect-kaolin allophane' or 'halloysite-like allophane' (Yoshinaga, 1986). Although some orthosilicate may still be present, the ^{29}Si NMR spectroscopy (Goodman et al., 1985; Shimizu et al., 1988) indicates that in this type of allophane the silicate group is polymerized with some Al^{3+} substituting for Si^{4+} in tetrahedral sites (Table 2.1). The IR spectrum shows an intense Si–O stretching band near 1020 cm^{-1} while the peak at 348 cm^{-1}, characteristic of proto-imogolite, imogolite, and imogolite-like allophane, is hardly detectable (Fig. 2.18).

The question arises whether the octahedral Al sheet still provides the structural framework in halloysite-like allophane as Parfitt (1990) proposed. A variant, suggested by MacKenzie et al. (1991), has the (isolated) orthosilicate groups penetrating the inner silica tetrahedral sheet through defect structures ('holes') in this sheet. Nevertheless, the possibility that the Si- or Si(Al)- tetrahedral sheet serves as the framework structure cannot be ruled out (van der Gaast et al., 1985). In any case, samples with Al/Si ratios between 1 and 2 are likely to be mixtures of halloysite- and imogolite-like allophanes. These mixtures may be of unit particles or of structures within particles (Parfitt, 1990).

On the other hand, there is little doubt that a curved halloysite-like layer structure constitutes the framework of 'stream-deposit allophane' from Silica Springs, New

Table 2.1. Types and structural features of allophane and imogolite (modified from Parfitt, 1990)

Features	Imogolite	Imogolite-like allophane (soil)[a]	Halloysite-like allophane (soil)[b]	Silica Springs allophane[c]
Al/Si ratio	2	~2	~1	1.1–1.9
Infrared bands (cm^{-1})	1000, 950, 700, 570, 500, 428, 348	975, 690, 570, 500, 428, 348	1020, 680, 580, 450	1020, 880, 670, 610, 450
^{29}Si NMR chemical shift (ppm)[d]	−78 (isolated orthosilicate)	−78 (isolated orthosilicate)	−90 (polymerized silicate) −78 (isolated orthosilicate)	–86 (sheet silicate)
^{27}Al NMR chemical shift (ppm)[e]	5 (Al^{VI})	5 (Al^{VI})	5 (Al^{VI}) 60 (Al^{IV})	3 (Al^{VI}) 51 (Al^{IV})

[a]Also known as 'Al-rich allophane' or 'proto-imogolite allophane'.
[b]Also known as 'Si-rich allophane' or 'defect-kaolin allophane'.
[c]Also known as 'stream-deposit allophane' or 'hydrous feldspathoid allophane'.
[d]Relative to tetramethylsilane.
[e]Relative to $Al(H_2O)_6^{3+}$.

Zealand (Wells et al., 1977). The XRD pattern of a Silica Springs allophane sample is shown in Fig. 2.13 and its IR spectrum in Fig. 2.18. The Al/Si ratio of Silica Springs allophanes varies between 1.1 and 1.9. As this ratio increases, the $^{[IV]}Al/^{[VI]}Al$ ratio decreases but the $^{[IV]}Al/^{[IV]}Si$ ratio remains invariant at 1/3. These observations led Childs et al. (1990) to suggest that a more or less complete tetrahedral sheet (containing one Al^{3+} for every three Si^{4+}) forms the outer, convex surface of the spherule wall while the inner $^{[VI]}Al^{3+}$ octahedral sheet is incomplete and fragmented (Fig. 2.19). These non-soil allophanes have also been referred to as hydrous felspathoids (Farmer et al., 1979; Farmer and Russell, 1990).

X-ray photoelectron spectroscopy (XPS) of Silica Springs allophane (Childs et al., 1997) indicates that the binding energies of Al, Si, and O electrons are similar to those for kaolinite, in agreement with the findings by He et al. (1995). The values are also closely similar to those measured for some framework silicates (feldspars) having 4-coordinate Al^{3+}. Atomic Al/Si, C/Si, and N/Si ratios by XPS further indicate that the surfaces of Silica Springs allophanes are enriched in Al, C, and N (Childs et al., 1997). The surface enrichment by Al may be explained in terms of the presence of Al-octahedral fragments (Fig. 2.18) at the surface of the allophane aggregates. Similarly, the surface enrichment by C and N may be ascribed to surface-adsorbed organic structures. Application of ^{27}Al NMR spectroscopy with high magnetic field strength, and fast MAS, has further revealed the presence of 5-coordinate Al^{3+} in Silica Springs allophanes (Childs et al., 1999). This Al species may be associated with the edges of octahedral sheet fragments. The presence of $^{[V]}Al^{3+}$ in Si-rich soil allophanes is yet to be established.

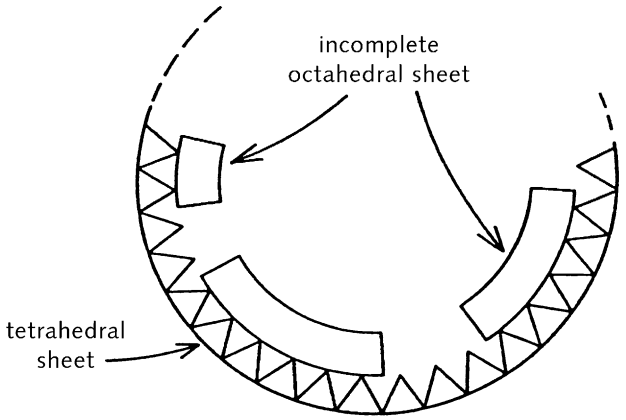

Fig. 2.19. Proposed structural model for the unit particle of Silica Springs allophane showing part of a hollow spherule with an outer diameter of 2–3 nm. Here the outer Si(Al)-tetrahedral sheet serves as the framework and the inner Al-octahedral sheet is incomplete (fragmented). From Childs et al. (1990).

2.9. PALYGORSKITE AND SEPIOLITE

Palygorskite and sepiolite are phyllosilicates inasmuch as they contain a continuous two-dimensional tetrahedral sheet; however, they differ from other layer silicates in that they lack continuous octahedral sheets. Their structure can be considered to contain ribbons of a 2:1 phyllosilicate structure, each ribbon being linked to the next inversion of SiO_4 tetrahedra along a set of Si–O bonds. Thus, tetrahedral apices point in opposite directions in adjacent ribbons. These ribbons extend parallel to the *X*-axis and have an average width along *Y* of three linked pyroxene-like single chains in sepiolite and two linked chains in palygorskite (Fig. 2.20); in this framework, rectangular channels run parallel to the *X*-axis between opposing 2:1 ribbons. As the octahedral sheet is discontinuous at each inversion of the tetrahedra, oxygen atoms in the octahedra at the edge of the ribbons are coordinated to cations on the ribbon side only, while coordination and charge balance are completed along the channels by protons, coordinated water and a small number of exchangeable cations. Furthermore, the channels contain a variable amount of zeolitic water (Galán, 1996).

Chain phyllosilicates have a fibrous habit (Fig. 2.21) with channels running parallel to the fibre length. Fibre sizes vary widely but generally range from about 10 to about 30 nm in width, and from about 5 to about10 nm in thickness (Jones and Galán, 1988; Galán, 1996).

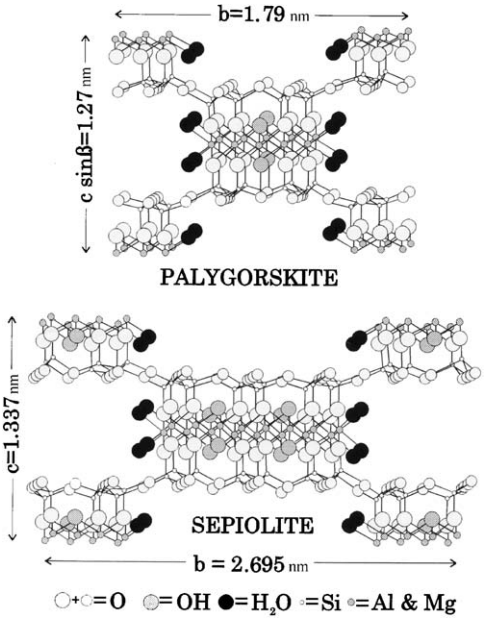

Fig. 2.20. Schematic structure of palygorskite (after Bradley (1940)) and sepiolite (after (Brauner and Preisinger, 1956; Jones and Galán, 1988)).

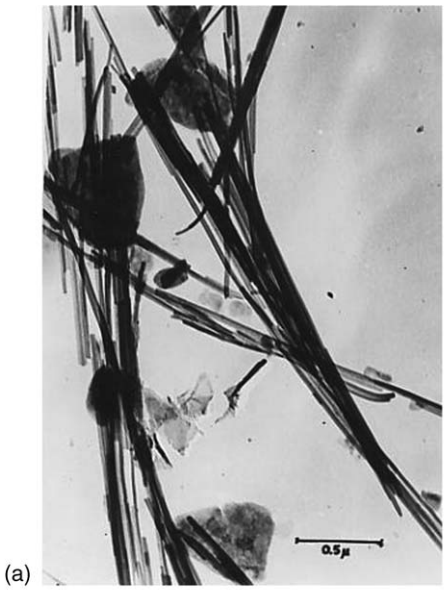

Fig. 2.21. (a) transmission electron micrograph of palygorskite (Torrejón, Spain); (b), scanning electron micrograph of sepiolite (Vallecas, Spain).

Early attempts at determining the sepiolite structure were carried out by Migeon (1936), Longchambon and Migeon (1936), Longchambon (1937), and Caillère (1951). The first structural pattern for sepiolite was proposed by Nagy and Bradley (1955) who suggested the $C2/m$ ($A2/m$) space group as being the most appropriate (Table 2.2). However, their interpretation from X-ray fibre photographs (using $0kl$ reflections) was not very conclusive.

Table 2.2. Some crystallographic data for sepiolite and palygorskite (Jones and Galán, 1988)

	a (nm)	*b* (nm)	*c* or *c* sin *β* (nm)	β (°)	Space group
Sepiolite					
Nagy and Bradley (1955)	0.530	2.70	1.34	?	*A*2/*m*
Brauner and Preisinger (1956)	0.528	2.680	1.340	90°	*Pnan*
Brindley (1959)	0.525	2.696	1.350	90°	——
Zvyagin et al. (1963)	0.524	2.72	1.34	90°	*Pnan*
Bailey (1980) (average)	0.528	2.695	1.337	90°	*Pnan*
Galán (unplublished, Vallecas sepiolite)	0.523	2.677	1.343	90°	*Pnan*
Palygorskite					
Bradley (1940)	0.52	1.80	1.29	?	*A*2/*m*
Zvyagin et al. (1963)	0.522	1.806	1.275	95.83°	*P*2/*a*
Christ et al. (1969) (Sapillo)	0.524	1.787	1.272	90°	*Pn*
Christ et al. (1969)	0.524	1.783	1.278	95.78°	*P*2/*a*
Drits and Sokolova (1971)	0.515	1.785	1.314	107°	*A*2/*m*
Bailey (1980) (average)	0.520	1.790	1.270	90°, 96°, 107°	

Later, Brauner and Preisinger (1956) and Preisinger (1959) proposed another model for sepiolite with space group *Pnan* (Fig. 2.20, Table 2.3). The fundamental difference between both models lies in whether the tetrahedral inversion at the edge of the ribbons occurs along the middle of the zig-zag Si–O–Si chains (Nagy and Bradley, 1955) or along their edges (Brauner and Preisinger, 1956). In the Brauner and Preisinger (1956) model, adjacent inverted ribbons are joined by a single basal oxygen (instead of two as in the Nagy–Bradley model), and there are eight octahedral sites in a ribbon (instead of nine), four OH (instead of six), and eight zeolitic water molecules (instead of six).

ED patterns from single fibres by Brindley (1959), Zvyagin (1967), and Gard and Follet (1968) have confirmed that the extinctions are in agreement with the space group *Pnan*. The Brauner–Preisinger model for sepiolite has also been confirmed and refined by Rautureau et al. (1972), Rautureau and Tchoubar (1974), Rautureau (1974), and Yucel et al. (1981).

The unit-cell parameters determined for sepiolite are: $a = 0.528$ nm, $b = 2.695$ nm, $c = 1.33$ nm, $\beta = 90°$ (Table 2.2). Channels in the structure are 0.37 nm × 1.06 nm in dimension.

Regarding the palygorskite structure, Bradley (1940) proposed a model with a probable *A*2/*m* space group (Table 2.2). The main difference from the sepiolite model is the shorter *b* dimension because only two linked pyroxene-like single chains are in the ribbon. Later, Drits and Sokolova (1971) confirmed the Bradley model and measured a *β*-angle of 107°. It would therefore appear that for both sepiolite and palygorskite, the linkage by two oxygens can be excluded.

Table 2.3. Octahedral and tetrahedral occupancy ranges for bulk and EDX analyses of sepiolite and palygorskite (in bracket mean value) (Galán and Carretero, 1999).

		Bulk analyses	EDX analyses by (Paquet et al., 1987)	Other EDX analyses from literature	EDX analyses by (Galán and Carretero, 1999)
Sepiolite	^{VI}R	6.95–8.11 (7.72)	6.93–8.5	7.61–7.87 (7.74)	7.93–7.98 (7.95)
	^{VI}Mg	4.96–8.1 (7.36)	5.6–8.5	6.05–7.73 (7.11)	7.93–7.98 (7.95)
	$^{VI}(R^2+R^3)$	0–2.28 (0.32)	0–1.8	0–1.8 (0.62)	0
	$^{IV}(Al+Fe^{3+})$	0–0.72 (0.19)	—	0–0.2 (0.10)	0
Palygorskite	^{VI}R	3.45–4.33 (3.96)	2.63–4.63	3.36–4.17 (3.88)	3.95–4.09 (4.00)
	^{VI}Mg	1.12–2.82 (2.00)	0.83–3.08	1.32–2.60 (1.97)	1.71–2.10 (1.96)
	$^{VI}(R^2+R^3)$	1.12–2.50 (1.96)	1.5–2.66	1.46–2.41 (1.91)	1.87–2.24 (2.04)
	$^{IV}(Al+Fe^{3+})$	0–0.67 (0.29)	—	0.07–0.49 (0.30)	0–0.29 (0.14)

^{VI}R = all octahedral cations.
$^{VI}(R^2+R^3)$ = octahedral cations other than Mg. They are mainly Al and Fe^{3+}.

Preisinger (1963) reported an orthorhombic model for palygorskite similar to the orthorhombic sepiolite of Brauner and Preisinger (1956) except for the ribbon width. Christ et al. (1969) studied five palygorskite samples by XRD and found three orthorhombic (Pn) and two different monoclinic cells. Although there are not sufficient data to define exactly the difference between them, it is clear that at least two symmetries are possible for palygorskite, one orthorhombic and another monoclinic. Monoclinic structures have an *n*-glide plane parallel to (1 0 0) (Table 2.2). One of the monoclinic symmetries is similar to the one proposed by Zvyagin et al. (1963) ($P2/a$, $\beta = 95.83^\circ$). The other, with the Z-axis as the monoclinic axis and $\gamma = 92.23^\circ$ for the monoclinic angle, has no structural interpretation up to the present time.

More recently, Chisholm (1992) analysed the structural models given by Christ et al. (1969) and other authors, and found two palygorskite structures, one orthorhombic (Pbmn≡Pnmb) and another monoclinic (C2/m≡A/2 m). Most palygorskite samples appear to contain both forms. There are samples of pure or nearly pure monoclinic palygorskite but there is no pure orthorhombic palygorskite. The coexistence of both structures lies behind the confusion that arises from indexing XRD patterns in terms of a single phase, and using different unit cells and space groups for palygorskite. The two structures determined by Chisholm (1992) agree with those

proposed by Drits and Sokolova (1971) for the monoclinic form (β about 105.2°, is not far from Drits and Sokolova's value of 107°), and that by Preisinger (1963) for the orthorhombic form.

Each form has some reflections (with $l \neq 0$) that are not shown by the other; these can be used for discrimination (Figs. 2.22 and 2.23). For example, the lines at 0.425 nm (121), 0.309 nm (123), and 0.2536 nm (161) indicate the presence of orthorhombic palygorskite, while those at 0.436 nm (120) and 0.251 nm (162, overlapping with 200) are indicative of monoclinic palygorskite. Two lines near 0.320 nm also indicate the presence of the monoclinic form, while a single line at 0.319 nm is expected for the orthorhombic forms. The *d*-values for monoclinic palygorskite depend on β, even in the narrow range of 106–108° (Figs. 2.22 and 2.23).

One palygorskite structure must be considered as orthorhombic: Pnmb (Preisinger, 1963) and another as monoclinic: $A2/m$ (Bradley, 1940; Drits and Sokolova, 1971). Monoclinic cells proposed by Zvyagin et al. (1963) and Christ et al. (1969) with smaller values of β may represent alternative choices of axes in the monoclinic system, as noted by Bailey (1980) who also gave the following unit-cell parameters: $a = 0.52$ nm, $b = 1.79$ nm, $c \sin \beta = 1.27$ nm, $\beta = 90$, 96 or 107°. Channels in the structure are 0.37×0.64 nm in dimension and run parallel to the fibre length. Powder XRD patterns of palygorskite and sepiolite are shown in Figs. 2.24 and 2.25.

Zoltai (1981) has described the palygorskite and sepiolite structures as biopyriboles (bio = biotite, pyr = pyroxenes, iboles = amphiboles) built of tri-di-octahedral modules, the tri-module being $M_3A_2Si_4O_{10}$, and di-module $M_2A_2Si_4O_{10}$. M is the octahedral cation and A is the anion not bonded to Si within to module; it can be oxygen when bonded to Si and is (OH) when bonded to more that one M cations. One half of each A anion is H_2O molecule when the anion bonded to only one M cation. The width of these modules is one tetrahedral chain, and their height (*t*) is four times the height of an ideal polyhedral layer. Combinations of these modules can give rise to complete crystal structures with a vertical displacement between the modules equal to $n \times t$ (with $n = 0$, 1/2, 3/4). If $n = 0$, the major layer silicates are produced. A sequence of $n = 0$ and 3/4 between modules produces palygorskite, and the sequence 0, 0, and 3/4 gives the sepiolite structure (Fig. 2.26). Symbol 0 is relative to the orientation of tetrahedral chains, indicating that the faces of adjacent tetrahedra point in opposite directions ('0' chains).

Although the crystallographic description by Zoltai (1981) is attractive, palygorskite and sepiolite should be considered as phyllosilicates (see above) with special features rather than as biopyriboles. This is because the physicochemical properties and genetic environments of palygorskite and sepiolite are akin to those of clay minerals. In common with many other phyllosilicates, a detailed single-crystal structure of sepiolite and palygorskite is still wanting. IR studies combined with powdered diffraction EM and TA have provided insight into the nature of the water in sepiolite and palygorskite, and the structural changes that occur after heating/dehydration (Hayashi et al., 1969; Serna et al., 1975, 1977; Mifsud et al., 1978; Van Scoyoc et al., 1979; Blanco et al., 1988).

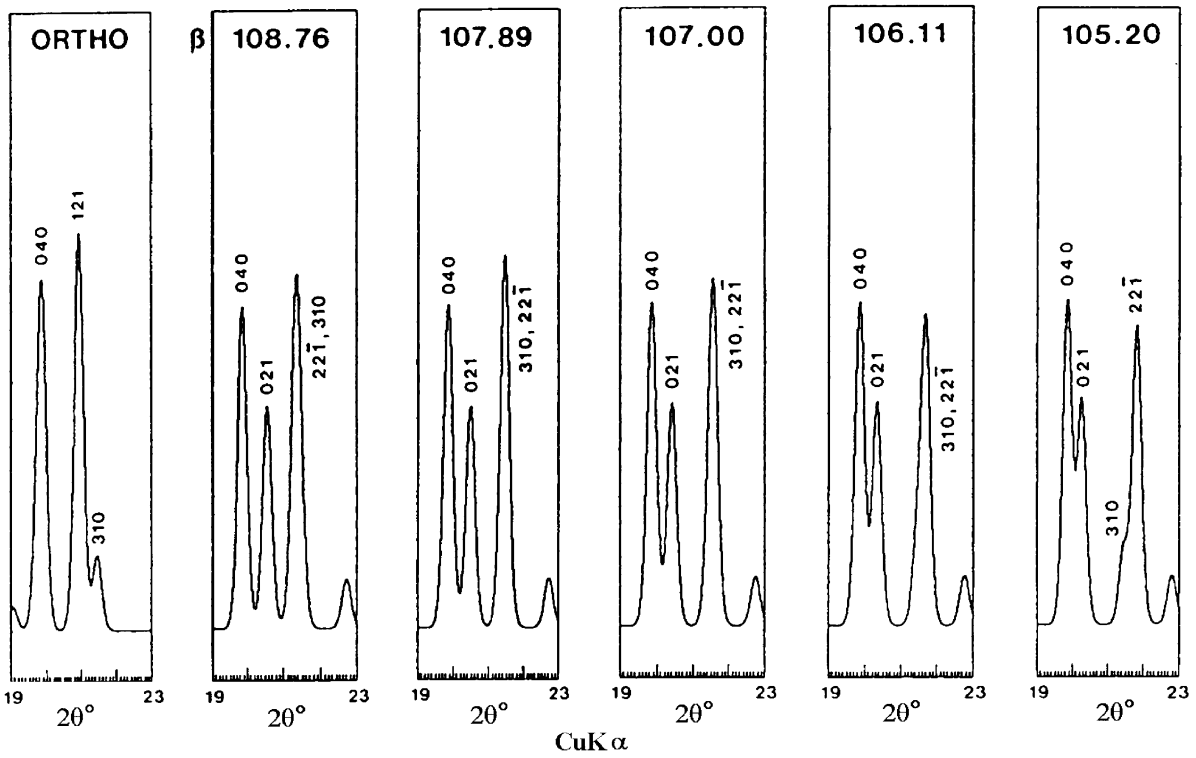

Fig. 2.22. XRD powder patterns in the 19–23° range of 2θ (Cu Kα radiation), showing the 0.40–0.45 nm diagnostic region calculated for idealized orthorhombic and monoclinic palygorskites. The 121 reflection is characteristic of the orthorhombic form, while the 021 and strong 22$\bar{1}$ reflections are characteristic of the monoclinic form. After Chisholm (1992).

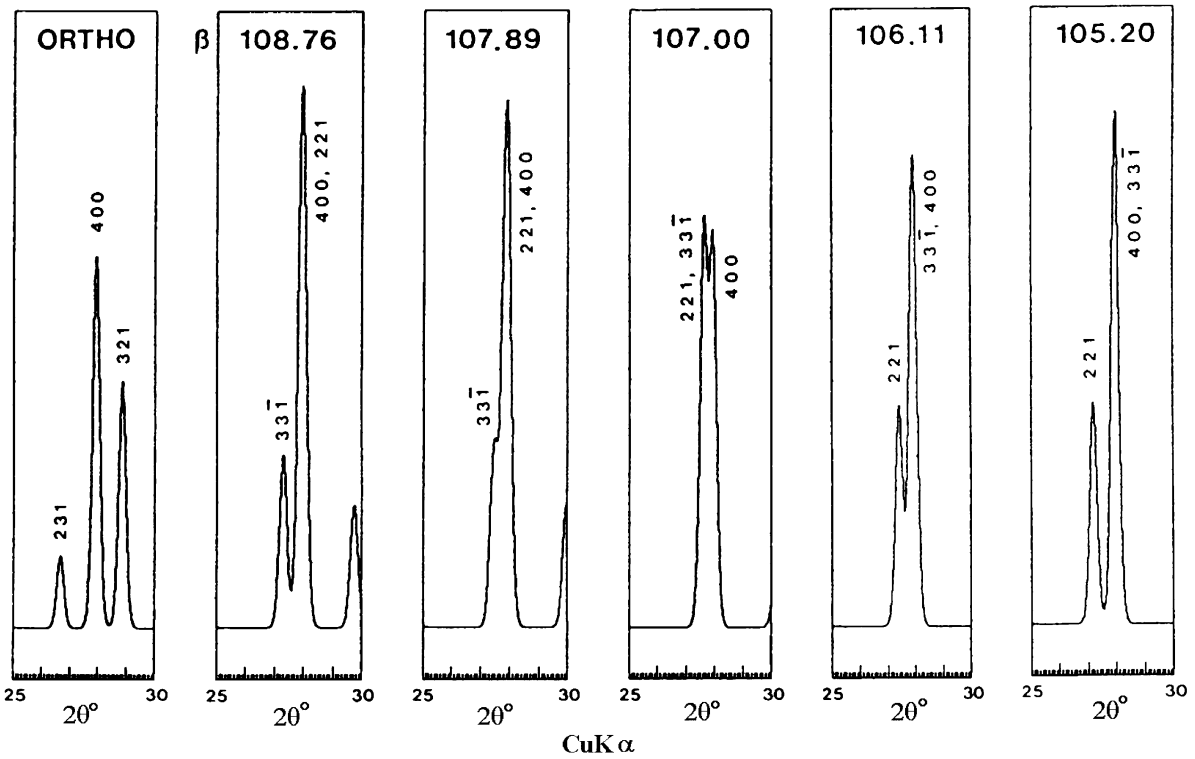

Fig. 2.23. XRD powder patterns in the 25–30° range of 2θ (Cu Kα radiation), showing the 0.305–0.33 nm diagnostic region calculated for idealized orthorhombic and monoclinic palygorskites. The 321 line is characteristic of the orthorhombic form. The appearance of two lines close together near 400 indicate the presence of the monoclinic form; the exact position of these lines is sensitive to the value of β in the range 106–108°. After Chisholm (1992).

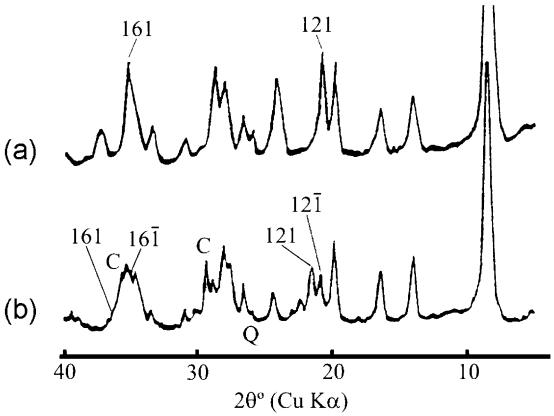

Fig. 2.24. XRD pattern of the orthorhombic form (a) and monoclinic form (b) of palygorskite (C = calcite, Q = quartz). After Christ et al. (1969). Indices for the monoclinic form are taken from Chisholm (1992).

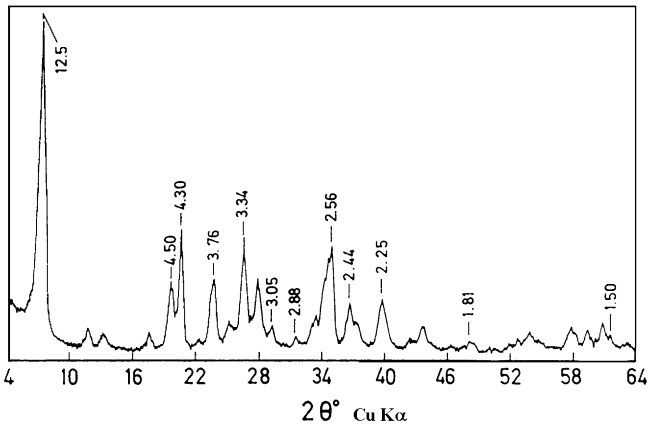

Fig. 2.25. XRD diagram of sepiolite from Vallecas. The numbers at the top of each peak refer to Ångstrom units (1 Å = 0.1 nm). After Pérez-Rodríguez and Galán (1994).

A more recent study by McKeown et al. (2002), using polarized Raman and FTIR spectroscopy, indicates that the Si–O stretching and O–Si–O bending force constants for palygorskite are similar to the corresponding values previously calculated for other phyllosilicates. However, the values for Mg–O stretching are about half of those obtained for the Al–O and Mg–O stretching force constants in other phyllosilicates (i.e., the octahedral sheets in micas). This finding suggests that the respective interatomic bonds within the octahedral ribbons of palygorskite and sepiolite are weaker than those in a continuous octahedral sheet.

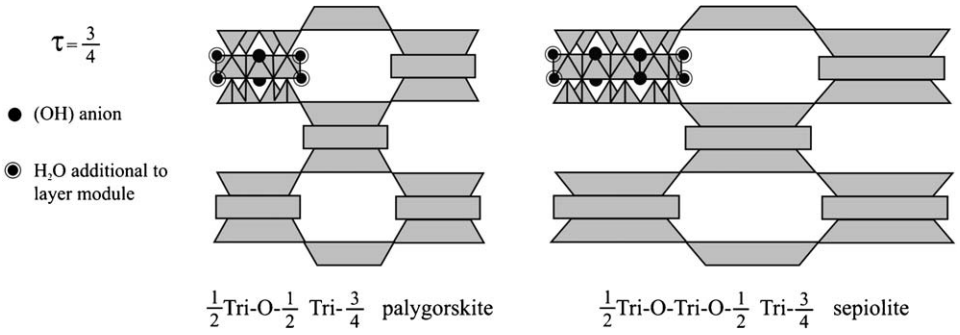

Fig. 2.26. Palygorskite and sepiolite structures. After Zoltai (1981). (τ = displacement between a pair of 1/2 Tri modules; 1/2 indicates that only half of the extra trioctahedral sites are occupied, that is, those sites between the two linked modules.)

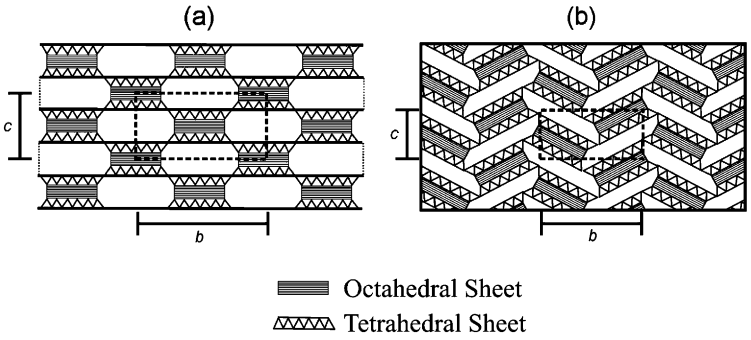

Fig. 2.27. General scheme for an unfolded (a) and folded (b) fibrous clay mineral. After Jones and Galán, 1988).

Four water molecules (zeolitic water) are present in the channels, and four others are bound to the octahedral edge inside the channels. Accordingly, the DTA curves can be divided into three parts: (i) the low-temperature region (<300 °C) where the minerals lose water adsorbed on outer surfaces and zeolitic water (peak at 120–150 °C); (ii) the central region (300–600 °C), where two endothermic peaks occur at about 350 °C and 500–550 °C for sepiolite, but only one (about 450–500 °C) for palygorskite; and (iii) the high-temperature region (> 600 °C) where an endothermic effect (at about 800 °C) is immediately followed by an exothermic maiximum.

In sepiolite, the first endotherm in the central region is narrower and more intense than the second one (Fig. 2.27). The first endothermic peak is ascribed to the loss of the first two water molecules coordinated to the inner octahedral edge, causing rotation of alternate ribbons and particle folding (Nagata et al., 1974; Serna et al., 1975; Van Scoyoc et al., 1979). The second central endotherm in sepiolite is due to the loss of the other two edge-coordinated water molecules that are 'trapped' inside

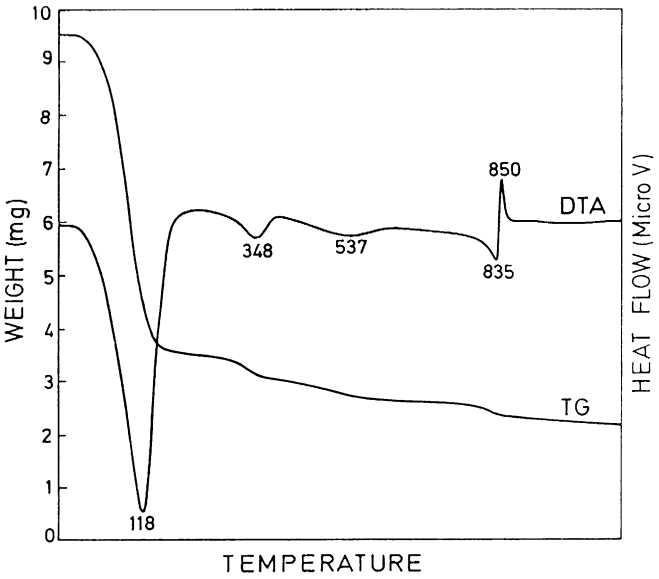

Fig. 2.28. DTA and TG curves of sepiolite from Vallecas. (temperature in °C, weight sample = 42 mg, heating rate = 12° min^{-1}, ambient conditions). After Pérez-Rodríguez and Galán (1994).

the collapsed channels (Pérez-Rodríguez and Galán, 1994). In palygorskite, coordination water is gradually lost through the whole interval, starting when zeolitic water is lost and ending when dehydroxylation begins (Mifsud et al., 1978). The high-temperature endotherm represents dehydroxylation of the structure, and the exothermic peak that follows is due to the formation of clinoenstatite. Typical DTA–TG curves for sepiolite are shown in Fig. 2.28.

The structural changes that occur on heating also lead to a decrease in the intensity of the principal XRD peaks. For instance, in sepiolite (Fig. 2.29) the reflections at 1.2, 0.45, 0.38, and 0.34 nm decrease when the mineral is heated at 250 °C for 1 h, while new reflections appear at 1.04 and 0.82 nm. Further heating to 450 °C increases the intensity of these new reflections, which persist up to 700 °C (Hayashi et al., 1969; Fernández álvarez, 1970; Nagata et al., 1974). In palygorskite, the intensity of the reflections at 1.05, 0.45, and 0.323 nm decreases on heating, and new peaks appear at 0.92 and 0.47 nm. On heating to 325 °C, these changes become more marked. Heating to 600 °C completely eliminates the 1.05 nm reflection. At the same time, the 0.92 nm peak becomes less intense (Hayashi et al., 1969) and shifts to 0.87 nm. At 700 °C, palygorskite is practically X-ray amorphous.

The decrease in intensity of the principal reflection occurs because structural disorder produced by heating is more prominent along the principal cleavage face (011) and less along the (040) plane (Lokanatha and Bhattacherjee, 1984). In the 200–300 °C range, the particle size of palygorskite slightly increases as water

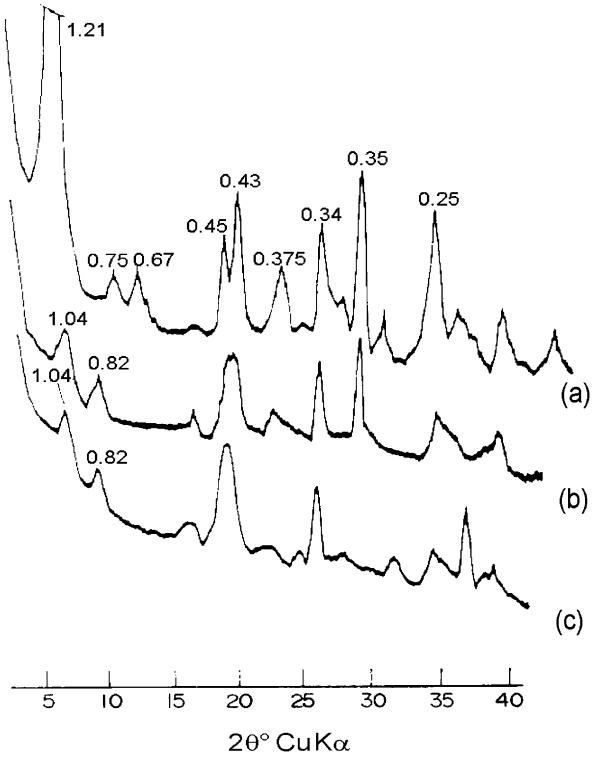

Fig. 2.29. XRD diffraction pattern of sepiolite recorded under vacuum at 25 °C, 4 h (a); 200 °C, 4 h (b); 530 °C, 6 h (c). After Serna et al. (1975).

molecules are expelled from the channels, but decreases markedly at 600 °C when the anhydrous stage is reached. As particle size decreases, the parameter *a* along the fibre axis increases until the structure collapses. Both palygorskite and sepiolite can rehydrate following particle folding. However, rehydration is difficult once the anhydrous state is reached when new interparticle bonds are formed.

From an historical point of view, the chemical analysis of sepiolite (in the form of a 'meerschaum' pipe from Turkey) was first attempted in the second half of the 18th century by Johann Christian Wiegleb. In 1794, Martin Heinrich Klaproth made a chemical analysis of a sepiolite from Eskişehir, Turkey. Since then most papers on sepiolite and palygorskite have information about their respective chemical compositions.

However, published analytical data mostly refer to bulk samples. As such, they are affected by both crystallochemical variations and admixed contaminants (other clay minerals and associated minerals). The most frequent admixtures in sepiolite and palygorskite are smectite, illite, chlorite, quartz, feldspars, carbonates, zeolites, iron, and silica gels.

Galán and Carretero (1999) have reviewed the literature on chemical analyses, including bulk chemical analyses, and EDX analyses of selected individual particles and pure samples. Their assessment indicates that sepiolite is a true trioctahedral mineral with eight octahedral positions filled by Mg^{2+} (Table 2.3) and negligible structural substitutions. A very pure (near end-member) specimen has close to the theoretical formula of

$$Mg_8Si_{12}O_{30}(OH)_4(OH_2)_4(H_2O)_8$$

Palygorskite is intermediate between di- and tri-octahedral. The octahedral sheet contains mainly Mg^{2+}, Al^{3+}, and Fe^{3+}, with an R^{2+}/R^{3+} ratio close to 1, and has four of the five structural positions occupied (Table 2.3). The theoretical formula is

$$(Mg_2^{2+}R_2^{3+}\square_1)(Si_{8-x}^{4+}Al_x^{3+})O_{20}(OH)_2(OH_2)_4 \times R_{x/2}^{2+}(H_2O)_4; \quad x = 0 - 0.5$$

The proposed formula is very close to that given by Smith and Norem (1986) for very pure palygorskite samples obtained by electron-microprobe analysis.

Figs. 2.30 and 2.31 indicate that the compositions of sepiolite and palygorskite are more limited than previously reported. The two minerals show no compositional gap if bulk analytical data are plotted on the Martin-Vivaldi and Cano (1956) diagram

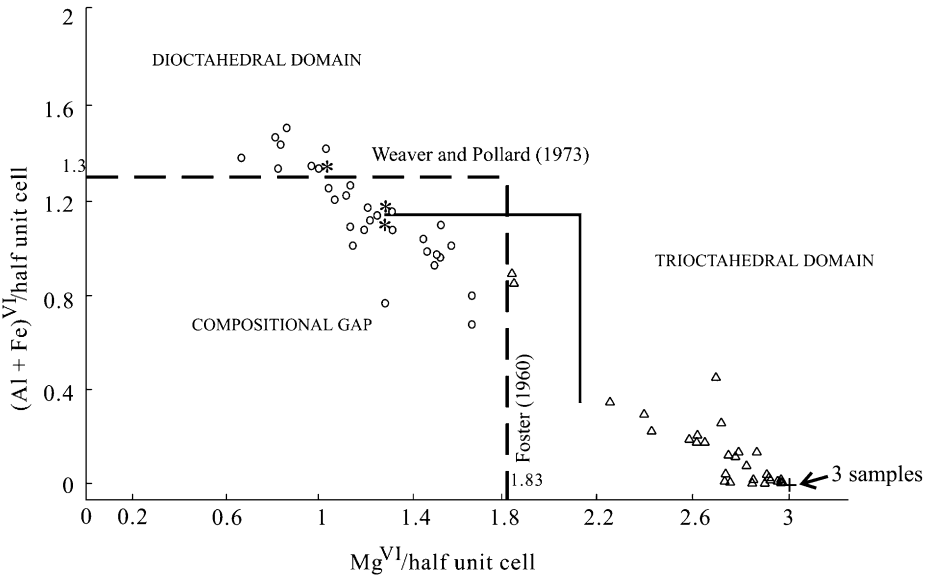

Fig. 2.30. Selected bulk analysis data for sepiolite and palygorskite, plotted as the content of 6-coordinate Mg atoms per half unit cell against the content of 6-coordinate (Al + Fe) atoms per half unit cell. (○): data for palygorskite from the literature; △: data for sepiolite from the literature. The EDX results for palygorskite (∗) and sepiolite (+) from Galán and Carretero (1999) are also included. Broken line represents the conventional plot; solid line denotes the relationship proposed by Paquet et al. (1987).

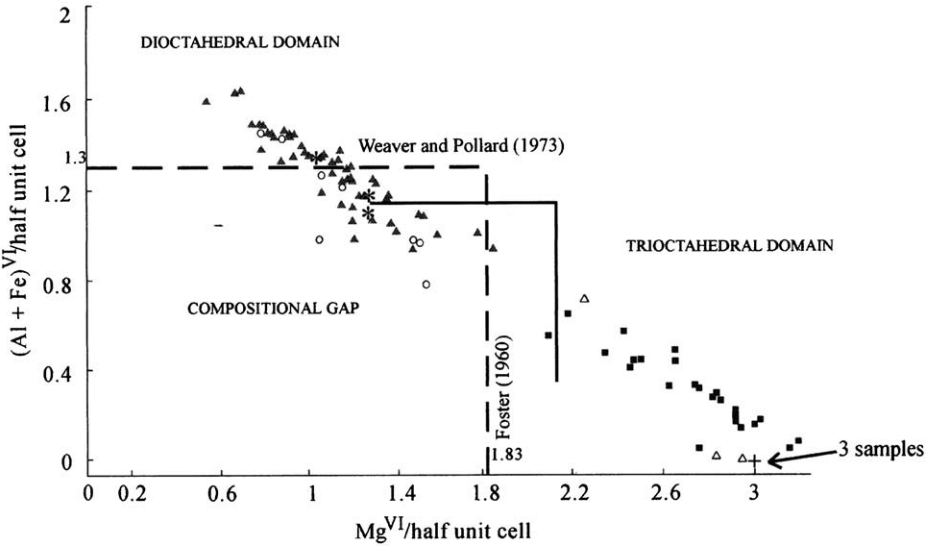

Fig. 2.31. EDX analysis data for sepiolite and palygorskite. ○: data for palygorskite from the literature; △: data for sepiolite from the literature. The results for palygorskite (∗) and sepiolite (+) from Galán and Carretero (1999) are also included. Broken line represents the conventional plot; solid line denotes the relationship proposed by Paquet et al. (1987) from their sepiolite (■) and palygorskite (▲) data.

(Fig. 2.32). On the contrary, a gap can be recognized if the EDX results alone are considered.

On the basis of trace elements content, sepiolite is a more 'restricted' mineral than palygorskite. According to Torres-Ruiz et al. (1994), sepiolite contains three or four times more trace elements than palygorskite. Both minerals are rich in F^- and Li^+. Sepiolite can contain up to 1.5% F^-, and 800 ppm Li^+ (Leguey et al., 1995; Torres-Ruiz et al., 1994). Inherited minerals have higher values of REE and transition-metal elements, and lower values of F^- and Li^+, than those formed by chemical precipitation in depositional basins (Torres-Ruiz et al., 1994; López-Galindo et al., 1996).

The CEC of both minerals is quite low, ranging from 4 to 40 cmol/kg; higher values are probably related to impurities (Galán, 1996).

In some sepiolites cations other than Mg^{2+} may occur in octahedral positions. If $Ni^{2+} > Mg^{2+}$ the species is known as falcondoite (Springer, 1976). Iron- and aluminium-rich varieties are named Fe^{3+}-sepiolite and Al^{3+}-sepiolite, respectively. Loughlinite is Na^+-sepiolite where two Na^+ substitute for two Mg^{2+}, and two Na^+ are in the channels (Fahey and Axelrod, 1948; Echle, 1978). Since it is very difficult to conceive of a stable sepiolite structure containing octahedral Na^+, Jones and Galán (1988) have suggested that the occurrence of loughlinite as a different mineral from sepiolite is still to be conclusively demonstrated. Other varieties of sepiolite are

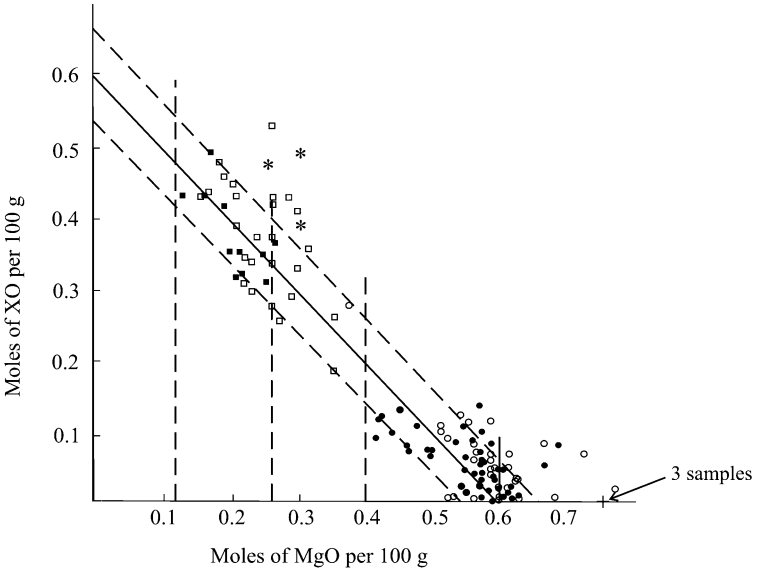

Fig. 2.32. Bulk analysis data for sepiolite and palygorskite, taken from the literature unless specified otherwise, plotted as moles of MgO per 100 g against moles of XO per 100 g where XO = $Al_2O_3 + Fe_2O_3 + FeO + MnO$. □ = palygorskite; ○ = sepiolite; ■ = palygorskite from Martín-Vivaldi and Cano (1956); ● = sepiolite from Martín-Vivaldi and Cano (1956). EDX results for palygorskite (*) and sepiolite (+) are taken from Galán and Carretero (1999).

Al^{3+}-sepiolite (Rogers et al., 1956; Firman, 1966), Mn^{2+}-sepiolite, and Mn^{2+}-Fe^{2+}-sepiolite (Semenov, 1969).

Among palygorskite varieties, Mn^{2+}-palygorskite and Mn^{2+}-ferropalygorskite are worthy of note (Semenov, 1969). Two new minerals, yofortierite (Perrault et al., 1975) and tuperssuatsiaite (Karup-Moller and Petersen, 1984), have been accepted as belonging to the palygorskite group. The former contains a high percentage of Mn^{2+} and a definite quantity of Zn^{2+} substituting for Al^{3+}. The latter can be considered a Na^{+}–Fe^{3+}-palygorskite.

The name attapulgite (for palygorskite), still widely used in industry and for deposits, was given by de Lapparent (1935) to a clay mineral found in fuller's earth from Attapulgus, Georgia, USA, and Mormoiron, France. Although 'attapulgite' is well established in industrial and trade circles because of the commercially available 'attapulgite clays' from the USA, the name 'palygorskite' has priority and should be used in preference (Bailey et al., 1971).

REFERENCES

Adams, J.M., 1983. Hydrogen atom positions in kaolinite by neutron profile refinement. Clays and Clay Minerals 31, 352–356.

Adams, J.M., Hewat, A.W., 1981. Hydrogen atom positions in dickite. Clays and Clay Minerals 29, 316–319.

Akiba, E., Hayakawa, H., Hayashi, S., Miyawaki, R., Tomura, S., Shibasaki, Y., Izumi, F., Asano, H., Kamiyama, T., 1997. Structure refinement of synthetic deuterated kaolinite by Rietveld analysis using time-of-flight neutron powder diffraction data. Clays and Clay Minerals 45, 781–788.

Alcover, J.F., Gatineau, L., 1980. Structure de l'espace interlamellaire de la vermiculite Mg bicouche. Clay Minerals 15, 25–35.

Altaner, S.P., Ylagan, R.E., 1997. Comparison of structural models of mixed layer illite/smectite and reactions mechanisms of smectite illitization. Clays and Clay Minerals 45, 517–533.

Anderson, C.S., Bailey, S.W., 1981. A new cation-ordering pattern in amesite-$2H_2$. American Mineralogist 66, 185–195.

Antonelli, F., Zane, A., Sassi, R., Lazzarini, L., Árkai, P., 2003. Illite Kübler index and chlorite "crystallinity" of marbles as indicators of metamorphic grade. Geophysical Research Abstracts 5, 21–42.

Aparicio, P., Ferrell, E., Galán, E., 1999. A new kaolinite crystallinity index from mathematical modeling of XRD data. Euroclay'99, Kraków, Program with Abstracts, p. 57.

Aparicio, P., Ferrell, E., Galán, E., 2001. Aplicación de la modelización matemática a los diagramas de DRX de la caolinita para mejorar el cálculo de indices de cristalinidad. In: Pascual Cosp, J., Zapatero Arenzana, J., Ramírez del Valle, A.J., Moya García, MV. (Eds.), Integración de Cienca-Tecnología de las arcillas en el Contexto Tecnológico-Social del Nuevo Milenio. Sociedad Española de Arcillas, Málaga, Spain, pp. 21–29.

Aparicio, P., Galán, E., 1999. Mineralogical interference on kaolinite crystallinity index measurements. Clays and Clay Minerals 47, 12–27.

Aruja, E., 1945. An X-ray study of the crystal structure of antigorite. Mineralogical Magazine 27, 65–74.

Backhaus, K.O., 1983. Structure refinement of a lepidolite-1M. Crystal Research and Technology 18, 1253–1260.

Bailey, S.W., 1963. Polymorphism of the kaolin minerals. American Mineralogist 48, 1196–1209.

Bailey, S.W., 1980. Structure of layer silicates. In: Brindley, G.W., Brown, G. (Eds.), Crystal Structures of Clay Minerals and Their X-ray Identification. Mineralogical Society, London, pp. 1–123.

Bailey, S.W., 1982. Nomenclature for regular interstratification. American Mineralogist 67, 394–398.

Bailey, S.W., 1984a. Classification and structures of the micas. In: Bailey, S.W. (Ed.), Micas. Reviews in Mineralogy, vol. 13. Mineralogical Society of America, Washington, DC, pp. 1–12.

Bailey, S.W., 1984b. Crystal chemistry of the true micas. In: Bailey, S.W. (Ed.), Micas. Reviews in Mineralogy, vol. 13. Mineralogical Society of America, Washington, DC, pp. 13–60.

Bailey, S.W., 1984c. Review of cation ordering in micas. Clays and Clay Minerals 32, 81–92.

Bailey, S.W., 1986. Report of the AIPEA Nomenclature Committee (illite, glauconite and volkonskoite). Supplement to the AIPEA Newsletter 22, 1–3.

Bailey, S.W., 1988a. Structure and composition of other trioctahedral 1:1 phyllosilicates. In: Bailey, S.W. (Ed.), Hydrous Phyllosilicates (Exclusive of Micas). Reviews in Mineralogy, vol.19. Mineralogical Society of America, Washington, DC, pp. 169–186.

Bailey, S.W., 1988b. Chlorites: structures and crystal chemistry. In: Bailey, S.W. (Ed.), Hydrous Phyllosilicates (Exclusive of Micas). Reviews in Mineralogy, vol. 19. Mineralogical Society of America, Washington, DC, pp. 347–403.

Bailey, S.W., Brindley, G.W., Jonhs, W.D., Martín, R.T., Ross, M., 1971. Clay minerals society report of nomenclature committee 1969–1970. Clays and Clay Minerals 19, 132–133.

Banfield, J.F., Bailey, S.W., 1996. Formation of regularly interstratified serpentine-chlorite minerals by inversion in long-period serpentine polytypes. American Mineralogist 81, 79–91.

Baronnet, A., 1978. Some aspects of polytypism in crystals. In: Progress in Crystal Growth Characterization, vol. 1. Pergamon Press, Oxford, pp. 111–151.

Baronnet, A., 1992. Polytypism and stacking disorder. In: Buseck, P.R. (Ed.), Minerals and Reactions at the Atomic Scale: Transmission Electron Microscopy. Reviews in Mineralogy, vol. 27. Mineralogical Society of America, Washington, DC, pp. 231–282.

Bayliss, P., 1975. Nomenclature of the trioctahedral chlorites. Canadian Mineralogist 13, 178–180.

Bayliss, P., 1989. Unit-cell dimensions of two-dimensional clay minerals. Powder Diffractions 4, 19–20.

Ben Haj Amara, A., Ben Brahim, J., Plançon, A., Ben Rhaiem, H., 1998. The structure of 8.4 Å hydrated and dehydrated nacrite determined by X-ray diffraction. Journal of Applied Crystallography 31, 654–662.

Ben Haj Amara, A., Ben Brahim, J., Plançon, A., Ben Rhaiem, H., Besson, G., 1997. Etude structurale d'une nacrite Tunisienne. Journal of Applied Crystallography 30, 338–344.

Benco, L., Tunega, D., Hafner, J., Lischka, H., 2001a. Orientation of OH groups in kaolinite and dickite: ab initio molecular dynamics study. American Mineralogist 86, 1057–1065.

Benco, L., Tunega, D., Hafner, J., Lischka, H., 2001b. Upper limit of the O–H–O hydrogen bond. Ab initio study of the kaolinite structure. Journal of Physical Chemistry B 105, 10812–10817.

Benco, L., Tunega, D., Hafner, J., Lischka, H., 2001c. Ab initio density functional theory applied to the structure and proton dynamics of clays. Chemical Physics Letters 333, 479–484.

Bethke, C.M., Altaner, S.P., 1986. Layer-by-layer mechanism of smectite illitization and application to a new rate law. Clays and Clay Minerals 34, 136–145.

Bhattacherjee, S., 1973. Dehydration transformation in metahalloysite. Proceedings of the Indian National Science Academy, Part A, vol. 39, pp. 54–61 (abstract).

Bish, D.L., 1993. Rietveld refinement of the kaolinite structure at 1.5 K. Clays and Clay Minerals 41, 738–744.

Bish, D.L., Johnston, C.T., 1993. Rietveld refinement and Fourier-transform infrared spectroscopic study of the dickite structure at low temperature. Clays and Clay Minerals 41, 297–304.

Bish, D.L., Von Dreele, R.B., 1989. Rietveld refinement of non-hydrogen atom position in kaolinite. Clays and Clay Minerals 37, 289–296.

Blanco, C., Herrero, J., Mendioroz, S., Pajares, J.A., 1988. Infrared studies of surface acidity and reversible folding in palygorskite. Clays and Clay Minerals 36, 364–368.

Blount, A.M., Threadgold, I.M., Bailey, S.W., 1969. Refinement of the crystal structure of nacrite. Clays and Clay Minerals 17, 185–194.

Boek, E.S., Sprik, M., 2003. Ab initio molecular dynamics study of the hydration of a sodium smectite clay. Journal of Physical Chemistry B 107, 3251–3256.

Bradley, W.F., 1940. The structural scheme of attapulgite. American Mineralogist 25, 405–410.

Bradley, W.F., 1959. Current progress in silicate structures. Clays and Clay Minerals 6, 18–25.

Brauner, K., Preisinger, A., 1956. Struktur und Entstehung des Sepioliths. Tschermaks Mineralogische und Petrographische Mitteilungen 6, 120–140.

Brigatti, M.F., Galli, E., Medici, L., Poppi, L., 1997. Crystal structure refinement of aluminian lizardite-2H2. American Mineralogist 82, 931–935.

Brigatti, M.F., Guggenheim, S., 2002. Mica crystal chemistry and the influence of pressure, temperature, and solid solution on atomistic models. In: Mottana, A., Sassi, F.P., Thompson, J.B., Guggenheim, S. (Eds.), Micas: Crystal Chemistry and Metamorphic Petrology. Reviews in Mineralogy and Geochemistry, vol. 46. Mineralogical Society of America, Washington, DC, pp. 1–97.

Brigatti, M.F., Lalonde, A.E., Medici, L., 1999. Crystal chemistry of $IVFe^{3+}$-rich phlogopites: a combined single-crystal X-ray and Mössbauer study. In: Kodama, H., Mermut, A.R., Torrance, J.K. (Eds.), Clays for our Future. Proceedings of the 11th International Clay Conference, Ottawa, pp. 317–327.

Brigatti, M.F., Lugli, C., Poppi, L., Foord, E.E., Kile, D.E., 2000. Crystal chemical variations in Li- and Fe-rich micas from Pikes Peak Batholith (central Colorado). American Mineralogist 85, 1275–1286.

Brigatti, M.F., Medici, L., Poppi, L., 1996b. Refinement of the structure of natural ferriphlogopite. Clays and Clay Minerals 44, 540–545.

Brigatti, M.F., Medici, L., Saccani, E., Vaccaro, C., 1996a. Crystal chemistry and petrologic significance of Fe^{3+}- rich phlogopite from the Tapira carbonatite complex, Brazil. American Mineralogist 81, 913–927.

Brindley, G.W., 1959. X-ray and electron diffraction data for sepiolite. American Mineralogist 44, 495–500.

Brindley, G.W., Brown, G. (Eds.), 1980. Crystal Structures of Clay minerals and Their X-ray Identification. Mineralogical Society, London.

Brindley, G.W., Robinson, K., 1945. Structure of kaolinite. Nature 156, 661–663.

Brindley, G.W., Robinson, K., 1946. The structure of kaolinite. Mineralogical Magazine 27, 242–253.

Brindley, G.W., Robinson, K., 1948. X-ray studies of halloysite and metahalloysite, I. The structure of metahalloysite, an example of random layer lattice. Mineralogical Magazine 28, 393–406.

Brindley, G.W., Wardle, R., 1970. Monoclinic and triclinic forms of pyrophyllite and pyrophyllite anhydride. American Mineralogist 55, 1259–1272.

Brown, B.E., 1978. The crystal structure of 3T lepidolite. American Mineralogist 63, 332–336.

Brown, B.E., Bailey, S.W., 1963. Chlorite polytypism, II. Crystal structure of one layer Cr-chlorite. American Mineralogist 48, 42–61.

Brown, G., Newman, A.C.D., Rayner, J.H., Weir, A.H., 1978. The structures and chemistry of soil clay minerals. In: Greenland, D.J., Hayes, M.H.B. (Eds.), The Chemistry of Soil Constituents. Wiley, Chichester, pp. 29–178.

Brown, G.E., Parks, G.A., O'Day, P.A., 1995. Sorption at mineral-water interfaces: macroscopic and microscopic perspectives. In: Vaughan, D.J., Pattrick, R.A.D. (Eds.), Mineral Surfaces. Mineralogical Society, Series 5. Chapman & Hall, London, pp. 129–183.

Bukin, A.S., Drits, V.A., Plançon, A., Tchoubar, C., 1989. Stacking faults in kaolin-group minerals in light of real structural features. Clays and Clay Minerals 37, 297–307.

Caillère, S., 1951. Sepiolite. In: Brindley, G.W. (Ed.), X-ray Identification and Structures of Clay Minerals. Mineralogical Society, London, pp. 224–233.

Cases, J.M., Liétard, O., Yvon, J., Delon, J.F., 1982. Étude des propiértés cristallochimiques, morphologiques, superficielles de kaolinites désordonnées. Bulletin de Minéralogie 105, 439–455.

Cases, J.M., Bérend, I., François, M., Uriot, J.P., Michot, L.J., Thomas, F., 1997. Mechanisms of adsorption and desorption of water vapor by homoionic montmorillonite: 3. The Mg^{2+}, Ca^{2+}, Sr^{2+}, and Ba^{2+} exchanged forms. Clays and Clay Minerals 45, 8–22.

Chatterjee, A., Iwasaki, T., Ebina, T., Miyamoto, A., 1999. A DFT study on clay–cation–water interaction in montmorillonite and beidellite. Computational Materials Science 14, 119–124.

Chernoski, J.V., 1975. Aggregate refractive indices and unit cell parameters of synthetic serpentine in the system MgO–Al_2O_3–SiO_2–H_2O. American Mineralogist 60, 2000–2008.

Childs, C.W., Hayashi, S., Newman, R.H., 1999. Five-coordinate aluminum in allophane. Clays and Clay Minerals 47, 64–69.

Childs, C.W., Inoue, K., Seyama, H., Soma, M., Theng, B.K.G., Yuan, G., 1997. X-ray photoelectron spectroscopic characterization of Silica Springs allophane. Clay Minerals 32, 565–572.

Childs, C.W., Parfitt, R.L., Newman, R.H., 1990. Structural studies of Silica Springs allophane. Clay Minerals 25, 329–341.

Chisholm, J.E., 1992. Powder diffraction patterns and structural models for palygorskite. Canadian Mineralogist 30, 61–73.

Christ, C.L., Hathaway, J.C., Hostetler, P.B., Shepard, A.O., 1969. Palygorskite: new X-ray data. American Mineralogist 54, 198–205.

Churchman, G.J., Theng, B.K.G., 1984. Interactions of halloysites with amides: mineralogical factors affecting complex formation. Clay Minerals 19, 161–175.

Compagnoni, R., Ferraris, G., Mellini, M., 1985. Carlosturanite, a new asbestiform rock-forming silicate from Val Variata, Italy. American Mineralogist 70, 767–772.

Costanzo, P.M., Giese, R.F. Jr., 1985. Dehydration of synthetic hydrated kaolinites: a model for the dehydration of halloysite (10 Å). Clays and Clay Minerals 33, 415–423.

Costanzo, P.M., Giese, R.F. Jr., Lipsicas, M., 1984. Static and dynamic structure of water in hydrated kaolinites, I. The static structure. Clays and Clay Minerals 32, 419–428.

Cradwick, P.D.G., Farmer, V.C., Russell, J.D., Masson, C.R., Wada, K., Yoshinaga, N., 1972. Imogolite, a hydrated aluminium silicate of tubular structure. Nature Physical Science 240, 187–189.

Cruciani, G., Zanazzi, P.F., 1994. Cation partitioning and substitution mechanism in 1M-phlogopite: a crystal chemical study. American Mineralogist 78, 289–301.

Cruciani, G., Zanazzi, P.F., Quartieri, S., 1995. Tetrahedral ferric iron in phlogopite. XANES and Mössbauer comparison to single-crystal X-ray data. European Journal of Mineralogy 7, 255–265.

de la Calle, C., Suquet, H., 1988. Vermiculite. In: Bailey, S.W. (Ed.), Hydrous Phyllosilicates (Exclusive of Micas). Reviews in Mineralogy, vol. 19. Mineralogical Society of America, Washington, DC, pp. 455–492.

de Lapparent, J., 1935. Sur un constituant essentiel des terres a foulon. Comptes Rendues de l'Académie des Sciences, Paris, vol. 201, pp. 481–482.

Donnay, G., Morimoto, N., Takeda, H., Donnay, J.D.H., 1964. Trioctahedral one-layer micas, I. Crystal structure of a synthetic iron mica. Acta Crystallographica 17, 1369–1373.

Dornberger-Schiff, K., Ďurovič, S., 1975. OD [order–disorder]-interpretation of kaolinite-type structures. I. Symmetry of kaolinite packets and their stacking possibilities. Clays and Clay Minerals 23, 219–229.

Drits, V.A., 1997. Mixed layer minerals. In: Merlino, S. (Ed.), Modular Aspects of Minerals, EMU Notes in Mineralogy, vol. 1. Eötvös University Press, Budapest, pp. 153–190.

Drits, V.A., Besson, G., Muller, F., 1996. X-ray diffraction study of structural transformations of aluminous 2:1 layer silicates during dehydroxylation. Journal de Physique IV 6 (C_4, Rayons X et Matière), 91–102.

Drits, V.A., Dainyak, L.G., Muller, F., Besson, G., Manceau, A., 1997a. Isomorphous cation distribution in celadonites, glauconites and Fe-illites determined by infrared, Mossbauer and EXAFS spectroscopies. Clay Minerals 32, 153–179.

Drits, V.A., Karavan, Yu, V., 1969. Polytypes of the two-packet chlorites. Acta Crystallographica B 25, 632–639.

Drits, V.A., Lindgreen, H., Salyn, A.L., 1997b. Determination by XRD of content and distribution of fixed ammonium in illite-smectite. Application to North Sea illite-smectite. American Mineralogist 82, 80–88.

Drits, V.A., Plançon, A., Sakharov, B.A., Besson, G., Tsipursky, S.I., Tchoubar, C., 1984. Diffraction effects calculated for structural models of K-saturated momtmorillonite containing different types of defects. Clay Minerals 19, 541–561.

Drits, V.A., Sokolova, G.V., 1971. Structure of palygorskite. Soviet Physics, Crystallography 16, 183–185.

Drits, V.A., Tchoubar, C., 1990. X-ray diffraction by disordered lamellar structures. Theory and application to microdivided silicates and carbons. Springer, Berlin.

Drits, V.A., Weber, F., Salyn, A.L., Tsipursky, S.I., 1993. X-ray identification of one-layer illite varieties; Application to the study of illite around uranium deposits of Canada. Clays and Clay Minerals 41, 389–398.

Ďurovíć, S., 1981. OD-caracther, Polytypie und Identifikation von Schichtsilikaten. Forschritte der Mineralogie 59, 191–226.

Ďurovíć, S., 1994. Classification of phyllosilicates according to the symmetry of their octahedral sheets. Ceramics—Silikàty 38, 81–84.

Ďurovič, S., 1997. Fundamentals of OD theory. In: Merlino, S. (Ed.), Modular Aspects of Minerals, EMU Notes in Mineralogy, vol. 1. Eötvös University Press, Budapest, pp. 1–28.

Ďurovič, S., 1999. Layer stacking in general polytypic structures. Section 9.2.2. In: Wilson, A.C.J., Prince, E. (Eds.), International Tables for Crystallography, vol. C. Kluwer Academic Publishers, Dordrecht, pp. 752–765.

Dyar, M.D., 1990. Mössbauer spectra of biotite from metapelites. American Mineralogist 75, 656–666.

Echle, W., 1978. The transformation sepiolite-loughlinite: experiments and field observations. Neues Jahrbuch fur Mineralogie, Abhandlungen 133, 303–321.

Eggleton, R.A., Tilley, D.B., 1998. Hisingerite a ferric kaolin mineral with curved morphology. Clays and Clay Minerals 46, 400–413.

Evans, B.W., Guggenheim, S., 1988. Talc, phyrophyllite, and related minerals. In: Bailey, S.W. (Ed.), Hydrous Phyllosilicates (Exclusive of Micas). Reviews in Mineralogy, vol. 19. Mineralogical Society of America, Washington, DC, pp. 225–280.

Fahey, J.J., Axelrod, J.M., 1948. Loughlinite, a new hydrous magnesium silicate. American Mineralogist 33, 195.

Farmer, L.G., Boettcher, A.I., 1981. Petrologic and crystal chemical significance of some deep-seated phlogopites. American Mineralogist 66, 1154–1163.

Farmer, V.C., Fraser, A.R., Tait, J.M., 1979. Characterization of the chemical structures of natural and synthetic aluminosilicate gels and sols by infrared spectroscopy. Geochimica et Cosmochimica Acta 43, 1417–1420.

Farmer, V.C., Russell, J.D., 1990. The structure and genesis of allophanes and imogolite: their distribution in non-volcanic soils. In: De Boodt, M.F., Hayes, M.H.B., Herbillon, A. (Eds.), Soil Colloids and Their Associations in Aggregates. Proceedings NATO Advanced Studies Workshop, Ghent 1985. Plenum Press, New York, pp. 165–178.

Fernández Álvarez, T., 1970. Superficie específica y estructura de poro de la sepiolita calentada a diferentes temperaturas. Proceedings Reunión Hispano-Belga de Minerales de la Arcilla, Madrid, 202–209.

Ferraris, G., Gula, A., Ivaldi, G., Nespolo, M., Soboleva, E., Khomyakov, A.P., Uvarova, Yu., 2000. First structural determination of a truly-polytypic mica-2O. In: Advances on Micas (Problems, Methods, Applications in Geodynamics). Accademia Nazionale dei Lincei, Roma, pp. 205–209.

Fieldes, M., Claridge, G.G.C., 1975. Allophane. In: Gieseking, J.E. (Ed.), Soil Components, Inorganic Components, vol. 2. Springer, New York, pp. 351–393.

Filut, A.M., Rule, A.C., Bailey, S.W., 1985. Crystal structure refinement of anandite 2Or, a barium- and sulfur-bearing trioctahedral mica. American Mineralogist 70, 1298–1308.

Firman, R.J., 1966. Sepiolite from the Malvern Hill. Mercian Geologist 1, 247–253.

Flehmig, W., 1973. Kristallinität und Infrarotspektroskopie natürlicher dioktaedrischer illite. Neues Jahrbuch für Mineralogie—Monatshefte, pp. 351–361.

Floran, R.J., Papike, J.J., 1975. Petrology of the low-grades rocks of the Gunflint iron-Formation, Ontario-Minnesota. Geological Society of America Bulletin 86, 1169–1190.

Frost, R.L., Rintoul, L., Eggleton, R.A., 1997. Structural aspects of hisingerite: a vibrational spectroscopic study. In: Kodama, H., Mermut, A.R., Torrance, J.K. (Eds.), Clays for Our Future. Proceedings of the 11th International Clay Conference, Ottawa, 1997, pp. 409–412.

Galán, E., 1996. Properties and applications of palygorskite-sepiolite clays. Clay Minerals 31, 443–453.

Galán, E., Carretero, M.I., 1999. A new approach to compositional limits for sepiolite and palygorskite. Clays and Clay Minerals 47, 399–409.

Gard, J.A., Follet, E.A., 1968. A structural scheme for palygorskite. Clay Minerals 7, 367–369.

Gast, R.G., 1977. Surface and colloid chemistry. In: Dixon, J.B., Weed, S.B. (Eds.), Minerals in Soil Environments. Soil Science Society of America, Madison, WI, pp. 27–73.
Giese, R.F. Jr., 1973. Hydroxyl Orientation in Pyrophyllite. Nature Physical Science 241, 151.
Giese, R.F., 1988. Kaolin minerals: structures and stabilities. In: Bailey, S.W. (Ed.), Hydrous Phyllosilicates (Exclusive of Micas). Reviews in Mineralogy, vol. 19. Mineralogical Society of America, Washington, DC, pp. 29–66.
Giese, R.F. Jr., Datta, P., 1973. Hydroxyl orientation in kaolinite, dickite, and nacrite. American Mineralogist 58, 471–479.
Giuseppetti, G., Tadini, C., 1972. The crystal structure of 2O brittle mica: anandite. Tschermaks Mineralogische und Petrographische Mitteilungen 18, 169–184.
Goodman, B.A., Russell, J.D., Montez, B., Oldfield, E., Kirkpatrick, R.J., 1985. Structural studies of imogolite and allophanes by aluminium-27 and silicon-29 nuclear magnetic resonance spectroscopy. Physics and Chemistry of Minerals 12, 342–346.
Gruner, J.W., 1932a. The crystal structure of dickite. Zeitschrift für Kristallographie, Kristallgeometrie, Kristallphysik, Kristallchemie 83, 394–404.
Gruner, J.W., 1932b. The crystal structure of kaolinite. Zeitschrift für Kristallographie, Kristallgeometrie, Kristallphysik, Kristallchemie 83, 75–80.
Gruner, J.W., 1934. The crystal structure of talc and pyrophyllite. Zeitschrift für Kristallographie, Kristallgeometrie, Kristallphysik, Kristallchemie 88, 412–419.
Guggenheim, S., Bailey, S.W., 1975. Refinement of the margarite structure in subgroup symmetry. American Mineralogist 60, 1023–1029.
Guggenheim, S., Bailey, S.W., 1977. The refinement of zinnwaldite-1M in subgroup symmetry. American Mineralogist 62, 1158–1167.
Guggenheim, S., Bailey, S.W., 1978. Refinement of the margarite structure in subgroup symmetry: correction, further refinement, and comments. American Mineralogist 63, 186–187.
Guggenheim, S., Bailey, S.W., Eggleton, R.A., Wikes, P., 1982. Structural aspect of greenalite and related minerals. Canadian Mineralogist 20, 1–18.
Guggenheim, S., Bain, D.C., Bergaya, F., Brigatti, M.F., Drits, V.A., Eberl, D.D., Formoso, M.L.L., Galán, E., Merriman, R.J., Peacor, D.R., Stanjek, H., Watanabe, T., 2002. Report of the Association Internationale Pour l'Étude des Argiles (AIPEA). Nomenclature Committee for 2001: order, disorder and crystallinity in phyllosilicates and the use of the crystallinity index. Clays and Clay Minerals 50, 406–409.
Guggenheim, S., Eggleton, R.A., 1998. The crystal structure of greenalite and caryopilite. Canadian Mineralogist 36, 163–179.
Guggenheim, S., Kato, T., 1984. Kinoshitalite and Mn phlogopites: trial refinements in subgroup symmetry and further refinement in ideal symmetry. Mineralogical Journal 12, 1–5.
Guggenheim, S., Zhan, W., 1998. Effect of temperature on the structures of lizardite-1T and lizardite-$2H_1$. Canadian Mineralogist 36, 1587–1594.
Güven, N., 1988. Smectites. In: Bailey, S.W. (Ed.), Hydrous Phyllosilicates (Exclusive of Micas), Reviews in Mineralogy, vol. 19. Mineralogical Society of America, Washington, DC, pp. 497–559.
Güven, N., 1992. Molecular aspects of clay-water interactions. In: Güven, N., Pollastro, R.M. (Eds.), Clay–Water Interface and its Rheological Implications, CMS Workshop Lectures, vol. 4. The Clay Minerals Society, Boulder, CO, pp. 1–80.
Güven, N., Burnham, C.W., 1967. The crystal structure of 3T muscovite. Zeitschrift für Kristallographie 125, 163–183.

Hall, P.L., Churchman, G.J., Theng, B.K.G., 1985. Size distribution of allophane unit particles in aqueous suspensions. Clays and Clay Minerals 33, 345–349.
Hall, S.H., Bailey, S.W., 1976. Amesite from Antarctica. American Mineralogist 61, 497–499.
Harsh, J., 2000. Poorly crystalline aluminosilicate clays. In: Sumner, M.E. (Ed.), Handbook of Soil Science. CRC Press, Boca Raton, FL, F-169–F-182.
Hashizume, H., Theng, B.K.G., 1999. Adsorption of DL-alanine by allophane: effect of pH and unit particle aggregation. Clay Minerals 34, 233–238.
Hashizume, H., Theng, B.K.G., Yamagishi, A., 2002. Adsorption and discrimination of alanine and alanyl-alanine enantiomers by allophane. Clay Minerals 37, 551–557.
Hayashi, H., Otsuka, R., Imai, N., 1969. Infrared study of sepiolite and palygorskite on heating. American Mineralogist 53, 1613–1624.
Hazen, R.M., Finger, L.W., Velde, D., 1981. Crystal structure of a silica- and alkali-rich trioctahedral mica. American Mineralogist 66, 586–591.
He, H., Barr, T.L., Klinowski, J., 1995. ESCA and solid-state NMR studies of allophane. Clay Minerals 30, 201–209.
Hendricks, S.B., 1938a. The crystal structure of talc and pyrophyllite. Zeitschrift für Kristallographie 99, 264–274.
Hendricks, S.B., 1938b. The crystal structure of the clay minerals: dickite, halloysite and hydrated halloysite. American Mineralogist 23, 295–301.
Hendricks, S.B., 1939. The crystal structure of nacrite, $Al_2O_3 \cdot 2SiO_2 \cdot 2H_2O$, and the polymorphism of the kaolin minerals. Zeitschrift für Kristallographie 100, 509–518.
Hendricks, S.B., Nelson, R.A., Alexander, L.T., 1940. Hydration mechanism of the clay mineral montmorillonite saturated with various cations. Journal of the American Chemical Society 62, 1457–1464.
Henmi, T., Wada, K., 1976. Morphology and composition of allophane. American Mineralogist 61, 379–390.
Hinckley, D., 1963. Variability in crystallinity values among the kaolin deposits of the Coastal Plain of Georgia and South Carolina. Clays and Clay Minerals 11, 229–235.
Hobbs, J.D., Cygan, R.T., Nagy, K.L., Schultz, P.A., Sears, M.P., 1997. All-atom ab initio energy minimization of the kaolinite crystal structure. American Mineralogist 82, 657–662.
Hofmann, U., Endell, K., Wilm, D., 1934. X-ray and colloid-chemical studies of clay. Angewandte Chemie 47, 539–547.
Huang, W.L., 1992. Illitic clay formation during experimental diagenesis of arkoses. In: Houseknecht, D.W., Pittman, E.D. (Eds.), Origin, Diagenesis, and Petrophysics of Clay Minerals in Sandstones. SEPM Special Publication. vol. 47, pp. 49–63.
Johnston, C.T., Agnew, S.F., Bish, D.L., 1990. Polarized single-crystal Fourier-transform infrared microscopy of Ouray dickite and Keokuk kaolinite. Clays and Clay Minerals 38, 573–583.
Jones, B.F., Galán, E., 1988. Sepiolite and palygorskite. In: Bailey, S.W. (Ed.), Hydrous Phyllosilicates (Exclusive of Micas). Reviews in Mineralogy, vol. 19. Mineralogical Society of America, Washington, DC, pp. 631–674.
Joswig, W., Amthauer, G., Takéuchi, Y., 1986. Neutron diffraction and Mössbauer spectroscopic study of clintonite (xanthophyllite). American Mineralogist 71, 1194–1197.
Joswig, W., Drits, V.A., 1986. The orientation of the hydroxyl groups in dickite by X-ray diffraction. Neues Jahrbuch für Mineralogie—Monatshefte, 19–22.

Karup-Moller, S., Petersen, O.V., 1984. Tuperssuatsiaite, a new mineral species from the Ilimaussaq intrusion in South Greenland. Neues Jahrbuch für Mineralogie—Monatshefte 11, 501–512.

Kassner, D., Baur, W.H., Joswig, W., Eichhorn, K., Wendschuh-Jostier, M., Kupčik, V., 1993. A test of the importance of weak reflections in resolving a space-group ambiguity involving the presence or absence of an inversion centre. Acta Crystallographica B 49, 646–654.

Kleppe, A.K., Jephcoat, A.P., Welch, M.D., 2003. The effect of pressure upon hydrogen bonding in chlorite: a Raman spectroscopic study of clinochlore to 26.5 GPa. American Mineralogist 88, 567–573.

Klevtsov, D.P., Krivoruchko, O.P., Mastikhin, V.M., Buyanov, R.A., Zolotovskii, B.P., Paramzin, S.M., 1987. Formation of [AlO_5] polyhedra during the dehydroxylation of layered compounds. Doklady Akademii Nauk SSSR 295, 381–384.

Kodama, H., 1959. Crystallo-chemical studies on pyrophyllite. Nendo Kagaku 1, 13–27.

Kohyama, N., Fukushima, K., Fukami, A., 1978. Observation of the hydrated form of tubular halloysite by an electron microscope equipped with an environmental cell. Clays and Clay Minerals 26, 25–40.

Kübler, B., 1964. Les argiles, indicateurs de métamorphisme. Revue de l'Institut Français du Pétrole 19, 1093–1112.

Kübler, B., 1967. La cristallinité de l'illite et les zones tout à fait supérieures du métamorphisme. In: Etages tectoniques. Colloque de Neuchâtel, 1966. Editions de la Baconnière, Neuchâtel, pp. 105–121.

Kübler, B., Goy-Eggenberger, D., 2001. The crystallinity of illite revisited: a review of knowledge acquired. Clay Minerals 36, 143–157.

Kunze, G., 1956. Die gewellte Struktur des Antigorits, I. Zeitschrift für Kristallographie 108, 82–107.

Kunze, G., 1958. Die gewellte Struktur des Antigorits, II. Zeitschrift für Kristallographie 110, 282–320.

Kunze, G., 1959. Fehlordnungen des Antigorits. Zeitschrift für Kristallographie 111, 190–212.

Laird, D.A., 1994. Evaluation of structural formulae and alkylammonium methods of determining layer charge. In: Mermut, A.R. (Ed.), Layer Charge Characteristics of 2:1 Silicate Clay Minerals. CMS Workshop Lectures. vol. 6, pp. 79–104.

Lee, H.-L., Guggenheim, S., 1981. Single crystal refinement of pyrophyllite-1Tc. American Mineralogist 66, 350–357.

Leguey, S., Martín Rubí, J.A., Casas, J., Marta, J., Cuevas, J., Álvarez, A., Median, J.A., 1995. Diagenetic evolution and mineral fabric in sepiolic materials from the Vicálvaro deposit (Madrid basin). In: Churchman, G.J., Fitzpatrick, R.W., Eggleton, R.A. (Eds.), Clays Controlling the Environment. Proceedings of the 10th International Clay Conference, Adelaide, 1993. CSIRO Publishing, Melbourne, pp. 383–392.

Liang, J.-J., Hawthorne, F.C., Novák, M., černý, P., Ottolini, L., 1995. Crystal-structure refinement of boromuscovite polytypes using a coupled Rietveld-static-structure energy-minimization method. Canadian Mineralogist 33, 859–865.

Liétard, O., 1977. Contribution à l'étude des propriétés physicochimiques, cristallographiques et morphologiques des kaolins. PhD thesis. University of Nancy, France, p. 322 (in French).

Lin, J.-C., Guggenheim, S., 1983. The crystal structure of a Li, Be-rich brittle mica: a dioctahedral-trioctahedral intermediate. American Mineralogist 68, 130–142.

Lindgreen, H., Hansen, P.L., Jakobsen, H.J., 1991. Diagenetic structural transformation in North Sea Jurassic illite/smectite. Clays and Clay Minerals 39, 54–69.

Lipkina, M.I., Drits, V.A., Tsipurskii, S.I., Ustinov, V.I., Strizhev, V.P., Yakusheva, I.N., Cherkashin, V.I., 1987. Dioctahedral Fe-rich layer silicates from hydrothermal rocks and sediments of volcanogenic mountains of Japan Sea. Izvestiya Akademii Nauk SSSR, seriya geologia 10, 92–111 (in Russian).

Lister, J.S., Bailey, S.W., 1967. Chlorite polytypism, IV. Regular two-layer structures. American Mineralogist 52, 1614–1631.

Lokanatha, S., Bhattacherjee, S., 1984. Structure defects in palygorskite. Clay Minerals 19, 253–255.

Longchambon, H., 1937. Thermal properties of sepiolites. Bulletin de la Société française de Minéralogie et de Cristallographie 60, 232–276.

Longchambon, H., Migeon, G., 1936. Sepiolite. Comptes Rendues de l'Académie des Sciences, Paris, vol. 203, pp. 431–433.

López-Galindo, A., Ben Abound, A., Fenoll Hach-Ali, P., Casas Ruiz, J., 1996. Mineralogical and geochemical characterization of palygorskite from Gabasa (NE Spain). Evidence of a detrital precursor. Clay Minerals 31, 33–44.

MacEwan, D.M.C., Wilson, M.J., 1980. Interlayer and intercalation complexes of clay minerals. In: Brindley, G.W., Brown, G. (Eds.), Crystal Structures of Clay Minerals and Their X-ray Identification. Mineralogical Society, London, pp. 197–248.

MacKenzie, K.J.D., Bowden, M.E., Meinhold, R.H., 1991. The structure and thermal transformations of allophanes studied by 29Si and 27Al high resolution solid-state NMR. Clays and Clay Minerals 39, 337–346.

Martín-Vivaldi, J.L., Cano, J., 1956. Contribution to the study of sepiolite, II. Some considerations regarding the mineralogical formula. Clays and Clay Minerals 4, 173–176.

Martin, R.T., Bailey, S.W., Eberl, D.D., Fanning, D.S., Guggenheim, S., Kodama, H., Pevear, D.R., Środoń, J., Wicks, F.J., 1991. Report of the Clay Minerals Society Nomenclature Committee: revised classification of clay materials. Clays and Clays Minerals 39, 333–335.

Mathieson, A.McL., Walker, G.F., 1954. Crystal structure of magnesium vermiculite. American Mineralogist 39, 231–255.

McBride, M.B., 1989. Surface chemistry of soil minerals. In: Dixon, J.B., Weed, S.B. (Eds.), Minerals in Soil Environments, 2nd edition. Soil Science Society of America, Madison, WI, pp. 35–88.

McKeown, D.A., Post, J.E., Etz, E.S., 2002. Vibrational analysis of palygorskite and sepiolite. Clays and Clay Minerals 50, 537–684.

Medici, L., 1996. Cristallochimica delle miche di Tapira (Brasile). PhD. thesis. University of Modena and Reggio Emilia, 140pp. (in Italian).

Mellini, M., 1982. The crystal structure of lizardite 1T: hydrogen bonds and polytypism. American Mineralogist 67, 587–598.

Mellini, M., Viti, C., 1994. Crystal structure of lizardite-1T from Elba, Italy. American Mineralogist 79, 1194–1198.

Mellini, M., Weiss, Z., Rieder, M., Drábek, M., 1996. Cs-ferriannite as a possible host for waste cesium: crystal structure and synthesis. European Journal of Mineralogy 8, 1265–1271.

Mellini, M., Zanazzi, P.F., 1987. Crystal structures of lizardite-1T and lizardite-2H1 from Coli, Italy. American Mineralogist 72, 943–948.
Mellini, M., Zanazzi, P.F., 1989. Effects of pressure on the structure of lizardite-1T. European Journal of Mineralogy 1, 13–19.
Mifsud, A., Rautureau, M., Fornes, V., 1978. Etude de l'eau dans la palygorskite à l'aide des analyses thermiques. Clay Minerals 13, 367–374.
Migeon, G., 1936. Sepiolites. Bulletin de la Société française de Minéralogie et de Cristallographie 59, 6–134.
Mizuki, K., Suzuki, M., Akiyama, H., 1985. Transformation of structure in heating of clay minerals. Kanzei Chuo Bunsekishoho 25, 49–57 (in Japanese, English abstract).
Mooney, R.W., Keenan, A.G., Wood, L.A., 1952. Adsorption of water vapor by montmorillonite, II Effect of exchangeable ions and lattice swelling as measured by X-ray diffraction. Journal of the American Chemical Society 74, 1371–1374.
Moore, D.M., Reynolds, R.C. Jr., 1989. X-Ray Diffraction and the Identification and Analysis of Clay Minerals. Oxford University Press, New York.
Murad, E., Wagner, U., 1996. The thermal behavior of an Fe-rich illite. Clay Minerals 31, 45–52.
Murray, H.H., 1954. Structural variations in some kaolinites in relation to dehydrated halloysite. American Mineralogist 39, 97–108.
Nadeau, P.H., Wilson, M.J., McHardy, W.J., Tait, J.M., 1984. Interstratified clays as fundamental particles. Science 225, 923–925.
Nadeau, P.H., Wilson, M.J., McHardy, W.J., Tait, M.J., 1985. The conversion of smectite to illite during diagenesis: Evidence from some illitic clays from bentonites and sandstones. Mineralogical Magazine 49, 393–400.
Nagata, M., Shimoda, S., Sudo, T., 1974. On dehydration of bound water of sepiolite. Clays and Clay Minerals 22, 285–293.
Nagy, B., Bradley, W.F., 1955. Structure of sepiolite. American Mineralogist 40, 885–892.
Neal, C.R., Taylor, L.A., 1989. The petrography and composition of phlogopite micas from the Blue Ball kimberlite, Arkansas: a record of chemical evolution during crystallization. Mineralogy and Petrology 40, 207–224.
Neder, R.B., Burghammer, M., Grasl, Th., Schulz, H., Bram, A., Fiedler, S., 1999. Refinement of the kaolinite structure from single-crystal synchrotron data. Clays and Clay Minerals 47, 487–494.
Nelson, D.O., Guggenheim, S., 1993. Inferred limitations to the oxidation of Fe in chlorite: a high-temperature single-crystal X-ray study. American Mineralogist 78, 1197–1207.
Nespolo, M., Takeda, H., Ferraris, G., 1997. Crystallography of mica polytypes. In: Merlino, S. (Ed.), Modular Aspects of Minerals, EMU Notes in Mineralogy, vol. 1. Eötvös University Press, Budapest, pp. 81–118.
Newman, A.C.D., 1987. The interaction of water with clay mineral surfaces. In: Newman, A.C.D. (Ed.), Chemistry of Clays and Clay Minerals, Mineralogical Society, Monograph 6. Wiley, New York, pp. 237–274.
Newnham, R.E., 1960. A refinement of the dickite structure and some remarks on polymorphism in kaolin minerals. Mineralogical Magazine 32, 683–704.
Newnham, R.E., Brindley, G.W., 1956. The crystal structure of dickite. Acta Crystallographica 9, 759–764.
Norrish, K., 1954. The swelling of montmorillonite. Discussions of the Faraday Society, No 18, 120–133.

Odom, I.E., 1984. Glauconite and celadonite minerals. In: Bailey, S.W. (Ed.), Micas. Reviews in Mineralogy, vol. 13. Mineralogical Society of America, Washington, DC, pp. 545–572.

Okada, K., Ossaka, J., 1983. Dehydration reaction of interlayer water of halloysite by heating. Faculty of Engineering, Tokyo Institute of Technology. Nendo Kagaku 23, 27–31.

Paquet, H., Duplay, J., Valleron-Blanc, M.M., Millot, G., 1987. Octahedral composition of individual particles in smectite-palygorskite and smectite-sepiolite assemblages. In: Schultz, L.G., van Olphen, H., Mumpton, F.A. (Eds.), Proceedings of the International Clay Conference, Denver, 1985. The Clay Minerals Society, Bloomington, IN, pp. 73–77.

Parfitt, R.L., 1990. Allophane in New Zealand—A review. Australian Journal of Soil Research 28, 343–360.

Parfitt, R.L., Henmi, T., 1980. Structure of some allophanes from New Zealand. Clays and Clay Minerals 28, 285–294.

Parfitt, R.L., Wilson, A.D., 1985. Estimation of allophane and halloysite in three sequences of volcanic soils, New Zealand. Catena Supplement 7, 1–8.

Parker, J.C., 1986. Hydrostatics of water in porous media. In: Sparks, D.L. (Ed.), Soil Physical Chemistry. CRC Press, Boca Raton, FL, pp. 209–296.

Pauling, L., 1930. The structures of the micas and related minerals. Proceedings of the National Academy of Sciences of the United States of America 16, 123–129.

Peacor, D.R., Bauluz, B., Dong, H., Tillick, D., Yan, Y., 2002. Transmission and analytical electron microscopy evidence for high Mg contents of 1M illite: absence of 1M polytypism in normal prograde diagenetic sequences of pelitic rocks. Clays and Clay Minerals 50, 757–765.

Pérez-Rodríguez, J.L., Galán, E., 1994. Determination of impurity in sepiolite by thermal analysis. Journal of Thermal Analysis 42, 131–141.

Perrault, G., Harvey, J., Pertsowwsky, R., 1975. La yofortierite, un noveau silicate de manganese de St. Hilare. Canadian Mineralogist 13, 68–74.

Plançon, A., Zacharie, C., 1990. An expert system for the structural charecterization of kaolinites. Clay Minerals 25, 249–260.

Plançon, A., Giese, R.F. Jr., Snyder, R., Drits, V.A., Bukin, A.S., 1989. Stacking faults in the kaolin-group minerals: defect structures of kaolinite. Clays and Clay Minerals 37, 203–210.

Preisinger, A., 1959. X-ray study of the structure of sepiolite. Clays and Clay Minerals 6, 61–67.

Preisinger, A., 1963. Sepiolite and related compounds: its stability and application. Clays and Clay Minerals 10, 365–371.

Radoslovich, E.W., 1961. Surface symmetry and cell dimensions of layer lattice silicates. Nature 191, 67–68.

Radoslovich, E.W., Norrish, K., 1962. The cell dimensions and symmetry of layer-lattice silicates, I. Some structural considerations. American Mineralogist 47, 599–616.

Rancourt, D.G., Dang, M.Z., Lalonde, A.E., 1992. Mössbauer spectroscopy of tetrahedral Fe^{3+} in trioctahedral micas. American Mineralogist 77, 34–93.

Range, K.J., Weiss, A., 1969. Über das Verhalten von kaolinitit bei hohen Drücken. Deutsche Keramische Gesellschaft 46, 231–288.

Rautureau, M., 1974. Analyse structurale de la sepiolite par microdiffraction electronique. Thesis. University of Orléans, France, 89pp.

Rautureau, M., Tchoubar, C., 1974. Precisions concernant l'analyse structurale de la sepiolite par microdiffraction electronique. Comptes Rendues de l'Académie des Sciences, Paris 278, 25–28.

Rautureau, M., Tchoubar, C., Méring, J., 1972. Analyse structurale de la sepiolite par microdiffraction electronique. Comptes Rendues de l'Académie des Sciences, Paris, vol. 274, pp. 269–271.

Rayner, J.H., Brown, G., 1966. Structure of pyrophyllite. Clays and Clay Minerals 14, 73–84.

Reynolds, R.C., 1988. Mixed layer chlorite minerals. In: Bailey, S.W. (Ed.), Hydrous Phyllosilicates (Exclusive of Micas). Reviews in Mineralogy, vol. 19. Mineralogical Society of America, Washington, DC, pp. 601–629.

Rieder, M., Cavazzini, G., D'yakonov, Y.S., Frank-Kamenetskii, V.A., Gottardi, G., Guggenheim, S., Koval, P.V., Müller, G., Neiva, A.M.R., Radoslovich, E.W., Robert, J-L., Sassi, F.P., Takeda, H., Weiss, Z., Wones, D.R., 1998. Nomenclature of the Micas. Clays and Clay Minerals 46, 586–595.

Rogers, L.E., Quirk, J.P., Norrish, K., 1956. Occurrence of an aluminium-sepiolite in a soil having unusual water relationships. Journal of Soil Science 7, 177–184.

Rosenberg, P.E., 2002. The nature, formation, and stability of end-member illite: a hypothesis. American Mineralogist 87, 103–107.

Rozhdestvenskaya, I.V., Bukin, A.S., Drits, V.A., Fin'ko, V.I., 1982. Proton position and structural features of dickite according to X-ray diffraction analysis data. Mineralogicheskii Zhurnal 4, 52–58.

Sainz-Diaz, C.I., Timon, V., Botella, V., Artacho, E., Hernandez-Laguna, A., 2002. Quantum mechanical calculations of dioctahedral 2:1 phyllosilicates: effect of octahedral cation distributions in pyrophyllite, illite, and smectite. American Mineralogist 87, 958–965.

Scheidegger, A.M., Lamble, G.M., Sparks, D.L., 1997. The kinetics of nickel sorption on pyrophyllite as monitored by X-ray absorption fine structure (XAFS) spectroscopy. Journal de Physique IV, 7 (C2, X-Ray Absorption Fine Structure, vol. 2), 773–775.

Semenov, E.I., 1969. Mineralogy of the Ilimaussaq Alkaline Massif, Southern Greenland. Inst. Mineral. Geokhim. Krystallokhim. Redk Elementov, Izdat. "Nauka" 1969, 164pp. (in Russian).

Semenova, T.F., Rozhdestvenskaya, I.V., Frank-Kamenetskii, V.A., 1977. Refinement of the crystal structure of tetraferriphlogopite. Soviet Physics, Crystallography 22, 680–683.

Sen Gupta, P.K., Schlemper, E.O., Johns, W.D., Ross, F., 1984. Hydrogen positions in dickite. Clays and Clay Minerals 32, 483–485.

Serna, C., Ahlrichs, J.L., Serratosa, J.M., 1975. Folding in sepiolite crystals. Clays and Clay Minerals 23, 452–457.

Serna, C., Van Scoyoc, G.E., Ahlrichs, J.L., 1977. Hydroxyl groups and water in palygorskite. American Mineralogist 62, 784–792.

Shimizu, H., Watanabe, T., Henmi, T., Masuda, A., Saito, H., 1988. Studies on allophane and imogolite by high-resolution solid-state 29Si- and 27Al-NMR and ESR. Geochemical Journal 22, 23–31.

Shirozu, H., Bailey, S.W., 1966. Crystal structure of a two-layer Mg-vermiculite. American Mineralogist 51, 1124–11143.

Shitov, V.A., Zvyagin, B.B., 1972. Relative stability of polytypal modifications of micalike minerals. Kristallografiya 17, 1162–1165.

Slade, P.G., Dean, C., Schultz, P.K., Self, P.G., 1987. Crystal structure of a vermiculite-anilinium intercalate. Clays and Clay Minerals 35, 177–188.
Slade, P.G., Stone, P.A., Radoslovich, E.W., 1985. Interlayer structures of the two layer hydrates of Na- and Ca-vermiculites. Clays and Clay Minerals 33, 51–61.
Smith, D.G.W., Norem, D., 1986. The electron-microprobe analysis of palygorskite. Canadian Mineralogist 24, 499–511.
Smrčok, L., Gyepesová, D., Chmielová, M., 1990. New X-ray Rietveld refinement of kaolinite from Keokuk, Iowa. Crystal Research and Technology 25, 105–110.
Smyth, J.R., Dyar, M.D., May, H.M., Bricker, O.P., Acker, J.G., 1997. Crystal structure refinement and Mössbauer spectroscopy of an ordered, triclinic clinochlore. Clays and Clay Minerals 45, 544–550.
Sokolova, T.N., 1982. Authigenic formation of silicate minerals of various salinization stages. Nauka, Moskva, 163pp. (in Russian).
Sposito, G., 1984. The Surface Chemistry of Soils. Oxford University Press, New York.
Sposito, G., Prost, R., 1982. Structure of water adsorbed on smectites. Chemical Reviews 82, 553–573.
Springer, G., 1976. Falcondoite, a nickel analogue of sepiolite. Canadian. Mineralogist 14, 407–409.
Środoń, J., 1989. Illite-smectite in the rock cycle. In: Perez-Rodriguez, J.L., Galan, E. (Eds.), Lectures-Conferencias, Euroclay'87, Sevilla. Sociedad Espanola de Arcillas, pp. 137–151.
Środoń, J., Eberl, D.D., 1984. Illite. In: Bailey, S.W., (Ed.), Micas, Mineralogical Society of America, Reviews in Mineralogy 13, pp. 495–544.
Środoń, J., Elsass, F., McHardy, W.J., Morgan, D.J., 1992. Chemistry of illite–smectite inferred from TEM measurements of fundamental particle. Clay Minerals 27, 137–158.
Steinfink, H., Brunton, G., 1956. The crystal structure of amesite. Acta Crystallographyca 9, 487–492.
Stoch, L., 1974. Mineraly Ilaste (Clay Minerals). Geological Publishers, Warsaw, 186–193.
Suquet, H., de la Calle, C., Pezerat, H., 1975. Swelling and structural organization of saponite. Clays and Clay Minerals 23, 1–9.
Suquet, H., Iiyama, J.T., Kodama, H., Pezerat, H., 1977. Sythesis and swelling properties of saponite with increasing layer charge. Clays and Clay Minerals 25, 231–242.
Suquet, H., Pezerat, H., 1987. Parameters influencing layer stacking types in saponite and vermiculite: a review. Clays and Clay Minerals 35, 353–362.
Takeda, H., Ross, M., 1995. Mica polytypism: identification and origin. American Mineralogist 80, 715–724.
Teppen, B.J., Rasmussen, K., Bertsch, P.M., Miller, D.M., Schaefer, L., 1997. Molecular dynamics modeling of clay minerals, 1. Gibbsite, kaolinite, pyrophyllite, and beidellite. Journal of Physical Chemistry 101, 1579–1587.
Theng, B.K.G., Russell, M., Churchman, G.J., Parfitt, R.L., 1982. Surface properties of allophane, halloysite, and imogolite. Clays and Clay Minerals 30, 143–149.
Thompson, J.G., Withers, R.L., 1987. A transmission electron microscopy contribution to the structure of kaolinite. Clays and Clay Minerals 35, 237–239.
Tien, P.-L., Leavens, P.B., Nelen, J.A., 1975. Swinefordite, a dioctahedral-trioctahedral lithium-rich member of the smectite group from Kings Mountain, North Carolina. American Mineralogist 60, 540–547.

Toraya, H., Iwai, S., Marumo, F., Hirao, M., 1978a. The crystal structures of germanate micas $KMg_2.5Ge_4O_{10}F_2$ and $KLiMg_2Ge_4O_{10}F_2$. Zeitschrift für Kristallographie 148, 65–81.

Toraya, H., Iwai, S., Marumo, F., Hirao, M., 1978b. The crystal structure of germanate micas $KMg_3Ge_3AlO_{10}F_2$. Mineralogical Journal 9, 221–230.

Toraya, H., Marumo, F., 1981. Structure variation with octahedral cation substitution in the system of germanate micas KMg_3-$xMnxGe_3AlO_{10}F_2$. Mineralogical Journal 10, 396–407.

Torres-Ruiz, J., López-Galindo, A., González-López, J.M., Delgado, A., 1994. Geochemistry of Spanish sepiolite-palygorskite deposits: genetic considerations based on trace elements and isotopes. Chemical Geology 112, 221–245.

Uehara, S., 1987. Serpentine minerals from Sasaguri area, Fukuoka Prefecture, Japan. Journal of the Japanese Association of Mineralogists, Petrologists and Economic Geologists 82, 106–118 (in Japanese, English abstract).

Uehara, S., Shirozu, H., 1985. Variations in chemical composition and structural properties of antigorites. Mineralogical Journal 12, 299–318.

Vahedi-Faridi, A., Guggenheim, S., 1997. Crystal structure of tetramethylammonium-exchanged vermiculite. Clays and Clay Minerals 45, 859–866.

Vahedi-Faridi, A., Guggenheim, S., 1999a. Structural study of TMP-exchanged vermiculite. Clays and Clay Minerals 47, 219–225.

Vahedi-Faridi, A., Guggenheim, S., 1999b. Structural study of monomethylammonium and dimethylammonium-exchanged vermiculite. Clays and Clay Minerals 47, 338–347.

van der Gaast, S.J., Wada, K., Wada, S.-I., Kakuto, Y., 1985. Small-angle X-ray powder diffraction, morphology, and structure of allophane and imogolite. Clays and Clay Minerals 33, 237–243.

van Olphen, H., 1965. Thermodynamics of interlayer adsorption of water in clays, I Sodium vermiculite. Journal of Colloid Science 20, 822–837.

van Olphen, H., 1969. Thermodynamics of interlayer adsorption of water in clays, II Magnesian vermiculite. In: Proceedings of the 3rd International Clay Conference, Tokyo. Israel University Press, Jerusalem, vol. 1, pp. 649–657.

Van Scoyoc, G.E., Serna, C., Ahlrichs, J.L., 1979. Structural changes in palygorskite during dehydration and dehydroxylation. American Mineralogist 64, 216–223.

Veblen, D.R., 1992. Electron microscopy applied to nonstoichiometry, polysomatism, and replacement reactions in minerals. In: Buseck, P.R. (Ed.), Minerals and Reactions at the Atomic Scale: transmission Electron Microscopy. Reviews in Mineralogy vol. 27, pp. 181–223.

Veblen, D.R., Wylie, A.G., 1993. Mineralogy of amphiboles and 1:1 layer silicates. In: Guthrie, G.D. Jr., Mossman, B. (Eds.), Health Effects of Mineral Dusts. Reviews in Mineralogy, vol. 28. Mineralogical Society of America, Washington, DC, pp. 61–131.

Velde, B., Köster, H.M., 1992. A kinetic model of the smectite-to-illite trasformation based on diagenetic mineral series. American Mineralogist 77, 967–976.

Wada, K., 1989. Allophane and imogolite. In: Dixon, J.B., Weed, S.B. (Eds.), Minerals in Soil Environments, 2nd edition. Soil Science Society of America, Madison, WI, pp. 1051–1087.

Wada, K., 1995. Structure and formation of non- and para-crystalline aluminosilicate clay minerals: a review. In: Churchman, G.J., Fitzpatrick, R.W., Eggleton, R.A. (Eds.), Clays: Controlling the Environment, Proceeedings of the 10th International Conference, Adelaide, 1993. CSIRO Publishing, Melbourne, pp. 443–448.

Wada, S.-I., Wada, K., 1977. Density and structure of allophane. Clay Minerals 12, 289–298.

Wardle, R., Brindley, G.W., 1972. Crystal structures of pyrophyllite, 1Tc, and of its dehydroxylate. American Mineralogist 57, 732–750.
Watanabe, T., 1988. The structural model of illite/smectite interstratified minerals and the diagram for its identifications. Clay Science 7, 97–114.
Weaver, C.E., 1960. Possible uses of clay minerals in search for oil. American Association of Petroleum Geologists Bulletin 44, 1505–1518.
Weber, K., 1972. Notes on the determination of illite crystallinity. Neues Jahrbuch fűr Mineralogie—Monatshefte, 267–276.
Weiss, Z., Ďurovič, S., 1984. Polytypism of pyrophyllite and talc. Silikáty 28, 289–309.
Welch, M.D., Marshall, W.G., 2001. High-pressure behavior of clinochlore. American Mineralogist 86, 1380–1386.
Wells, N., Childs, C.W., Downes, C.J., 1977. Silica Springs, Tongariro National Park, New Zealand—analyis of the spring water and characterization of the alumino-silicate deposit. Geochimica et Cosmochimica Acta 41, 1497–1506.
Wicks, F.J., O'Hanley, D.S., 1988. Serpentine minerals: structure and petrology. In: Bailey, S.W. (Ed.), Hydrous Phyllosilicates (Exclusive of Micas) Reviews in Mineralogy, vol. 19. Mineralogical Society of America, Washington, DC, pp. 91–159.
Wicks, F.J., Whittaker, E.J.W., 1975. A reapparisal of the structures of the serpentine minerals. Canadian Mineralogist 13, 227–243.
Wiewióra, A., Rausell-Colom, J.A., García-González, T., 1991. The crystal structure of amesite from Mount Sobotka: a nonstandard polytype. American Mineralogist 76, 647–652.
Wiewióra, A., Weiss, Z., 1990. Crystallochemical classifications of phyllosilicates based on the unified system of projection of chemical composition, II. The chlorite group. Clay Minerals 25, 83–92.
Yoshinaga, N., 1986. Recent clay mineralogical studies of Ando soils—a review. Nendo Kagaku 26 (4), 281–291.
Yuan, G., Theng, B.K.G., Parfitt, R.L., Percival, H.J., 2000. Interactions of allophane with humic acid and cations. European Journal of Soil Science 51, 35–41.
Yucel, A.M., Rautureau, M., Tchoubar, D., Tchoubar, C., 1981. Calculation of the X-ray powder reflection profiles of very small needle-like crystal, II. Quantitative results on Eskischir sepiolite fibers. Journal of Applied Crystallography 14, 431–454.
Zheng, H., Bailey, S.W., 1994. Refinement of the nacrite structure. Clays and Clay Minerals 42, 46–52.
Zheng, H., Bailey, S.W., 1997. Refinement of an amesite—$2H_1$ polytype from Postmasburg, South Africa. Clays and Clay Minerals 45, 301–310.
Zöller, M., Brockamp, O., 1997. 1M- and 2M1-illites: different minerals and not polytypes. Results from single-crystal investigations at the transmission electron microscope (TEM). European Journal of Mineralogy 9, 821–827.
Zoltai, T., 1981. Amphibole asbestos mineralogy. In: Veblen, D.R. (Ed.), Amphiboles and Other Hydrous Pyriboles. Reviews in Mineralogy, vol. 9. Mineralogical Society of America, Washington, DC, pp. 237–278.
Zussman, J., 1954. Investigation of the crystal structure of antigorite. Mineralogical Magazine 30, 498–512.
Zvyagin, B.B., 1957. Determination of the structure of celadonite by electron diffraction. Soviet Physics, Crystallography 2, 388–394.

Zvyagin, B.B., 1963. The theory of polymorphism in chlorite. Kristallografiya 8, 32–38 (abstract).
Zvyagin, B.B., 1967. Electron Diffraction Analysis of Clay Mineral Structures. Plenum Press, New York.
Zvyagin, B.B., Berkhin, S.I., Gorshkov, A.I., 1966. Structural characteristics of halloysite based on X-ray and electron-diffraction patterns. Akademii Nauk SSSR, 69–93 (in Russian, English abstract).
Zvyagin, B.B., Drits, V.A., 1996. Interrelated features of structure and stacking of kaolin mineral layers. Clays and Clay Minerals 44, 297–303.
Zvyagin, B.B., Mishchenko, K.S., 1965. Diagnostics of one-stacking semirandom polymorphic modifications of chlorites. Kristallografiya 10, 555–557 (abstract).
Zvyagin, B.B., Mishchenko, K.S., Shitov, V.A., 1963. Electron diffraction data on the structures of sepiolita and palygorskite. Soviet Physics, Crystallography 8, 148–153.
Zvyagin, B.B., Mishchenko, K.S., Soboleva, S.V., 1968. Structures of pyrophyllite and talc in the light of the multiplicity of types of mica-like. Kristallografiya 13, 599–604.
Zvyagin, B.B., Soboleva, S.V., Fedotov, A.F., 1972. Refinement of nacrite structure by a high-voltage electron-diffraction method. Kristallografiya 17, 514–520.
Zvyagin, B.B., Soboleva, S.V., Fedotov, A.F., 1979. Determination of the crystal structures of layer silicates, 4. Crystal structure of nacrite. In: Drits, V.A. (Ed.), Vysokovol'tnaya Elektronogr. Issled. Sloistykh Miner. vol. 171–177. Izd. Nauka, Moscow, pp. 216–223.